April 2010

Pneumatic Spring Mass System

Brendan R. White
Worcester Polytechnic Institute

Kazim Naqvi
Worcester Polytechnic Institute

Richard M. MacKendrick
Worcester Polytechnic Institute

Pneumatic Test Bed

A Major Qualifying Project Report

Submitted to the faculty of

WORCESTER POLYTECHNIC INSTITUTE

In partial fulfillment of the requirements for the

Degree of Bachelor of Science

By

Richard MacKendrick
rmack10@wpi.edu

Syed Kazim Naqvi
sknaqvi@wpi.edu

Brendan White
whitebr@wpi.edu

Date of Submission: 22nd April 2010

Approved:

Professor Eben C. Cobb

eccobb@wpi.edu

Abstract

To enhance the learning experience of students in WPI's mechatronics class, a pneumatic piston-spring assembly was designed and fabricated. Mathematical and bond graph analysis was performed to obtain theoretical metrics for the device's operation. These theoretical metrics were compared with experimental results using sensors and data acquisition methods. The theoretical and experimental values were determined to have an acceptable deviation and can be reproduced by future students for the purpose of demonstrating the limits of theoretical metrics.

Table of Contents

Table of Figures

Table of Tables

Executive Summary

An increasing number of systems today are mechatronic, meaning they combine mechanical, electrical, computer, and control engineering together. This major qualifying project, incorporating the endeavors of Richard MacKendrick, Kazim Naqvi, and Brendan White, is aimed at the development of a device to be used as a teaching aid for the Mechatronics class at Worcester Polytechnic Institute (WPI).

This project called for both the design and fabrication of a pneumatic spring-mass system that includes electronic sensors and controls, as well as the creation of a detailed mathematical analysis and bond graph analysis of the system. As a teaching aid, the device will collect experimental data that can be compared to the theoretical data generated by the bond graph approach. The expectation is that the theoretical and experimental data will not match, but it will be shown how refinement would allow the theoretical calculations to approach the experimental determined values.

Background research was conducted to fully understand the components needed to develop a pneumatic spring-mass system. This research investigated the components of a pneumatic system, such as a piston, solenoid valve, and compressed air handling. Electronics such as sensors that measured pressure and force, as well as controllers that would manage the system were also examined.

The afore-mentioned pneumatic spring-mass system can be designed using several approaches. A list of task specifications was compiled to narrow the scope of this system and understand the limitations within which its design needed to be encompassed. One essential task specification was the constraint that the device should be desktop sized and portable. Another was that device should have a facility for measuring and recording pressure at various physical locations throughout the duration of its operation.

A mathematical model of this system based on a differential equation for a general pneumatic spring-mass system was then developed. This completed a full understanding of the requirements of the device, its expected mechanical behavior, and the design parameters that needed to be modified for improving the design.

Concurrent to the development of the mathematical model, the design of the physical device was conducted. The initial design was developed entirely out of VEX components, due to their availability and conduciveness to rapid prototyping. This design consisted of a pneumatic piston, actuated by a solenoid valve and controller that moved a sliding rail. The need for a low-friction linear

slider to replace the sliding rail as well as a guide rod for the spring was identified during this stage. The next design iteration incorporated these changes, consequently improving the overall functionality of the device. This iteration also identified the need for accurate alignment of the piston, spring, and linear slider, since no components of the force exerted by the piston were desired in non-axial directions. If all of the force were to be transferred axially, it would result in a direct compression or expansion force acting on the spring, consequently lowering the gap between theoretical calculations and experimental results.

The final design of the device incorporated the use of an aluminum plate for mounting the piston assembly, linear slide, spring, and guide rod together as a sub-assembly. Both vertical and horizontal alignment of all components was achieved by drilling holes with high clearance on the base plate, which allowed the components to be adjusted with respect to each other. A wooden base was chosen to mount the steel plate, as well as sensors, pneumatic components, and electrical equipment. An annotated image of the overall design is provided in Figure 1.

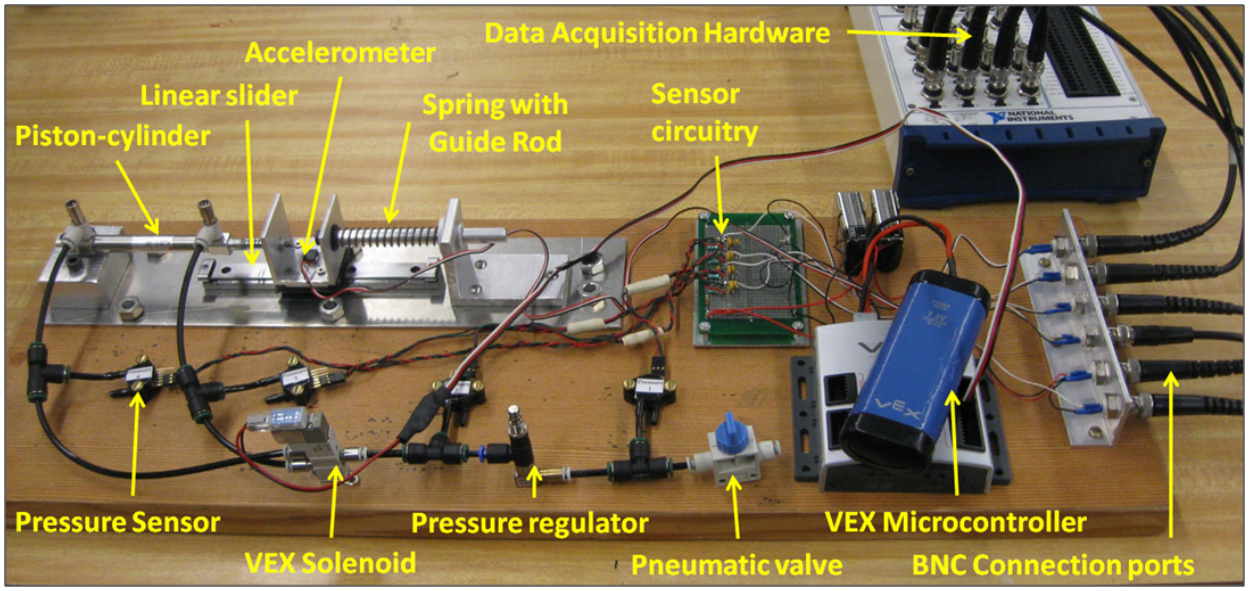

Figure 1 Annotated diagram of final design

The system shown above is operated by turning the pneumatic switch to its 'on' position, turning on the VEX microcontroller, and connecting the switch to a pressure source such as a tank or a regulated air supply, and connecting the device to a computer. BNC connections were used to transfer data from the sensor circuitry to a National Instruments Data Acquisition Board (DAQ), which was then analyzed using a system developed in LabVIEW. The LabVIEW program written for this device reads and

converts the electrical signals acquired by the DAQ to the appropriate pressure, acceleration, and force quantities, and then displays on screen and records to file the experimental data.

Testing was conducted on four types of springs that had varying spring constants, and one had varying geometry. Three of the springs had a constant free length and a constant outside diameter, which were marked with color to denote spring rates. The “red” spring has a spring rate of 15.59 lb/in, the ”yellow” 5.27 lb/in, and the “green” 3.31 lb/in. Additionally, a short spring that was about half the size of the other springs was used with a spring rate of 3.14 lb/in. The orientation of the accelerometer provides results in values that are positive in the direction of the piston being pushed out (outward stroke), and negative when pulled in (return stroke).

Table 1 below summarizes the results of experimental analysis of the final design. All values are of the resultant acceleration of the pneumatic spring-mass system in units of Newtons. It is important to note that the positive and negative values of acceleration are extremely high on the outward stroke for the control experiment (in the absence of springs). This is because one of the valves in the piston-cylinder was adjusted to compensate for a higher force required to compress a compression spring on the outward stroke, and is expected behavior of the system.

Table 1 - Experimental Result Summary

Spring	Pressure (psi)	Outward Stroke		Return Stroke	
		Positive	Negative	Positive	Negative
Red	52.3	5.74	2.76	1.77	3.88
Yellow	52.1	7.04	3.93	2.05	3.56
Green	54.3	6.30	3.35	1.88	1.90
Control	49.9	16.35	53.48	0.55	0.83

A comparison is now made between the final iteration of the mathematical model, and the final iteration of the bond graph model, describe further in Section 7.2. For the variation of pressure with respect to time, the bond graph method did not provide a function that was similar to the original function in magnitude or behavior.

Figure 2 shows the overall behavior of the fluid component of the pneumatic spring-mass system as modeled using a differential mathematical analysis and a bond graph approach. The

differential analysis shows a consistent sinusoidal curve for pressure variation on the right, whereas the bond graph approach shows a decaying sinusoidal curve for force variation on the left. Since pressure is directly proportional to force, a comparison between the two plots can be made. When compared to physical system behavior of the device, the bond graph function shows better relation to the behavior, as the motion of the system quickly ceases with a spring installed.

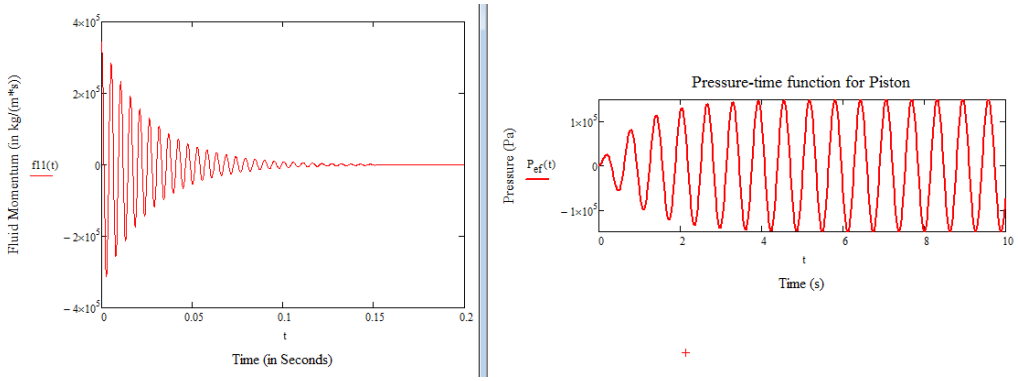

Figure 2- Fluid Momentum versus time functions

The theoretical results are slightly different from experimental values obtained, as was expected at the outset of the design process. This is because there are several external conditions that influence the actual behavior of the system, such as friction inside the piston, the compressibility of air, the response time of the overall system, as well as the accuracy of the measurement devices. These factors contribute to a slight variation between theoretical and experimental values which cannot be avoided without making the theoretical computations extremely tedious and time consuming.

Over the three terms that this MQP was designed, engineered, fabricated, and tested, our group gained valuable insight into the design process and advanced our knowledge in pneumatic systems and engineering in general. We feel that the constructed device can be used as a valuable teaching tool in Professor Cobb's Modeling and Analysis of Mechatronic Systems course, whose value could be greatly improved through subsequent project work.

The device constructed fulfils the goals and objectives that were established at the beginning of this project, and will be a beneficial teaching aid to convey the differences and similarities between a bond graph model of a system and a system's actual behavior. As a teaching tool, this device will assist students in learning what assumptions to make and when they are valid. Throughout this process, familiarity with electrical, mechanical, and pneumatic systems will be improved.

In final conclusion, this MQP was an overall success, meeting the project's goals and objectives, and providing a launching point for the continuation of this project. Our hope is that future MQP groups improve the pneumatic test bed, following our recommendations and expanding it to fulfill the device's needs.

1 Introduction

An increasing number of systems today are mechatronic, meaning they combine mechanical, electrical, computer, and control engineering together. One way of modeling and analyzing a mechatronic system is through the use of a bond graph, which allows mechanical and electrical systems to be modeled together in terms of effort and flow. Due to the complexity of even the most simple mechatronic system, assumptions and simplifications need to be made to allow for a bond graph that is both accurate enough to reasonably predict the actions of the system, but not too complex as to require excessive computational power.

Since the 2006-2007 academic year, the mechanical engineering and robotics engineering departments of WPI have offered a course in the Modeling and Analysis of Mechatronic Systems, taught by Professor Eben C. Cobb. "This course introduces students to the modeling and analysis of mechatronic systems," as well as the "creation of dynamic models and analysis of model response using the bond graph modeling language."[1]

Professor Cobb desires a device to be used as a teaching aid in the class that can be modeled and tested by the class. Once the device was modeled theoretically with a bond graph, the actual device can be tested experimentally through the use of sensors. The expectation is that the theoretical and experimental data will not match, but it will be shown how the simple theoretical model can be refined to account for errors and eventually allow the theoretical calculations to approach the experimental determined values.

This project called for the design and fabrication of a pneumatic spring-mass system that includes electronic sensors and controls, in addition to the creation of a detailed mathematical analysis and bond graph analysis of the system. This report follows the design process by first detailing the project description, then covering the required background research, and resulting task specifications. The methodology of the design and fabrication of the device is then covered, followed by the design description of the resulting product. Additionally, the mathematical, bond graph, and experimental results are discussed proceeded by the results and conclusions.

2 Background Research

In order to develop a pneumatic cylinder test bed, it was necessary to fully understand the workings of pneumatic theory and the systems they require to function. Research into commercially available products was also conducted in order to source components for this project. In addition, an introduction to bond graphs is included for the benefit of the reader.

2.1 Equipment

The equipment required to assemble a pneumatic system were researched. These components included pneumatic cylinders, solenoids, regulators, force and pressure transducers, springs, pneumatic tubing, dryers, filters, and other components.

2.1.1 Pneumatic Cylinders

Pneumatic cylinders are devices that convert compressed gas into linear movement. Although compressed air is most common due to its availability, other gasses such as compressed nitrogen and carbon dioxide are also used when requirements necessitate their use. Pneumatic cylinders are comprised of two primary components: the main cylinder, and an enclosed piston. They also come in two different principle styles, namely single and double acting cylinders. A single acting cylinder as shown on the left in Figure 3 allows pressurized gas to flow through one end of the cylinder to advance the piston, and may contain a spring that returns the piston back to its original position. A double acting cylinder as shown on the right in Figure 3 allows the gas to enter on both sides of the piston, permitting control in both directions.

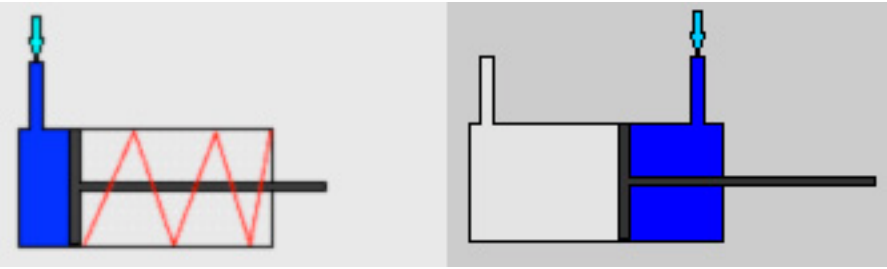

Figure 3 - Single (Left) and Double (Right) Acting Cylinder – Source: Wikimedia Commons

The primary formula that describes a pneumatic cylinder is as follows, where the force (F) is equal to the pressure (P) times the area (A). [2]

$$F=PA$$

It should be noted that the area of the piston on the return stroke of a double acting piston is smaller by the cross section of the piston rod, thus reducing the potential force.

When choosing the correct size for a pneumatic cylinder, several factors have to be taken into consideration. One of the main design considerations, is the output force required, which as detailed before, is determined by the diameter of the piston and the amount of pressure used. The force that the cylinder is capable of producing should be greater than the required force, to allow for proper movement that does not produce "slow, jerky, and uncontrolled motion." [2] At the same time, the pneumatic cylinder should not overly excessive, as to cause waste and added cost. Since compressed gas can be potently dangerous if accidently released, just 30 psi of compressed air can cause eye and ear damage, the required system pressure should be taken into consideration. [3]

2.1.2 Solenoid Valve

Solenoid valves are electronically controlled valves for controlling fluid flow. A solenoid consists of a cylinder, called a plunger that is housed around an electric magnetic field. When the magnetic field is activated, the plunger is retracted, and the solenoid will remain open until the field is turned off, resulting in the solenoid closing by means of a spring. [4] The small volume of flow that results from this is called a direct acting valve, but like a transistor, this fluid flow can be used to control a larger volumetric flow, called a diaphragm piloted valve. When the solenoid is closed, as seen in Figure 4, pressure from the fluid flow directed through the diaphragm forces it closed, until the solenoid opens and releases the pressure, resulting in the diaphragm releasing the fluid through the valve.

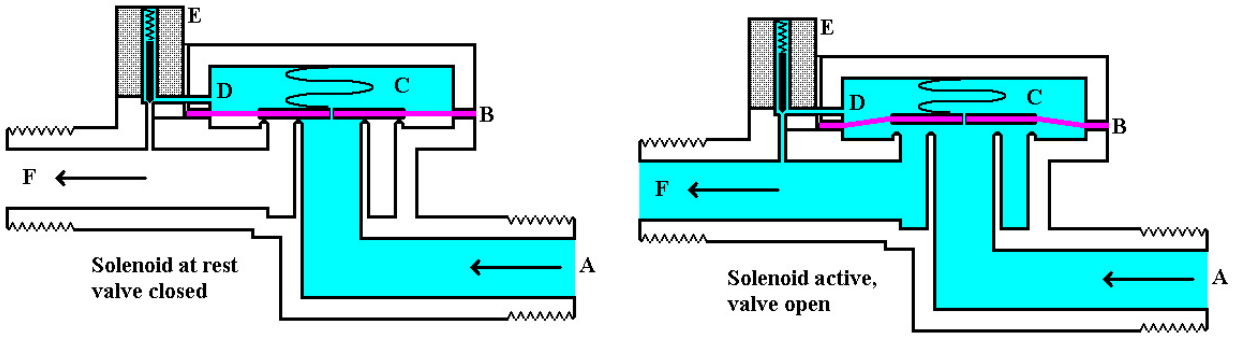

Figure 4 - Solenoid Valve Closed (Left) and Open (Right) [5]

2.1.3 Pressure Regulators

Pressure regulators are used to allow for constant output pressure independent from the input pressure. Regulators are a type of valve that consists of "integral loading, sensing, actuating, and control components." To allow for regulation of the pressure, a wide variety of springs are used in conjunction with a diaphragm or piston for pressure sensing. Pressure regulators work best when the desired pressure is in the "center one-third" of the source pressure. This prevents the spring from being compressed too much or too little. When using a pressure regulator, the consequence of its failure has to be considered. Relief valves can be used to prevent fluid at a high pressure from causing damage further downstream, or injuring nearby people. [6]

2.1.4 Pressure Transducer

Pressure transducers are designed to produce an analog signal that varies based on the pressure it is reading. Most pressure transducers work by measuring the strain produced by the deformation of a diaphragm between a high and low pressure using a strain gage. Pressure transducers come in a variety of styles that allow for different sizes and geometries, as well as high pressure, high accuracy, and other applications. [7]

2.1.5 Force Transducer

Force transducers are used to measure an applied force. Classic force transducers relied on the deformation of a spring to measure the applied force, but were plagued by small ranges of measurement, large deflections, and inaccuracies. Modern force transducers rely on hydraulics or pneumatics, strain gauges, quartz crystals, and other assorted methods.

Hydraulic force transducers are designed for high load applications and utilize a force balancing principle, and can achieve an accuracy of 0.25%. Pneumatic transducers work on the same force balancing principle, but have a higher accuracy at the cost of increased response time. [8]

Strain gauge force transducers are becoming increasingly popular, and work by converting mechanical deflection to an electrical signal using a strain gauge. Typically "four strain gages are used to obtain maximum sensitivity and temperature compensation," and are mounted, two in tension and two in compression to "a beam or structural member that deforms when weight is applied." These strain gauges can achieve accuracies up to 0.03% of a load varying from 10-5000 lb. [9]

Piezoelectric sensors, which typically use quartz crystals to "produce an electric charge proportional to the mechanical load applied," are another type of force transducers. These transducers

allow for a large range of measurements with an accuracy of 0.03% with deflections in the micron range, but have a high cost and have a non-linear output. [9]

Force can also be determined using the moving mass and its acceleration, which can be measured using an accelerometer. Accelerometers are also piezoelectric, and determine acceleration through the squeezing of a quartz crystal. When specifying an accelerometer some important terms have to be taken into consideration. One such term is the dynamic range, or the maximum amplitude that can be measured before the data is cutoff. The resonance frequency is the frequency at which the sensor will resonate, and should be well above the frequencies measured. Sensitivity, which affects the output voltage, is counterintuitive where high accelerations are best measured by low output accelerometers, and low accelerations by high output accelerometers. Mounting also has to be taken into consideration, and manufacturers offer a wide range of options for different applications. [10]

Force can also be determined using integrated position or velocity measurements. A wide variety of technology and devices exist to measure the velocity of an object, which include but are not limited to devices that work on the same principles of accelerometers, magnetic based systems, to ultrasonic based systems that take repeated distance measurements. Similarly, distance measuring devices employ a breadth of technology such as linear potentiometers, whose resistive value changes with position, or optical based systems. The benefits and detractors of the different technologies include accuracy, precision, sampling rate, and the lack or requirement of a physical connection to the object being measured.

2.1.6 Springs

Springs can be manufactured from a variety of materials, although music wire and stainless steel are commonplace. Springs are specified by their diameter, both inner and outer, along with wire diameter, free length and solid height. Free length is used to describe the length of the spring when no forces are acting upon it, and solid height is the length of the spring when fully compressed. The spring rate specifies the stiffness of the spring and is measured in units of force over distance. [11] The spring rate is determined through Hooke's law, which states that the deformation of a spring is directly proportional to the force acting on it. [12]

$$F=-kx$$

2.1.7 Pneumatic Tubing

Pneumatic tubing can be formed from polyurethane, polyethylene, or nylon 11, all of which have unique physical properties. Polyethylene is designed primarily for food applications; polyurethane and nylon 11 see more industrial uses. While polyurethane features greater flexibility, kink resistance, and low permeability, nylon 11 can be used under greater working pressures and has lower expansion under pressure. [13]

2.1.8 Compressed Air Dryer and Filter

Compressed air from a compressor is neither clean nor dry, compressed air contains water due to the humidity of the source air, as well dirt and other particulates. Oil also makes its way into the compressed air, both through discharge from the compressor and added in some cases for the maintenance and lubrication of compressed air equipment. Dryers and filters can be used to remove undesired components from the air. [14]

A dryer is used to eliminate water vapor from the compressed air once any liquid water formed during compression is removed. There are three primary types of dryers available, namely refrigerant, regenerative adsorbent desiccant and deliquescent absorbent dryers. Refrigerant dryers utilize the thermodynamic cycle and heat exchangers to purge water vapor from the compressed air, while desiccant and deliquescent based systems absorb the water vapor using adsorbent media. A comparison of the different types of dryers is shown in Figure 5, and highlights the cost and maintenance required for each.

COMPRESSED AIR DRYER COMPARISON

Dryer Type	Pressure Dew Point	Atmospheric Dew Point	Drying Media Replacement	Power Consumption	Initial Cost	Pre Filters	After Filters	Maintenance Cost
Refrigerated	2°C	23°C	Nil	For refrigeration motor	Medium	General purpose and coalescing	None	Regular maintenance of refrigeration motor
Regenerative Desiccant	–40°C	–57°C	Infrequent	For drying desiccant	High	General purpose and coalescing	Coalescing	Small
Deliquescent	10°C	–15°C	Regularly, minimum 6 monthly	Nil	Low	General purpose and coalescing	Coalescing	Recharging container

Figure 5 - Comparison of compressed air dryer types [14]

Filters are designed to remove unwanted particulates and contaminants from the compressed air. Most air filters will remove coarse, or larger than 40 microns, particles. Systems requiring removal of

fine, smaller than 40 microns, require more specialized filtration. “High speed pneumatic tools” require flirtation in the rage of 10 to 25 microns. Since filters will become clogged faster with finer filtration, choosing a filter with the lowest required filtration size is important. Most filters will remove the majority of oil that is introduced to the compressed air from an oil lubricated compressor, while this is sufficient for most industrial processes, the air is not oil free, thus not for human consumption.

2.2 Bond Graph Introduction

The bond graph approach utilizes a simple mathematical consequence of several systems in order to create equations that predict the behavior of said systems. The power of the bond graph system comes from its ability to traverse multiple types of systems (pneumatic to mechanical, electrical to rotational, etc.) with incredible ease. This is because power can measurable as an effort multiplied by a flow for all types of systems. For mechanical systems, power is force (effort) times velocity (flow). For fluid systems, power is pressure (effort) times volumetric flow rate (flow).

Using the two variables of effort and flow, the bond graph is a general purpose tool for modeling the behavior of several systems. To model system properties, such as mass or compliance, bond graphs use elements and junctions. Junctions set a condition on the efforts and flows moving into and out of them, while elements set relations between the quantities entering them. Junctions can either be 1 or 0 junctions, while elements are resistors, inertances, and capacitances.

In the bond graph approach, elements are joined by bonds. The direction of the bonds indicates the direction of power application when the flow and effort associated with the bond are positive. Bonds are drawn as a half arrow, and may have a causal mark added to either end. The causal mark is important in the mathematical analysis of the graph, as it indicates the junction or element (attached to a bond) which has the effort of the bond used as an input into its mathematical functions.

3 Goals and Objectives

The overall goal of our group's project is to design and construct a device which will enable a controlled application of force to a spring mass system, and provide sensor output that will match theoretical results as closely as possible. To accomplish this goal, we pursued the following objectives:

(1) Design a system to be constructed that meets the design requirements. After a complete understanding of the project was achieved, and specifications created, the iterative method of design was employed. After multiple attempts, a design that functioned as required was constructed.

(2) Purchase or make the components required to meet the requirements of the device. In order to choose the correct components and materials, our group researched sensors, pneumatic theory, and commercial products to make educated decisions. When required components were not readily available, they were designed and fabricated to meet the project's needs.

(3) Create a means of reading and recording the sensors measuring the application of force. When the mechanical system was created, an electrical module was designed and constructed. Electronic control and computer software were used to operate the device and convert the electrical signals to meaningful data.

(4) Create a mathematical and bond graph model of the designed device. Theoretical modeling of the device was conducted in two manners. Scientific theory and mathematical equations were used to produce one model, while a bond graph was employed for the other.

(5) Analyze and compare the mathematical, bond graph, and experimental results. The underlying intention of this project is to demonstrate the differences between the two theoretical models and the experimental results.

These objectives were established to guide our progress toward the creation and completion of the pneumatic test bed project. The methodology we established allowed us to ensure a high quality deliverable for use by Professor Cobb. The objectives were worked on in parallel whenever possible, and broken down into numerous different tasks.

4 Task Specifications

It is important to review the task specifications of any project or problem before beginning the design stage. Task specifications can be further broken down into performance specifications and design specifications. For example, the performance specifications for a hand glove would be that it needs to maintain insulation at temperatures as low as 0° F, whereas the design specifications would require that it needs to be at least 1/8 inch thick. This section will enlist the performance and design specifications for our major qualifying project, and explain them individually.

4.1 Performance specifications

The following performance specifications were given to us and/or used as initial parameters before starting the design stage for our project.

1. The device needs to operate at room temperature and pressure
2. The device should be capable of withstanding a shock of up to 5 g's (to reduce breakage if dropped)
3. It should operate from a standard electrical outlet for 110 V, 15 A and/or run off of shop air.
4. The components should have an operational life of a minimum of 10 years
5. The device should be able to deliver its output results in the form of a graph when integrated with system analysis software, such as LabVIEW/SimuLink.
6. The device should not cost more than $450 to design, manufacture, and deliver (shipping and handling excluded) to the customer.
7. The device should operate for pressures lower than 100 psi.

4.2 Design specifications

Design specifications are also important, since they are used as initial parameters for drafting possible designs of the device. The following design specifications were required for this project

8. The device should be portable with dimensions less than 2 feet by 3 feet by 6 inches).
9. It should be easy to carry with a gross weight of less than 35 lbs
10. The device should not require manual input during operation, to improve repeatability of results
11. Since the device is pneumatic, all components allowing air flow in the device should be able to withstand pressures of up to 70 psi.
12. The device should have a facility for measuring and recording pressure at various physical locations throughout the duration of its operation

5 Methodology

The design of the pneumatic test bed took a very iterative path, encompassing numerous prototype models that varied widely. An initial design intended for rapid prototyping and exploration of the project was quickly made in the beginning, this design was followed by more refined and complete designs, which would lead to a finished product. This section will detail each design iteration, and the problems discovered and rectified throughout the process.

5.1 1st Iteration – VEX construction

The first iteration of our model was developed entirely using VEX components. It consisted of a reservoir capable of handling up to 150 psi of air pressure, a pressure regulator, solenoid, and two-way piston capable of withstanding pressures up to 100 psi. These components were connected using VEX tubing and the solenoid was controlled by the VEX controller. The piston selected was capable of moving a guide rod that was attached to a spring. This would complete the piston-spring assembly and ensure linearity of motion during the compression and expansion strokes.

This model did not have any springs attached to it, and consequently there was no mechanism for preventing the springs from bending during compression. The entire model was built on a collection of VEX plates bolted together to form a large rectangular base with space in the middle for housing the VEX controller. For visualization purposes, a CAD illustration of this model is attached and shown below in Figure 6.

The model was constructed in merely a couple of days to give the team a vision of performance requirements, drawbacks, and the project scope. Hence, there were no sensors installed for monitoring pressure at various points in the model. The VEX slider gave us ideas on what kinds of sensors could be used for measuring the force of the piston on the spring and vice versa. A linear potentiometer, accelerometer, force sensor, and velocity transducer were some of the sensors considered during this phase.

The first iteration of our project was easy to assemble, and the components required for its development were readily available in WPI's robotics lab. This made it an ideal model as a teaching tool for the Mechatronics class, which was its primary purpose as mentioned in the project's objectives and goals. The development of this model gave us insight on additional (non-VEX) components required for measuring pressure and force during operation of the device.

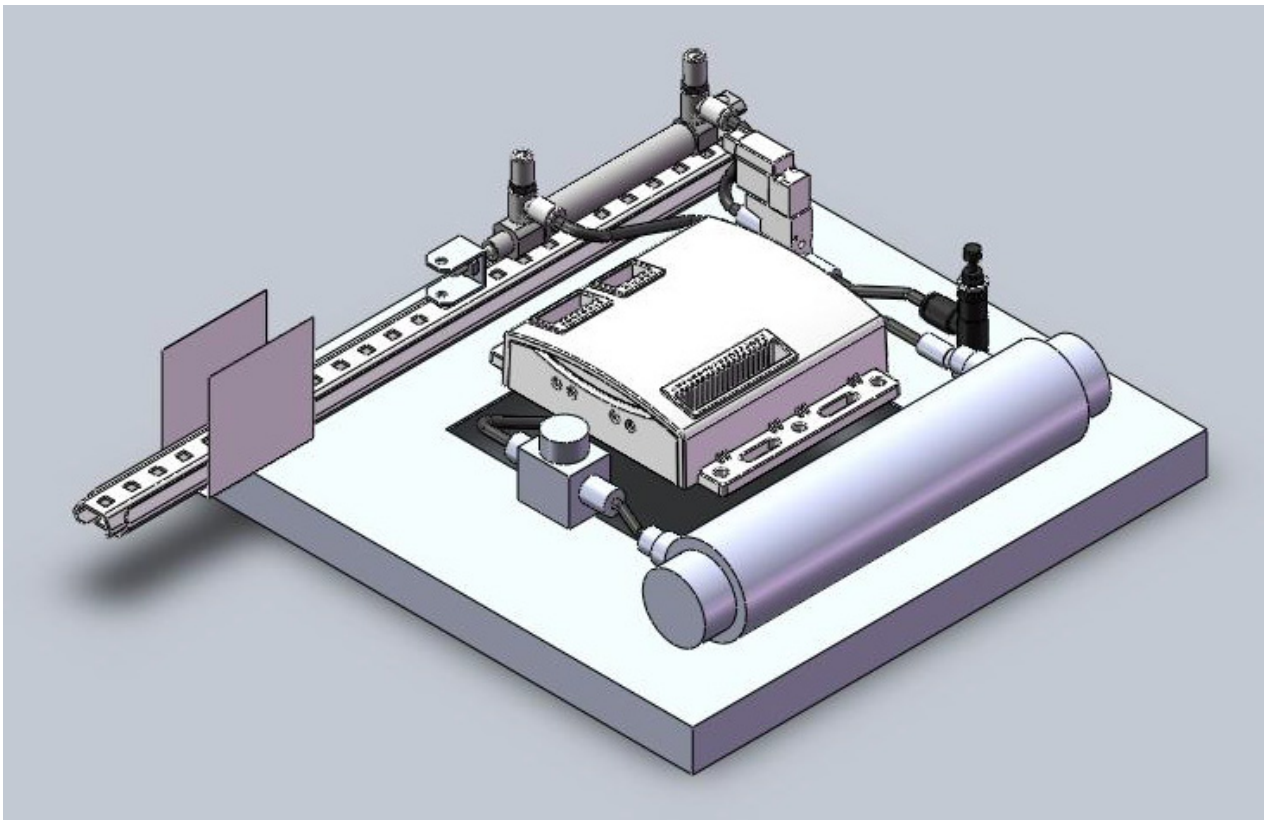

Figure 6 - CAD rendering of the first iteration of the device

5.1.1 Design limitations

Since it was our first iteration, this model had some inevitable drawbacks that forced us back to the drawing board. One such drawback was that the VEX slider was noisy and generated a large amount of friction during motion, which would have added an additional and undesired parameter into the experimental results. There was also no straightforward way of adding a spring and guide rod to the piston and slider in a way that kept them aligned. The inability to align the components was due to the design of the VEX plates used for construction, which featured pre-spaced holes that were not conducive to aligning our components.

In addition, the VEX reservoir was not capable of holding large amounts of air, which reduced the model's functionality to 10 cycles of compression and expansion. The reservoir was also bulky and occupied an unacceptable amount of space on the base plate of the model.

It was also found that the VEX base was lacking robustness, which resulted in flimsy connections between the VEX components and the base. This resulted in the connections loosening during operation

of the device, and it was noted that operational stability needed to be improved in the next iteration of the model.

5.2 2nd Iteration

The second iteration of our model took into account the limitations and drawbacks observed in the first iteration, and positioned the removal of these drawbacks as the primary goal for the second iteration. The entire design was concentrated on efforts to align the piston with the slider, guide rod, and spring. VEX components were used in this iteration for the purpose of raising the height of the piston to properly align with the slider. This enabled the platform attached to the slider to be aligned to the piston. An illustration of the final CAD model for this iteration is shown below in Figure 7.

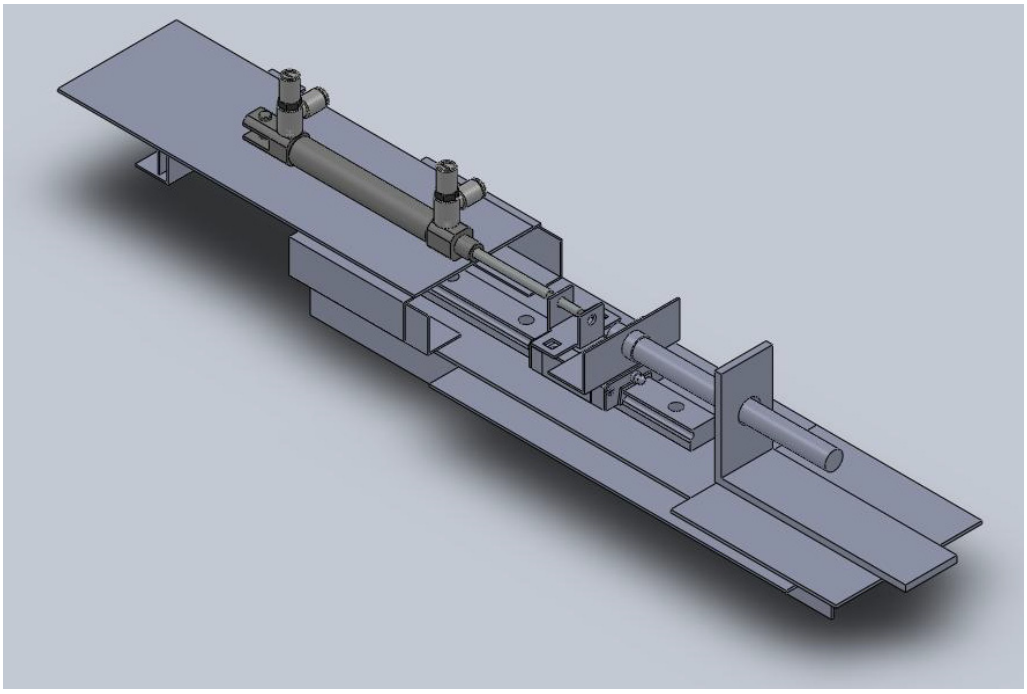

Figure 7 - CAD rendering of the second iteration of the device

5.2.1 Linear slider replacement

A replacement slider, manufactured by THK, was purchased to reduce friction and noise during operation. This slider had a limited range of travel in comparison to the VEX slider, but it was noted that the range of travel of the piston was less, thus the operational limits of our first model were not compromised.

5.2.2 Potentiometer vs. accelerometer dilemma

A linear potentiometer was also purchased, and attached to the slider to measure of the distance traveled during motion. This resulted in alignment issues, since the piston, slider, potentiometer, spring, and guide rod had to move in the same plane and lineup with each other. The issues were resolved by mounting the potentiometer parallel to the slider, and introducing a linking bracket between the moving knob of the potentiometer and the platform of the slider.

It was also discovered that the potentiometer could not display a linear change in displacement during the operation of the device, but rather showed a jump in the measured value of electrical resistance during motion. This behavior was similar to a trapezoidal change in resistance and drastically compromised the accuracy of the experimental results.

At this point, it was decided to discard the potentiometer and use a piezoelectric accelerometer in its place. A separate circuit and a LabVIEW interface were developed for the accelerometer. The accelerometer was also compact, allowing it to be mounted on the base of the linear slide without a major compromise in the model design.

5.2.3 Mounting brackets and guide rod

A bracket was mounted on the linear slide to enable a guide rod to be horizontally attached to the linear slide. This ensured linearity of the guide rod with respect to the slider during operation. The accelerometer was attached to this bracket to measure the acceleration, and consequently the force, subjected on the spring.

The guide rod was obtained from scrap metal available in the work area of Washburn Shops at WPI. This rod conveniently had a threaded hole, which allowed it to be attached to the bracket using a bolt. The guide rod functioned as a support for the spring during its tension and compression, and allowed for quick release and adjustment of the spring.

Another bracket was fixtured at the extreme end of the assembly to support the guide rod horizontally and restrict free motion of the spring in the forward direction. In order to mount this bracket, an additional metal plate was attached to the VEX support structure since the previously base was not long enough. An illustration of the final CAD model for this iteration was shown previously in Figure 7.

6 Final Design Selection

The final design was developed after taking into account the limitations and drawbacks that were observed for both the first and second designs. This design involved the use of custom plates to ensure the piston assembly, linear slide assembly, guide rod, and spring line up both horizontally and vertically during operation. Every component used in the project, including the breadboard, VEX controller, BNC connectors, pneumatic tubing and fittings, as well as the plate containing the dynamic assembly were mounted on a wood base for increased stability. The following section illustrates the design considerations and challenges faced for this project, and the solutions that were deemed most applicable to the issues, as well as a description of the final design.

6.1 System schematic

The first phase in the final design of the pneumatic test bed was the creation of a system schematic that encompasses all aspects of the system and describes the system variables concisely and precisely. The schematic is shown below in Figure 8 with all its components.

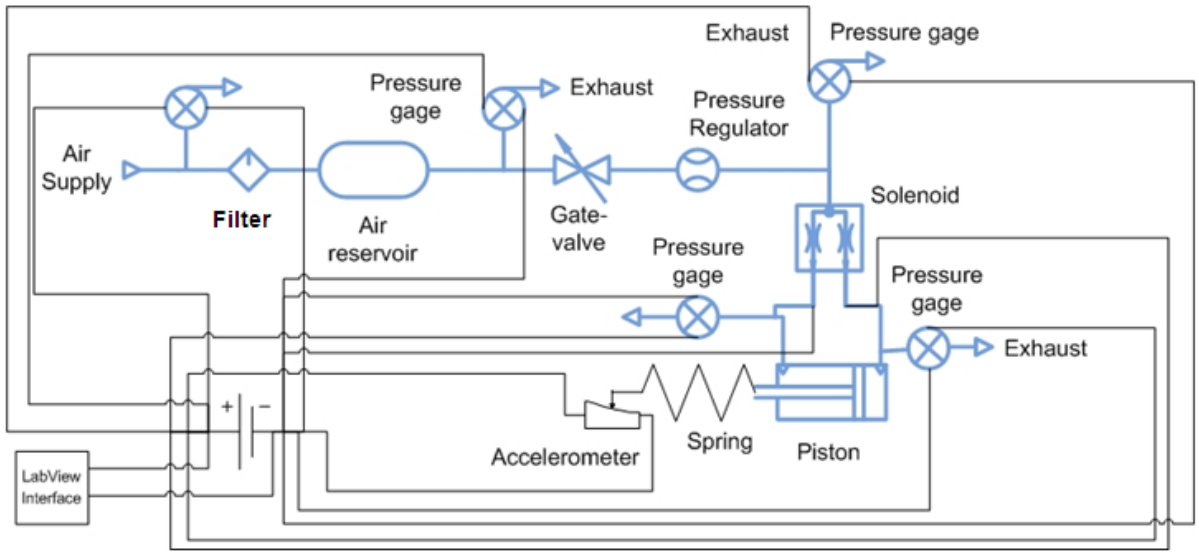

Figure 8 - System schematic of final design

This schematic is an integration of all the pneumatic, electrical, and mechanical components of the assembly. The pneumatic components depicted by the schematic include the piston assembly, solenoid, pressure regulator, on-off valve, and tubing for connections. The electrical components consist of pressure sensors, an accelerometer, and circuitry for sensor output to the LabVIEW interface. The

latter has not been shown in intrinsic detail, as its function is not critical for understanding the dynamics of the entire system.

The first phase of the schematic shows how the compressed shop air enters the system and is regulated before entry into the pneumatic connections. Ideally this air would also be dried, but the cost of a dryer was prohibitively expensive, and would not have significantly improved the quality of the air. Drying compressed air intended for pneumatic applications serves two primary purposes. From a mechanical standpoint dry air prevents rust from forming inside pneumatic components during extended usage. Dry air is also preferred from a scientific standpoint, since the validity of modeling air as an inviscid fluid is improved, resulting in experimental results closer to their theoretical values.

In the second phase of the schematic, the air is stored in a pressurized gas cylinder to be used when the on-off valve is opened. The pressure from the gas cylinder is also regulated for additional control of the dynamics of our experiment using a VEX regulator. The pressure at the inlet and after the regulator is monitored using pressure sensors.

The third phase of the schematic shows how the air output from the regulator is fed into a five-way solenoid valve. The solenoid valve is operated using a simple program loaded into the VEX controller that switches which output ports, A or B, is connected to the pressurized air, and which is vented to atmospheric pressure. The VEX controller is not included in the system schematic however.

The two output valves A and B are connected by way of pneumatic tubing to the two inlets of the piston assembly. The pressure in each of these connections is also monitored using the same pressure sensor used previously.

The final phase of the system schematic involves the conversion of potential energy in the piston to kinetic energy of the spring and moving mass, and vice versa. Several springs with varying spring constants were obtained for use with this system (for further detail, please refer to Section 6.2.4). The accelerometer is a common version available at WPI and was used for easy replacement and its availability.

Finally, a linear slider and guide rod were used to keep the dynamic assembly aligned and to prevent components from having forces in the perpendicular axes during operation. Both components have not been depicted in the system schematic; however the linear slider has been described in greater detail in Section 6.2.3.

6.2 Design compliance and accuracy

The primary goal for the final design of this system was to arrive at a solution that was compliant in all configurations during motion and reasonably accurate in the experimental results. The need to have a compliant design meant that the device should function as expected within its mechanical and pneumatic limits and show visual results that are repeatable during every operation of the system. This implied that no nuts or bolts should become undone as a result of extended operation of the device, and that no vertical motion of any of the moving components of the device with respect to ground occurred during operation.

Achieving a compliant design required the creation of detailed drawings that outlined the alignment and separation distance of each component with respect to the other. These efforts are further outlined in Appendix E. Obtaining reasonably accurate data from the experiment, on the other hand, required further development of the LabVIEW interface, and secure connections for the circuitry between the sensors and the DAQ interface. These improvements are described further in this section.

6.2.1 Tolerance Issues

Setting the right tolerances for each dimension for the final iteration was very important. This is because the entire final design was developed using calipers. Since CNC machining was not utilized for any part of the final design assembly, high tolerances on the initial design were not desired. Additionally, the tolerances needed to be less than 10% of the original dimension, without which the design would not function as intended. With dimensions as small as 1/32”, selecting the right tolerances became a challenge.

This problem was resolved by selecting tolerances that were 120% of the original dimension for all the critical dimensions, which were located on the aluminum base plate and required to align the piston, slider, and spring bracket. The tolerances were made greater than 10% to allow for precise alignment of the piston riser, linear slide, and bushing bracket.

6.2.2 Alignment of piston-spring assembly

The alignment of the piston assembly, linear slide, and bushing bracket in the same plane with respect to each other was very important for proper movement, and resulting accurate experimental results. The alignment was required in two planes: one parallel to the aluminum base plate, which ensured that all components were mounted at the same level; and the other axially through the

components, which ensured that all the force exerted by the piston was directed in the x-direction, and not in the y and z directions.

Whenever the device is assembled, alignment of the piston assembly, linear slider and busing bracket must be performed to ensure proper motion, a step by step tutorial on the recommended alignment procedures can be found in Appendix A.

6.2.3 Linear Slider

The linear slide assembly made by THK caused more than its fair share of problems throughout the life of the project. After receiving the linear slide assembly, it was discovered that it exhibited a large amount of friction. After contacting THK, it was discovered that the linear slide assembly did not ship lubricated, and that lubrication with Lithium Soap Based #2 grease was recommended. THK additionally stated that their recommended lubrication method was to use their MG70 grease gun to apply the grease through the nipple found on the linear slide block [15]. In addition, the bracket preventing the linear slide rail from coming off the linear slide block failed, resulting in the linear slide block falling off and dispersing its ball bearings across the floor. As a result the linear slide assembly operates with fewer ball bearings than it was designed for.

Based on the recommendations of THK and personal judgments, a set of possible options were created to deal with the lubrication issue. The first option involved not lubricating the linear slide assembly, which would have been free and simple, but was decided against since the plastic bearings in the linear slide block could eventually wear out, and lubrication would help with the resistance and non-linear movement exhibited by the linear slide block. Option two consisted of purchasing the recommended grease gun and lubrication through THK. This option totaled more than $150 and would have cost more than twice the price of the linear slide assembly, and was deemed too expensive and not necessary for the loads and usage expected [16]. Option three was similar but involved purchasing the THK grease gun through eBay for $20 and the grease through THK for another $20 [16, 17]. This option was thought to still be too expensive at that point in time, but reserved for use at a later point. Option four was to use a grease gun in Washburn Shops and purchase the correct type of lubricant for it. Although an ideal choice, Washburn Shops did not have any grease guns that fit the small nipple of linear slide block. Option five was to purchase a tube of Lithium Soap Based #2 grease for $5.00 and apply it manually to the linear slide rail. Although crude and not as effective as the other choices it was simple and inexpensive.

The final decision was to use option five and apply the lubricant manually since it was inexpensive and easy, and the requirements for the linear slide were not that high. After applying the lithium based soap grease, the resistance was not reduced as much as desired, so additional lubricant in the form of WD-40 was used and was found to have effective results.

6.2.4 Spring considerations

Several springs were considered for the final design of the pneumatic test bed. All the springs were purchased from MSC Direct and were made of stainless steel. Most had an uncompressed length of 3 inches since the distance between the edge of the sliding bracket and the bushing in the bushing bracket was this length. Compression springs were used for the final design as the mechanism of the device ensures that the spring is not subjected to tension during any phase of the piston assembly's motion.

Three inch springs with spring constants of 3.31, 5.27, and 15.59 lb/in were selected for the final design, and are referred to as green, yellow, and red springs respectfully. The short spring can also be used in the design to display the results of no resistance for part of the cycle, but due to its low spring rate of 3.14 lb/in its use causes destructive forces and can only be used at low pressures. The small diameter spring, or piston rod spring, was manually shorted to be mounted on the piston rod between the sliding bracket and the piston cylinder, to reduce the amount of slamming that occurs during the return stroke of the piston. An additional three inch long spring was also purchased to add an additional spring constant value between the red and yellow springs, but the inner diameter was later found to be too small and would have had to be forced around the guide rod, resulting in it being unfit for use with the device, but is mentioned here for completeness.

The product information for each spring purchased, including free length, spring constant, outer diameter, MSC Direct product number, price and quantity per package, is shown below in Table 2. The list of springs and other components used in the final design is also available in Appendix D

Table 2 - All springs purchased for use with device with pertinent information

Spring	Free Length	k (lb/in)	OD	Number in Pack	Price	MSC Direct Product Number
Red	3"	15.59	0.48"	5	15.06	2314441
Yellow	3"	5.27	0.48"	5	3.45	6812077
Green	3"	3.31	0.48"	5	3.45	6811996
Short	1.44"	3.14	0.61"	10	16.52	2312031
Piston Rod	2.5"	3.73	0.25"	12	7.91	2311611
Unused	3"	8.67	0.48"	5	3.57	6812150

6.3 Final assembly

The final design of our device utilized a modular construction, which enabled us to conduct the assembly of the device in different stages. Each of the stages required for assembling the device will be described here in greater detail.

The first stage of the assembly operation involved the aluminum base plate. For this stage the tolerances for all holes in the aluminum base plate were checked to ensure that they would cause no interference with the wooden base when attached to it. Next, the linear slide, bushing bracket, and piston assembly with piston riser were attached to the aluminum plate. At this step, it was essential to confirm that all three aforementioned components were aligned.

The aluminum plate was then attached to the wooden base with six countersunk bolts and nuts. It was deemed important at this stage to ensure that the aluminum plate remained parallel to the wooden base when mounted, as the device would then be perfectly horizontal and reduce vibrations during operation. Some interference was caused by the washers attached the piston-block to the base plate, but this issue was resolved by slightly widening the edges of the clearance holes on the wooden base. The first stage of the assembly operation was completed by mounting the sliding bracket containing the accelerometer to the linear slide, attaching a spring to the guide rod, and screwing the guide rod to the sliding bracket with a bolt.

The second stage of the assembly operation required mounting the electrical components of the device to the wooden base. These components consisted of the BNC bracket, the bread board consisting

of sensor circuitry, and holding stands for two 9V batteries. The BNC connectors were first attached to the BNC bracket, which was then screwed to the wooden base. Next, the breadboard was mounted to an aluminum plate, and then the plate was screwed to the wooden base. Finally, mounting stands for the batteries were attached to the wooden base with simple nails.

The final stage of the assembly operation involved cutting the pneumatic tubing to proper lengths and mounting all the tubes on to the wooden base. Since each tube had an associated pressure sensor, it was deemed appropriate to mount the pressure sensors with wood screws first. The pneumatic tubing was then routed to each sensor, the solenoid, regulator, and on-off valve, and placed appropriately between the connections such that they did not require additional support to staying fixed during operation. The last step required cutting the electrical wires to the pressure sensors to the right lengths for connection with the sensor circuitry, placing the VEX controller in an easily assessable location on the wooden base, and connecting the solenoid to the VEX controller using an extended jumper wire.

6.4 Circuitry for Sensor Output

The intent of the circuit board was to allow a compact and reliable means to both power and collect data from the four pressure sensors. In order to power the sensors, resistors were used to regulate the voltage from two 9V batteries, attached in parallel.

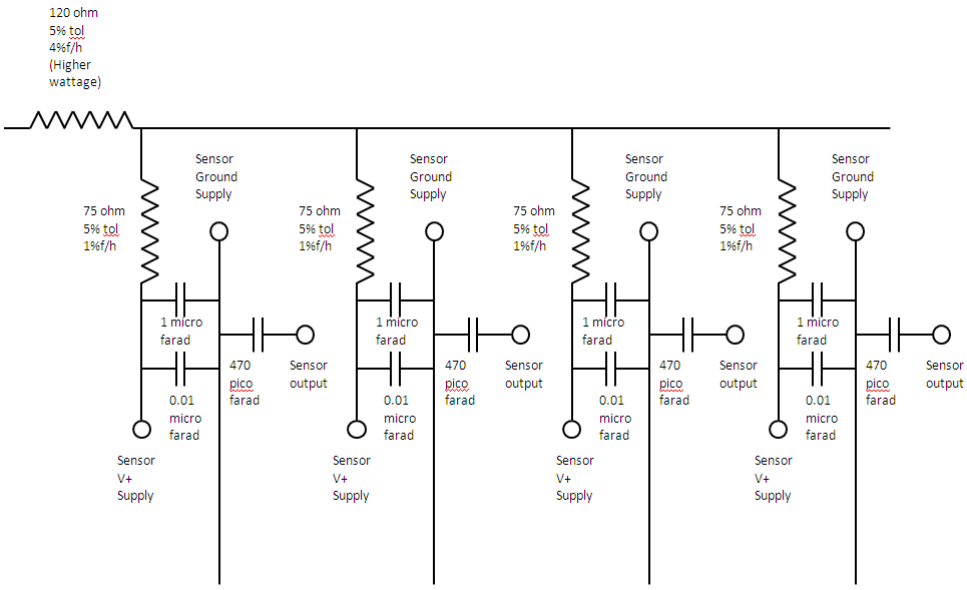

Figure 9- Circuit Diagram for the pneumatic test bed

The diagram above is that of the circuit as it currently stands in the MQP. The leads traveling to the bottom of the diagram connect to ground. Also connected to the ground are the appropriate leads from the BNC connections to the DAQ. Also connected to the sensor output junctions (though not shown above) are other leads from the BNC connections. These leads allow the DAQ to measure the voltages supplied by the output, thus allowing pressure measurement.

To ensure accurate readings, Sensor Decoupling Circuits (SDC) s were added to the circuit board. The SDC design was taken directly from the data sheet for the pressure sensor. The decoupling circuits, through the use of capacitors, reduce the power fluctuations experienced by the sensors, as well as noise in the sensor output. The power supply decoupling and output filtering diagram provided in the pressure sensor data sheet, is shown below in Figure 6.

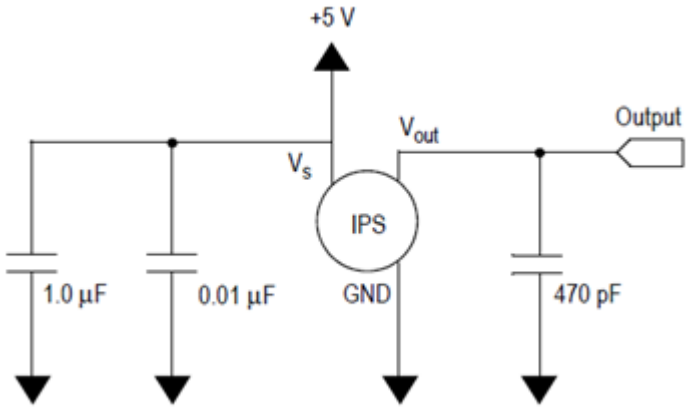

Figure 10 - Recommended power supply decoupling and output filtering for the pneumatic test bed

The individual circuit modules on the circuit board feature their own input voltage protection resistor. This resistor was selected to ensure that there would be more than enough protection for the individual sensor even if the batteries were to supply surplus power. This was accomplished by selecting a resistor that would offer acceptable current with the maximum rated voltage was applied to the sensor.

As seen in Figure 10, there is also a resistor in series with the positive power bus of the circuit. The reason for this resistor, and why each individual circuit had its own power protection circuit, was that a linear potentiometer was originally attached to the circuit board to measure the linear displacement of the piston rod. This potentiometer was later found to be defective, and was removed for the reasons discussed previously.

A resistor was added before all other elements in the circuit. This is because the potentiometer and sensors operated at different voltages and currents. The potentiometer was run at 5.25V (its maximum rated value) to ensure the largest possible voltage difference for LabVIEW to read. The LabVIEW program could have potentially picked up microscopic vibrations in the system and the potentiometer lead if the potentiometer functioned as intended.

During prototype development, a problem with the pressure sensor readings was discovered. The problem was that the voltage output of the pressure sensors would need repeated calibration. This is caused by the use of resistors to regulate a diminishing power supply, which results in a variable voltage supply to the pressure sensors, resulting in a varying pressure to voltage ratio. While this adversely affects sensor accuracy, the lack of sufficiently precise calibrated sensors to calibrate those on the MQP makes the addition of a voltage regulating IC almost irrelevant. If sufficiently precise sensors are found, however, then the circuit would optimally have a voltage regulator incorporated. Due to the design of the current system, however, the circuitry would require a redesign in its entirety.

6.5 Data Gathering

In order to collect, modify, and store the data generated by the pressure sensors and accelerometer, a computer program had to be created, and data acquisition hardware had to be used. National Instruments' LabVIEW software and corresponding DAQ devices were a clear choice due to their availability and common use within WPI.

6.5.1 DAQ Interface Design Decision

When considering the method for transferring the electronic connections from the device to the computer on the outside, numerous means were considered. In the end it was decided to mount BNC connectors to the device and have the end user utilize a NI USB-6259 BNC found in HL 031.

Throughout the prototyping stage, connections were made using alligator clips from the large DAQ board to the various wires connected to the device. Since this method was confusing even to the designers of the device, in addition to being messy and prone to faulty connections, a better method was desired for the final design.

An initial possible solution was to create a board that had a compact and labeled area for alligator clip connections. This idea was quickly discarded due to the fact that it improved but did not solve many of the problems.

Mounting a DAQ board to the device was also considered since only a USB connection would be required, but this idea was also quickly discarded. Two different DAQ boards were considered, the NI USB-6259 BNC and NI USB-6008, which cost $2,600 and $169 respectfully [18]. Neither were chosen for the final design since both were expensive, the resolution and sampling rate for the low-cost device was in question, and portability was not greatly reduced since the device still required multiple external connections.

The final chosen design utilizes BNC connectors mounted on the device, and requires six BNC cables to be connected from the device to a NI USB-6259 BNC device (or other comparable device). Some minor variations of this design considered include the use loose BNC cables and various different BNC connection types. The final mounting decision simplifies the electronic connections from twelve scattered, loose connections to six sturdy localized connections. Although this design forces the use of a BNC style DAQ board, this constraint was deemed negligible since the device will likely be used near the DAQ boards, and in a worst case scenario a DAQ board would have to be moved.

6.5.2 Programming Logic

The LabVIEW Virtual Instrument (VI), whose block diagram can be seen in Figure 11 and Figure 12, was required to first communicate with the DAQ, then perform calculations on the voltage data collected, display the calculated data, and finally write the data to a spreadsheet. Portions of the VI are based on a highly modified version of the “Cell Phone VI” constructed by Professor Sullivan for his ME3901 class.

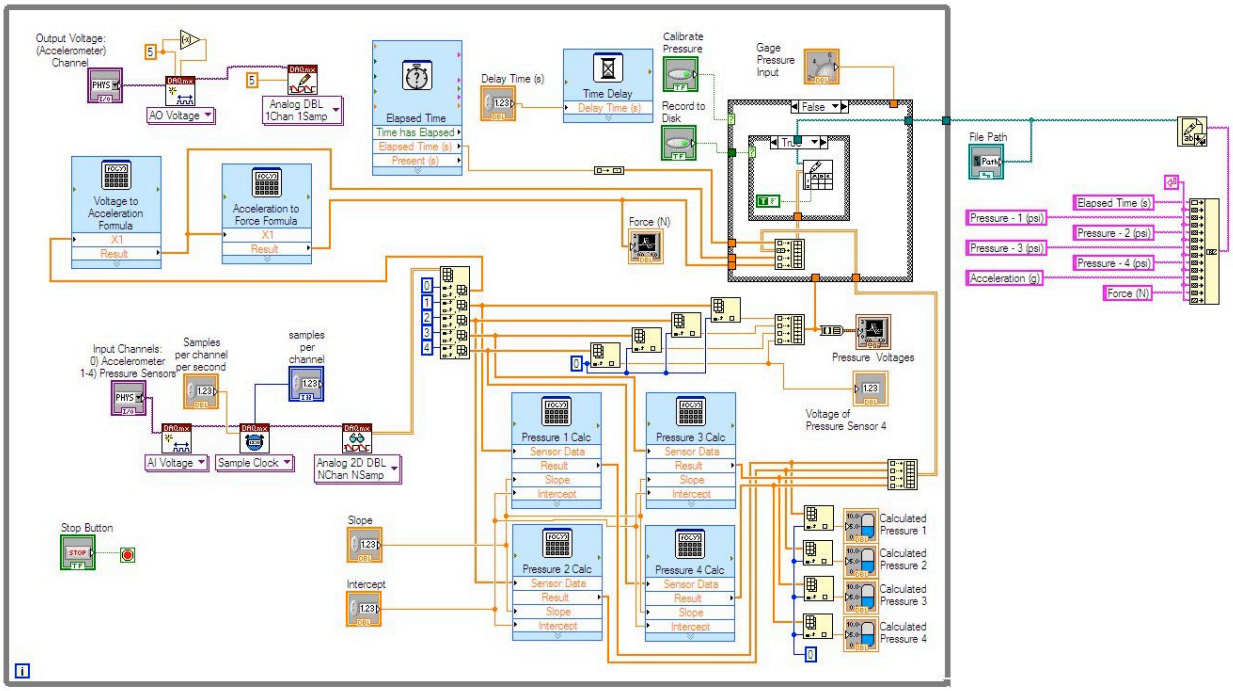

Figure 11 - Programming logic of the VI's block diagram for the pneumatic test bed

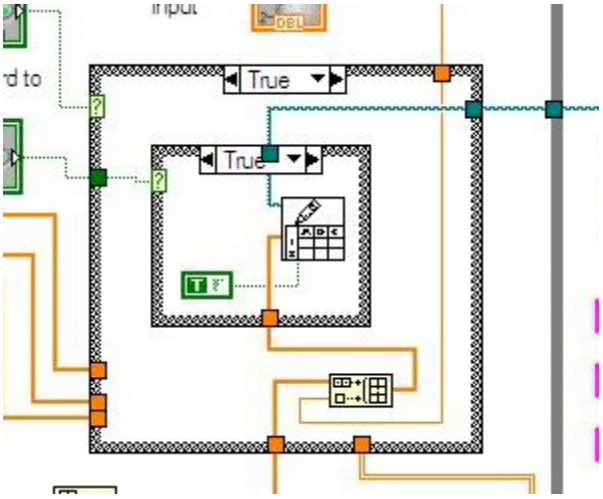

Figure 12 - Alternate view of True/False loop for the pneumatic test bed

Communication with the DAQ includes both sending a constant voltage of 5 volts to the accelerometer, and reading the voltage difference of the four pressure sensors and accelerometer. The resulting data array is then divided so that the accelerometer data (set 0) can be converted from voltage to acceleration, as described in the section below, and then converted to force by multiplying the acceleration by the moving mass and converting to Newtons, this data is then graphed and written to

file. The pressure data (sets 1-4) are also stripped from the array and then multiplied by the slope and added to the intercept to convert the data to pressure that is displayed and written to file.

The VI also contains a true/false loop for calibrating the pressure sensors that records the voltage difference of each pressure sensor along with a user entered pressure value. This calibration mode can be enabled in the diagnostic section of the VI, which also displays the voltage of the first sensor in real time, and includes input areas for gage pressure, slope and intercept values. This allows the user to calculate the slope and intercept of the pressure sensor, as described in Appendix C.

The VI writes all of the recorded data to an Excel spreadsheet so that the data generated can be studied and analyzed later. For a complete explanation of the Excel spreadsheet output, reference Appendix B.

6.5.3 Accelerometer calculations

In order to convert the electrical signal from the accelerometer into a mechanical measurement, a conversion has to be made. Analog Devices provides the conversion equation as shown in Equation 1, as well as the constants for the ADXL276 (AD22237) model as shown in Equation 2.

Equation 1 - Conversion equation from Analog Devices

$$V_{out}(accel, V_s) = \frac{V_s}{2} - \left[(accel)\cdot\left(b\cdot V_s + c\cdot V_s^{\,2}\right)\right]$$

Equation 2 - Constant for ADXL276 (AD22237) model

$$b = 8.284\cdot 10^{-3}\,\frac{1}{g} \qquad c = 0.542\cdot 10^{-3}\,\frac{1}{g\cdot V}$$

After simplifying, the equation that describes the acceleration in terms of output voltage is displayed below in Equation 3.

Equation 3 - Acceleration in terms of both variables and calculated values

$$accel = \frac{\frac{V_s}{2} - V_{out}}{b\cdot V_s + c\cdot V_s^{\,2}}$$

Analog Devices recommends a supply voltage of 5V, which is supplied by the DAQ at a slightly lower 4.97V, which is taken into account in the equation used.

Due to the fact that the accelerometer was accidently mounted to the sliding bracket with the positive axis pointing into the device, the acceleration calculation corrects for this by computing a negative acceleration.

To calibrate the sensor further, an offset was calculated by measuring the steady state acceleration at two known points, namely zero when the axis of the accelerometer was parallel to the ground, and 1g ($9.81 m/s^2$) when the axis was perpendicular to the ground. The final equation used to calculate the acceleration is shown below in Equation 4.

Equation 4 - Final acceleration equation taking into account supply voltage, constants, reversed accelerometer, and calibration offset

$$accel = \frac{V_{out} - 2.485}{.054559} - 0.075$$

6.5.4 Front Panel

The VI's front panel, as shown in Figure 13, includes the main section, and a lower hidden diagnostic section. The main section includes a graph of the acceleration data and the pressure readings from all four pressure sensors. In addition, there are sections that ask for the input and output channels along with the file path for the Excel spreadsheet. The diagnostic section located below the main section includes voltage plots of the sensors, along with a place to input the gage pressure, along with input boxes for the corresponding slope and intercept. Also available for optional modification are the sampling rates and delay time of the VI.

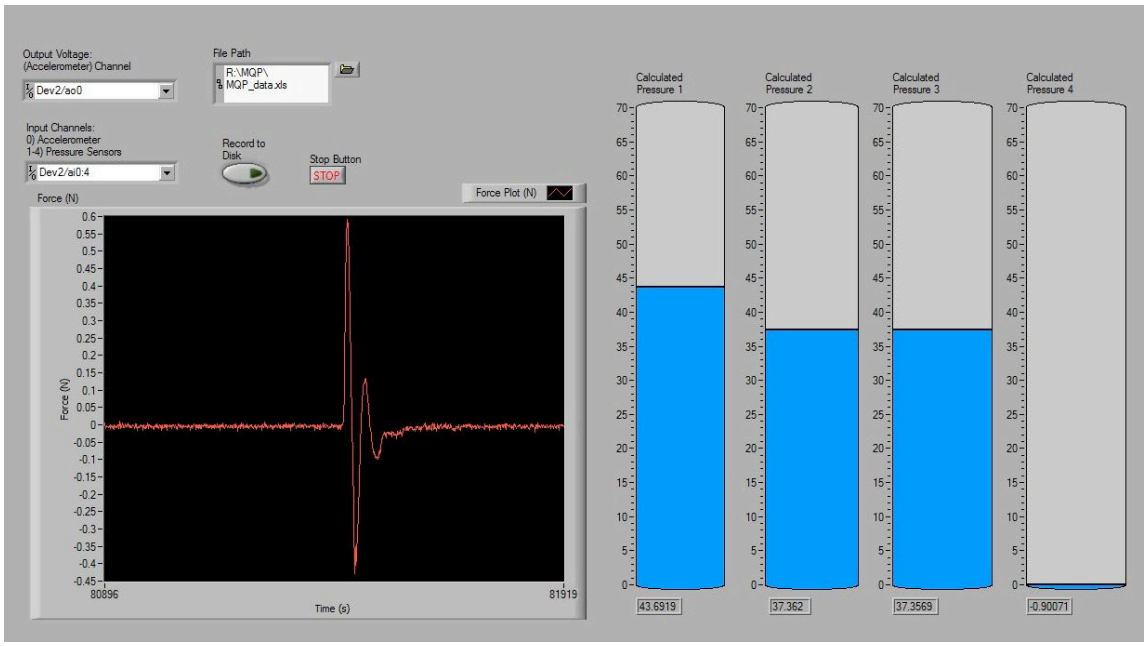

Figure 13 - Front panel of the VI, showing acceleration plot and pressure sensors

6.6 The Final Product

After multiple iterations the final dynamic design is shown below in Figure 14. This device is made up of many purchased and made parts, the purchased parts are detailed in Appendix D, and the engineering drawings for the machined components can be found in Appendix E. The assembly instructions for putting the device together can be found in Appendix A.

Since the design requirements specified a desktop device which was portable, the entire dynamic assembly was mounted on a wooden base along with the components that are required for its operation. As seen in Figure 15, the final design is self contained, except for the input of compressed air, and six BNC cables required to monitor the sensors on the device.

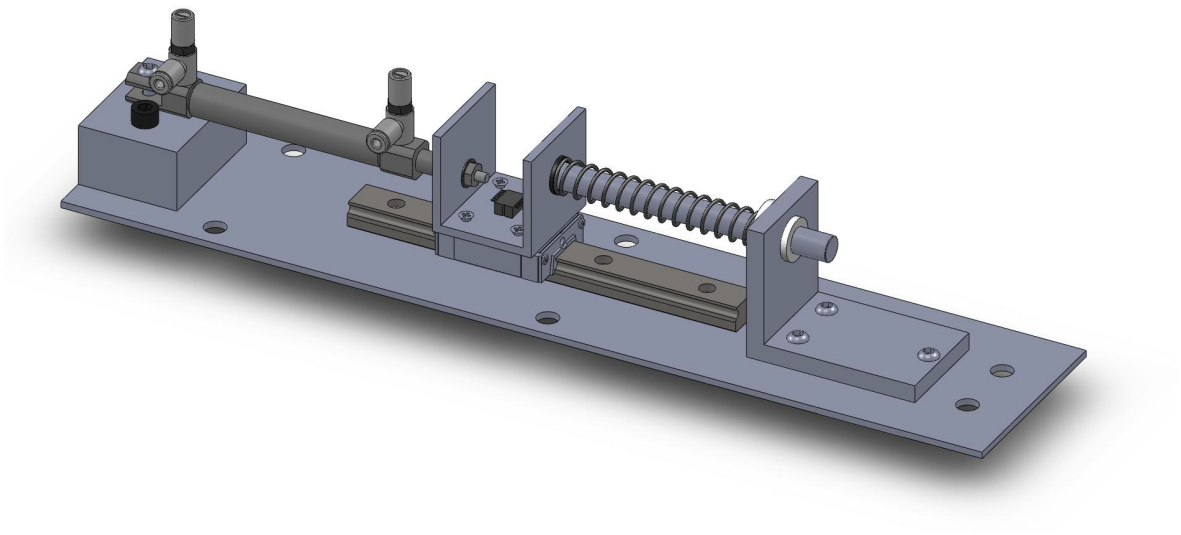

Figure 14 - CAD image of final design of dynamic assembly

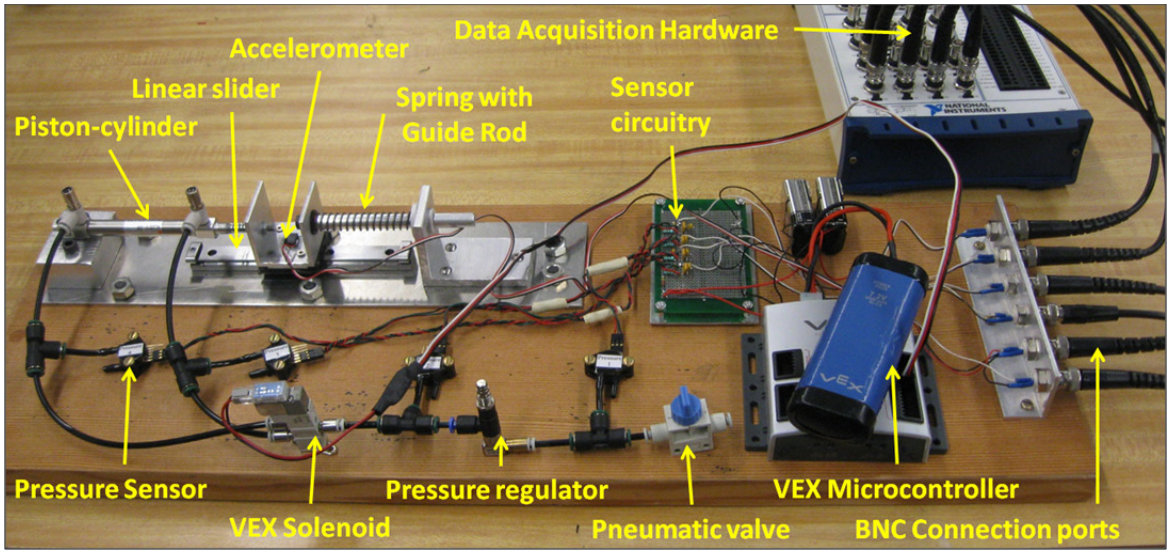

Figure 15 - Annotated picture of the entire device

7 Results and Analysis

The results and analysis will show the relationship between the theory associated with this device, namely the mathematical system of equations and the bond graph approach, and the experimental results gathered through sensor data recorded during actual operation.

7.1 Mathematical system of equations

A system of equations was developed to understand the dynamics of motion for the piston-spring assembly. Initial calculations include several simplifying assumptions, such as the negligence of damping and impact force. These are factored into our calculations at later stages once the fundamental behavior of the system as depicted by equations has been fully developed and understood. The changes in behavior of the piston-spring assembly are assessed at each stage of refinement of the system of equations modeling its behavior. The final set of calculations is presented in this section.

7.1.1 Initial known parameters

This section outlines the initial known parameters for the piston-spring assembly system. These parameters are static and form a part of the design of the entire system. They will not be changed in any of the iterations for our calculations. Since our final model is required to fit on a desk, considerably small values for the model's piston and shaft are being considered. The system starts at rest, and all equations of motion consequently assume zero displacement and velocity as the boundary conditions.

The diameter of the shaft and piston have been obtained directly from the manufacturer

Diameter of piston $d_{piston} := .01 \quad m$

Contact area of piston $A_{piston} := \pi \cdot \frac{d_{piston}^2}{4}$

$A_{piston} = 7.854 \times 10^{-5} \ m^2$

Diameter of shaft $d_{shaft} := .004 \quad m$

Contact area of shaft $A_{shaft} := \pi \cdot \frac{d_{shaft}^2}{4}$

$A_{shaft} = 1.257 \times 10^{-5} \ m^2$

The mass of all components of our system that are in motion has been considered to achieve accurate results for the time shapes of displacement, velocity, and acceleration. The acceleration due to gravity on earth is an important constant in any discussion of kinematics, and hence it has been spelled out in this section as well.

As the boundary condition, the initial displacement and velocity of the piston-spring assembly is taken as zero

Initial velocity of mechanical model	$v_i := 0 \frac{m}{s}$
Displacement offset of spring	$x_i := 0 \ m$

The following masses have been calculated by assuming Aluminum alloy 2080 and calculated mass properties from the CAD model in Solidworks

Mass of block	$m_{slider} := .01134 \ kg$
Mass of spring	$m_{spring} := .0136 \ kg$
Mass of piston	$m_{piston} := 0.00241 \ kg$
Total mass in motion	$m_{total} := m_{slider} \cdots = 0. \ kg$ $+ m_{spring} \cdots$ $+ m_{piston}$
Acceleration due to gravity	$A_{grav} := 9.8 \frac{m}{s^2}$

7.1.2 Initial test parameters

This section outlines the initial test parameters for the piston-spring assembly. These parameters are dynamic and form a part of the analysis of the entire system. They will be changed in several of the iterations for our calculations, until the best (most feasible) value is achieved.

The forcing frequency of the mechanical model is a parameter that can be switched on or off. This parameter affects the initial vibrations experienced by the piston-spring assembly and factor the undesirable 'chattering' effect into the oscillations of the piston and spring.

The spring damping ratio is an experimental parameter that directly affects the oscillatory behavior of the piston-spring assembly. It can be used to control the damping of the system, which can be under damped, critically damped, and over damped. Currently we desire a continued oscillation for our system, due to which the spring damping ratio chosen has a value such that the system is under damped.

Forcing frequency of mechanical model	$\omega_f := 10 \ \frac{rad}{s}$
Spring damping ratio	$\zeta := .01 \ dmnl$
Inlet pressure	$P_{in} := 150 \cdot 10^3 \ Pa$
Spring constant	$k_{spring} := 100 \ \frac{N}{m}$
Coeffecient of friction (for slider)	$\mu_{slider} := .9 \ dmnl$
Time constant for pressure variation	$\tau := 1 \ s$

The inlet pressure is initially set at low values, but will be increased incrementally during our experiments to conduct an analysis of the behavior of our system at all ranges of pressure. It is understood that for simplification, the piston-spring assembly has been considered an adiabatic system, which implies that pressure is a static parameter. For most practical applications, this is a valid

assumption, but it increases the discrepancy between experimental and theoretical calculations of parameters within our system.

The spring constant is a value obtained from the data sheet and properties associated with each spring used in our iterations. A set of springs will be used in this experiment, with progressively higher spring constants, starting with a value that is closest to the ratio of the maximum force exerted by the piston to the maximum displacement of the spring allowed by our assembly.

The coefficient of friction for the linear slider is an important parameter that will affect the dynamics of motion in the piston-spring assembly. This coefficient varies between 0 and 1, and a lowest possible value is desired, since this implies smooth motion of the piston, spring, and slider, which translates into a more accurate reading of the displacement and consequent resultant force of the assembly.

The time constant for pressure variation is effectively the period of oscillation of the impact force caused by the exertion of pressure into the piston. This parameter changes the response of the piston-spring assembly to the impact force.

7.1.3 Calculated parameters of model

The following parameters of our model are important quantities that will change the behavior of our system. They have been calculated from the known and test parameters previously outlined.

Effective fluid contact area	$A_{ef} := A_{piston} - A_{shaft}$ $A_{ef} = 6.597 \times 10^{-5}\ m^2$
Natural Frequency of spring	$\omega_n := \sqrt{\frac{k_{spring}}{m_{total}}} = 60.467\ \frac{rad}{s}$
Damping coefficient (spring)	$c_{spring} := 2 \cdot \zeta \cdot m_{spring} \cdot \omega_n = 0.016$
Damped Frequency of spring	$\omega_d := \omega_n \cdot \sqrt{1 - \zeta^2} = 60.464\ \frac{rad}{s}$
Switch for sinusoidal pressure input	$sw_1 := 1$

It can be observed that the natural and damped frequency of the spring are very similar, which implies that the system may undergo resonant motion. Since the damping coefficient directly effects the damped frequency of the spring, the former will be adjusted in successive iterations to increase the difference between the damped and natural frequency of the spring and hence avoid resonance from occuring in the system. To observe the response of our piston-spring assembly to sinusoidal motion, an oscillatory function has been included in the pressure input with a switch, which allows a comparative study of the behavior of our system in the presence and absence of sinusoidal pressure input. Finally, it can also be noted that the effective fluid contact area is quite small, so that a very large force is produced for an average pressure input.

Effective fluid pressure	$P_{ef}(t) := P_{in}\cdot\left(1 - e^{\frac{-t}{\tau}}\right)\cdot\left(\sin\left(\omega_f\cdot t\right)\right)^{sw_1}$
Periodic fluid force	$F_p(t) := P_{ef}(t)\cdot A_{ef}$
Differential equation of motion	$m_{total}\cdot x''(t) + k_{spring}\cdot x(t) + c_{spring}\cdot x'(t) = F_p(t)$

7.1.4 Equations of motion for model

This section presents the resultant equations of motion for our piston-spring assembly. The effective fluid pressure is a combination of an exponential function that stabilizes after becoming equal to the inlet pressure, and a sinusoidal function that introduces oscillations into the effective fluid pressure with controllable amplitude. The fluid force is simply the product of the effective fluid contact area and the effective fluid pressure. Finally, the differential equation of motion is obtained by considering the sum of forces in the horizontal (x) direction. This shows that the impact force due to pressure input to the piston is equivalent to the sum of the motion of the piston, spring, and block, the force caused by the extension of the spring, and the resistive feedback force due to the damping of the spring.

The fundamental differential equation for our piston-spring assembly has a known solution for displacement, which has been studied extensively in texts on dynamic vibration analysis. The following solution has been obtained from Tongue [19].

General solution of differential equation

$$x(t) := \frac{F_p(t)}{k_{spring}}\left(1 - e^{-\zeta\cdot\omega_n\cdot t}\cdot\cos\left(\omega_d\cdot t\right)\right) \ldots + \frac{-\zeta\cdot F_p(t)}{k_{spring}\cdot\sqrt{\left(1-\zeta^2\right)^3}}\cdot e^{-\zeta\cdot\omega_n\cdot t}\cdot\sin\left(\omega_d\cdot t\right)$$

The general solution of the differential equation shows a variation in displacement with respect to time of the piston-spring assembly. It takes into account the damping force of the spring and the frictional force resisting motion. Since both the damping force and friction changes direction and magnitude at the forward and reverse stroke of the piston, this general solution contains exponential and sinusoidal functions. These functions accurately account for the rapidly changing net force on the system at each interval in time.

This solution was differentiated using symbolic calculus in MathCAD to obtain the variation in velocity along the x-axis for the piston-spring assembly. Since several exponential and sinusoidal functions that account for the damping force of the spring and the friction in the slider are present as multiples in the general solution, it can be seen that the velocity versus time equation becomes more complex than the general solution that describes displacement.

Velocity for piston-spring assembly

$$v(t) := \frac{F_p(t)}{k_{spring}}\left(1 + \zeta\cdot\omega_n\cdot\cos\left(\omega_d\cdot t\right)\cdot e^{-\zeta\cdot\omega_n\cdot t} + \omega_d\cdot\sin\left(\omega_d\cdot t\right)\cdot e^{-\zeta\cdot\omega_n\cdot t}\right) \ldots + \frac{\zeta\cdot F_p(t)}{k_{spring}\cdot\sqrt{1-\zeta^2}}\cdot\left(\zeta\cdot\omega_n\cdot e^{-\zeta\cdot\omega_n\cdot t}\cdot\sin\left(\omega_d\cdot t\right) - \omega_d\cdot\cos\left(\omega_d\cdot t\right)\cdot e^{-\zeta\cdot\omega_n\cdot t}\right)$$

Finally, the variation in acceleration for the piston-spring assembly was computed via symbolic differentiation in MathCAD. This equation is directly proportional to the resultant force in the system at any given point in time, and hence is important as a function that describes the overall dynamics of our system. The equation for acceleration contains the spring damping ratio in both first and second orders multiples. This implies that, in contrast with displacement, the spring damping ratio has a considerable impact on the resultant force in the piston-spring assembly.

Acceleration for piston-spring assembly.

$$\alpha(t) := \frac{F_p(t)}{k_{spring}} \cdot \left(\begin{array}{l} 1 - \zeta \cdot \omega_n \cdot \omega_d \cdot \sin\left(\omega_d \cdot t\right) \cdot e^{-\zeta \cdot \omega_n \cdot t} - \zeta^2 \cdot \omega_n{}^2 \cdot \cos\left(\omega_d \cdot t\right) \ldots \\ + \omega_d{}^2 \cdot \cos\left(\omega_d \cdot t\right) \cdot e^{-\zeta \cdot \omega_n \cdot t} - \zeta \cdot \omega_n \cdot \omega_d \cdot \sin\left(\omega_d \cdot t\right) \cdot e^{-\zeta \cdot \omega_n \cdot t} \end{array} \right) \ldots$$
$$+ \left(\frac{\zeta \cdot F_p(t) \cdot e^{-\zeta \cdot \omega_n \cdot t}}{k_{spring} \cdot \sqrt{1 - \zeta^2}} \right) \left[\begin{array}{l} \zeta \cdot \omega_n \cdot \omega_d \cdot \cos\left(\omega_d \cdot t\right) + \omega_d{}^2 \cdot \sin\left(\omega_d \cdot t\right) \ldots \\ + \zeta \cdot \omega_n \cdot \left(\omega_d \cdot \cos\left(\omega_d \cdot t\right) - \zeta \cdot \omega_n \cdot \sin\left(\omega_d \cdot t\right)\right) \end{array} \right]$$

7.1.5 Graphical representation of model dynamics

This section will discuss the time variation of the various parameters of model dynamics. It will provide a better understanding of the theory of motion in the piston-spring assembly and the expectations from the final model.

The first time-variation under consideration is that of displacement. The overall graph is presented below and demonstrates behavior that is generally expected from a standard spring oscillatory system. The spring starts up with jerky motions that are indicated by the jagged lines during the first 2-3 seconds of motion. This is due to the forces impacted on the spring by the piston as well as the resultant force impacted by the spring on the system. Both components require a small time interval to adjust to the resultant force in the system.

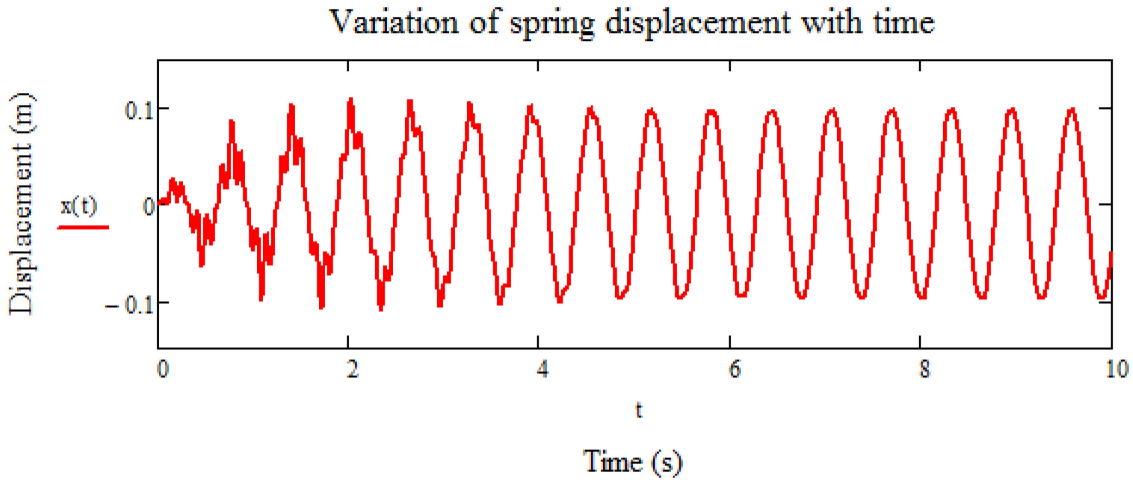

Moreover, the oscillations begin with small amplitude which gradually increases to a constant value. This accounts for the frictional forces in the slider and other moving components in the system that are eventually overcome. Finally, the piston-spring assembly continues to oscillate in a steady, rhythmic fashion. The second time variation is that of velocity shown below over the same interval as displacement of 10 seconds.

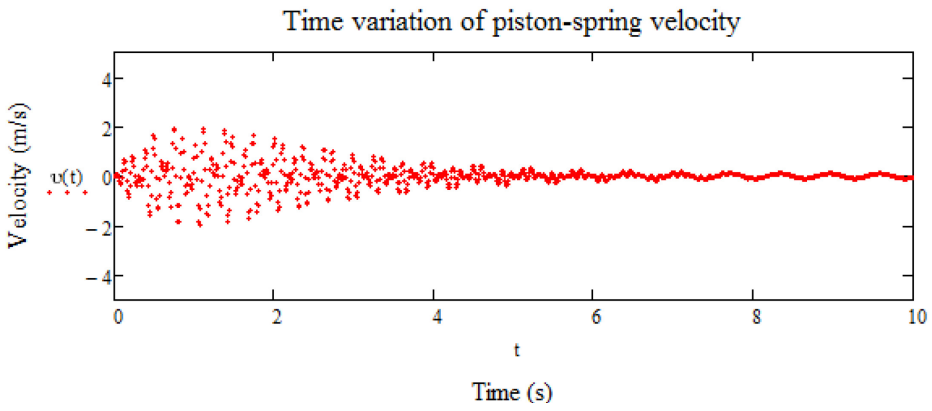

Since the velocity of the piston-spring assembly is the differential of its displacement, the initial agitation seen in the velocity variation in the first 2-3 seconds accounts for the initial irregularities in the time variation of displacement shown previously. The magnitude of the initial velocity is also much higher, as the system 'jolts' into motion, but ebbs down to a nominal value of 0.1 m/s. This is an acceptable value since the system under consideration has a travel distance of merely .08m (3").

Another time variation that must be considered is acceleration of the piston-spring assembly. Immediately after the piston-spring assembly is set in motion, resistive forces such as friction and the spring compression start acting to lower the resultant force.

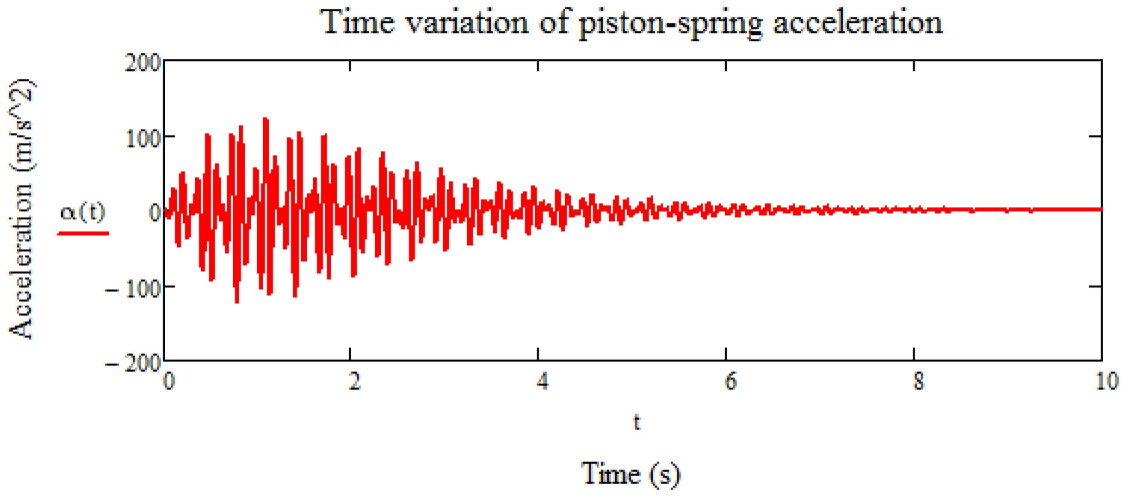

These forces reach a maximum at t=1 s, and then are gradually cancelled out by the force of the piston. As desired for any system in motion, the resultant acceleration (and consequently force) on the piston-spring assembly becomes negligible after t=7 s. Dynamic equilibrium of the system is achieved at this point, and the sum of forces of the piston, spring, and friction equal zero.

The fourth parameter of the dynamics of motion for the piston-spring assembly is the force impacted by the piston. This is inevitably different from the resultant force on the system, and is the result of a cyclic opening and closing of valves in a solenoid activated by a VEX controller.

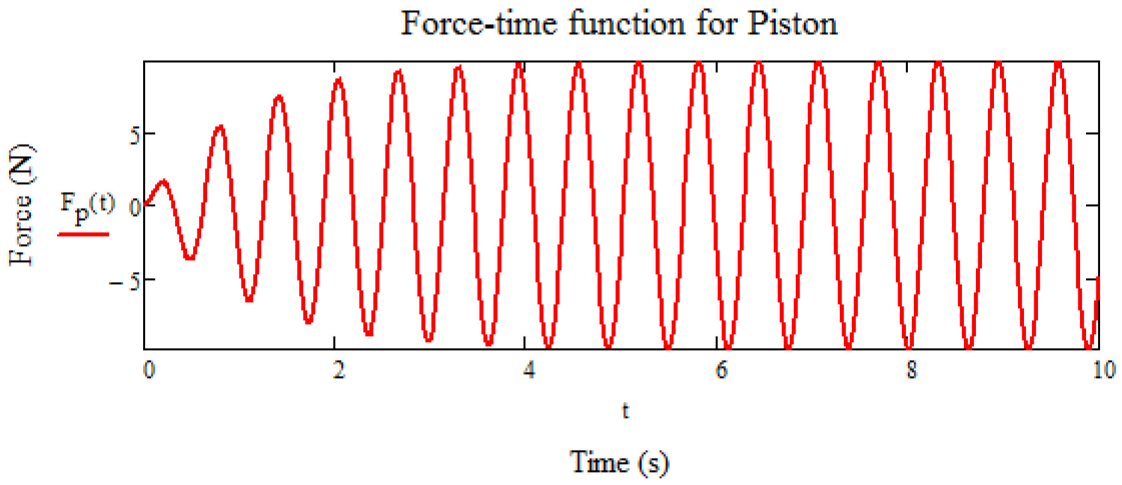

Finally, the time variation of the pressure in the piston will be considered. As the area of the piston rod inside the piston cylinder is constant, this function is directly proportional to the resultant force inside the piston, and consequently has the same graphical shape.

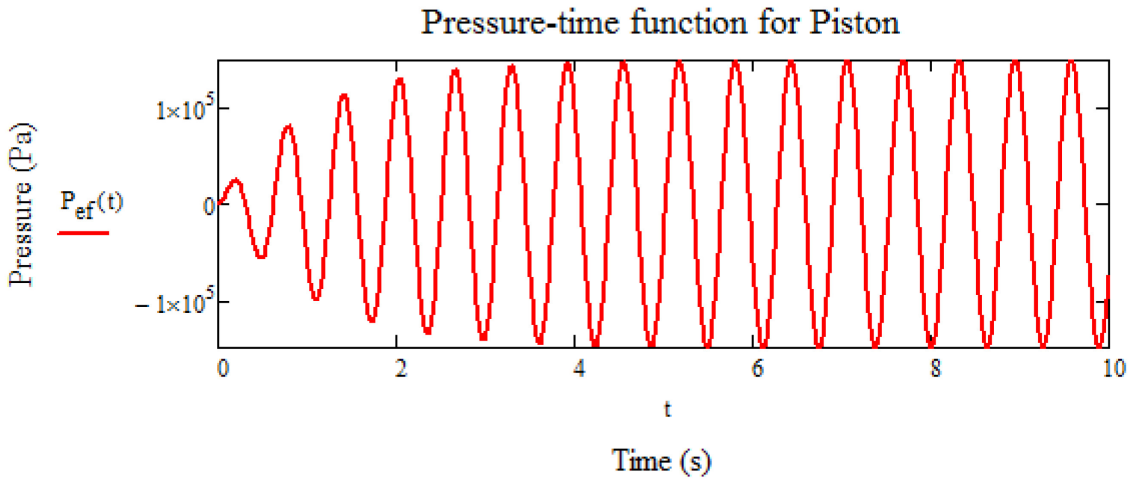

7.2 Bond Graph Approach

In order to best meet the teaching aid requirement of the project, a bond graph based model of the system had to be derived. This is due to the fact that the bond graph approach to analyzing systems is a cornerstone to the mechatronics course curriculum. The following section discusses the creation and use of the bond graphs for this project.

In order to accurately model a system, each aspect of the system must be well known. To fully understand the system, an initial bond graph, shown below in Figure 16, was constructed to account for as many elements as possible.

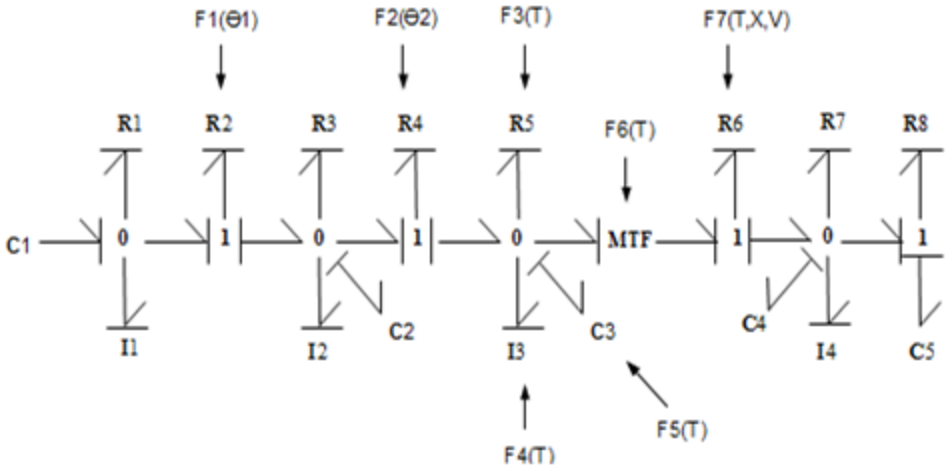

Figure 16 - Initial bond graph for the pneumatic test bed

This initial graph was later proven to be incorrect in some of its assumptions, as was a simplified three capacitance and three inertance variant. The model that was eventually used modeled the entire fluid system before and including the regulator as a constant source of pressure. As a regulator is designed to maintain a pressure output, this was believed a viable assumption. The assumptions that eventually invalidated the first iterations were those that pertained to the fluid regulator and the fluid system in general.

The incorrect assumption was that the pressure in the pipe could be accurately modeled by assuming that the pressure only dropped across resistances, where the flow of the fluid varied. This was later proven wrong by an inability to generate mathematical equations for modeling that were remotely accurate, and by considering that the flow of air would less likely be affected than the pressure of the air during its travel through a pipe. To demonstrate the change that this alteration of assumptions made,

the three capacitance three inertance bond graph, along with the final two-inertance, two-capacitance model, are shown below in figure 13.

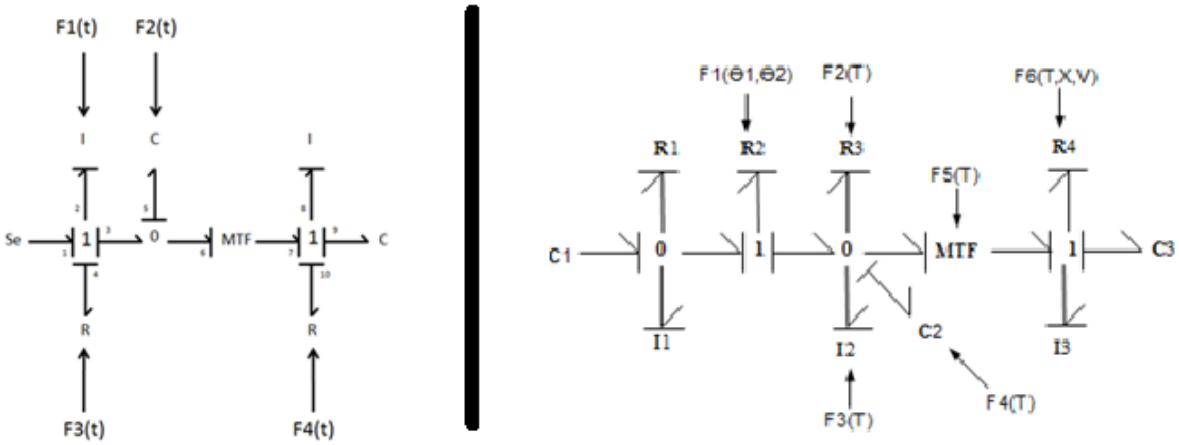

Figure 17 - Final two inertance two capacitance model (left) and three capacitance three inertance bond graph (right) for the pneumatic test bed

The difference in the bond graphs in Figure 17 above, besides the labeling and line thickness, is the simplicity. By simplifying the system, mathematical modeling became more feasible. It was also assumed that pressure would drop moving through a tube, but fluid capacitance would eventually reach an equilibrium charge, thus allowing the capacitance to be placed on a zero junction. The inertance and resistance of the fluid system were placed on the one junction, along with the source of effort that modeled the regulator.

The construction of the final bond graph was an iterative process. The lessons learned from the previous bond graphs carried through each stage of design. An examination of the 3-capacitance, 3-inertance (3C3I) model resulted in its revision, in which the final junction for the mechanical system was changed from a zero junction to a zero and a one junction.

The following list defines what aspect of the system is represented by each portion of the graph.

Se - Source of effort modeling the air tank and the regulator.

I_2 - The fluid inertia of the system after the regulator leading to the piston. This is signal controlled because the solenoid in the system forces the air to take different paths at different times.

R_4 - The fluid resistance of the system after the regulator leading to the piston. This is signal controlled because the solenoid in the system forces the air to take different paths at different times.

C_5 - The fluid capacitance of the system after the regulator leading to the piston. This is signal controlled as the solenoid forces the air to take a different path depending on the time.

MTF_{67} - This is the piston itself. As the air enters different chambers of the piston at different times (thanks to the solenoid) the piston is signal controlled

I_8 - This is the inertia of the moving mass of the system.

C_9 - This is the resistance spring of the system

R_{10} - This is the limped frictional and piston damper resistance in the mechanical system. It is signal controlled due to the different dampening settings of the piston release valves. This quantity was determined experimentally.

Table 3 below displays the mathematical relationships of all the elements. The P' or Q' variables are the momentum or charge derivatives. These measure system properties later on, and are compared to the MathCAD model and system observations to examine the utility of the bond graph method.

Table 3 - Mathematical relationships of all the elements used in the pneumatic test bed

Element	IN	OUT	Equations	
Se_1	f_1	e_1	$e_1=P_{sp}$	
I_2	e_2	f_2	$P'_2=e_2$	$f_2=P_2/m_2$
R_4	f_4	e_4	$e4=R_4f_4$	
1_{1234}	e_1	f_1	$f_1=f_2$	
	f_2	e_2	$e_2=e_1-e_4-e_3$	
	e_3	f_3	$f_3=f_2$	
	e_4	f_4	$f_4=f_2$	
C_5	f_5	e_5	$Q'_5=f_5$	$e_5=k_5Q_5$
0_{356}	f_3	e_3	$e_3=e_5$	
	e_5	f_5	$f_5=f_3-f_6$	
	f_6	e_6	$e_6=e_5$	
MTF_{67}	e_6	f_6	$e_7=e_6/G$	
	f_7	e_7	$f_6=f_7/G$	
I_8	e_8	f_8	$P'_8=e_8$	$f8=P_8/m_8$
C_9	f_9	e_9	$Q'_9=f_9$	$e_9=k_9Q_9$
R_{10}	f_{10}	e_{10}	$e_{10}=R_{10}f_{10}$	
1_{78910}	e_7	f_7	$f_7=f_8$	
	f_8	e_8	$e_8=e_7-e_9-e_{10}$	
	e_9	f_9	$f_9=f_8$	
	e_{10}	f_{10}	$f_{10}=f_8$	

The mathematical formulas in Table 3 were the basis of the creation of a MATLAB script to create and analyze a matrix, the standard form of equations in the bond graph method. The MATLAB script would have a set of values calculated by a separate MathCAD file input as system parameters. These system parameters would be used to create a matrix based on a hand derived matrix. This numerical matrix was then used to extract a characteristic equation and polynomial. These features serve more as diagnostic tools to determine whether or not the results are worth investigating with the MathCAD program. Similar features in similar previous scripts indicated that there was a problem with the 3C3I model.

The MathCAD program was used derive the system properties for the MATLAB script based on Karnopp's [20] equations for fluid system elements. Laminar air flow was assumed in order to use the resistance formula, while air compressibility and tube elasticity were accounted for in tube capacitance. The effects of junctions on the system were neglected in the equations, and the effects of the tubes that connected tee-fittings to sensors, rather than down the system, were only accounted for in their resistance and capacitance, and were considered a single section of pipe.

One of the variables entered in the MathCAD program was the mechanical resistance. This data was taken from sensor data for acceleration from 0. The bond graph approach was used to create an equation that could translate acceleration data into resistance data. The resulting equation transformed velocity, which was integrated from acceleration, into resistance values. The equation used was as follows.

$$R2 = -\frac{m}{t}\ln\left(\frac{m}{Fa} * \int A(t)dt\right)$$

In this equation, R2 is the mechanical resistance, m is the sliding mass, 'Fa' is the force applied by the piston (assumed constant) and A (t) is the accelerometer data. The integration was taken from a sixth degree polynomial trend line (in Excel). The R2 values used in the bond graph utilized the average value of the values that Excel returned using the above equation. Shown in 0 are Excel plots for the acceleration data, with the trend lines integrated for velocity data. These plots came from data that was trimmed to ensure that only the motion of the device, and not the noise of the accelerometer, was used. The acceleration is positive in the direction of intended piston motion (positive axis in the direction of the outward stroke). The bond graph element values calculated in MathCAD, after entry into MATLAB, were used to create a vector of Laplace Domain equations for the state equations for the

system. These were entered into MathCAD, which produced functions that were graphed, and then compared to the MathCAD models for the standard system of equations.

7.3 Experimental Results

Testing was conducted on four types of springs that had varying spring constants, and one had varying geometry. Three of the springs had a constant free length of three inches and a constant outside diameter of 0.48 inches (inside diameter varied slightly due to wire diameter). These springs were marked with color to denote spring rates, and will be reference by respective color henceforth. The "red" spring denotes a spring rate of 15.59 lb/in, the "yellow" spring denotes a spring rate of 5.27 lb/in, and the "green" spring denotes a spring rate of 3.31 lb/in. Additionally, a short spring was used that had a free length of 1.44 inches, an outside diameter of 0.61 inches, and a spring rate of 3.14 lb/in. All of the data is available in the Excel spreadsheets provided with this report. In addition, the orientation of the accelerometer results in values that are positive in the direction of the piston being pushed out (outward stroke), and negative when pulled in (return stroke).

When calculating the forces in the system based on the acceleration, the moving mass of the system was required. This mass was determined to be 122.84 grams through the combination of three values as shown in Table 4. The mass of the moving components and the linear slide rail were weighed as one unit since the linear slide rail and block could not be separated. The mass of the rail was then calculated in SolidWorks using the model provided by THK, and assuming the density of stainless steel. The measured mass less the calculated mass of the linear slide rail, results in a moving mass of 122.84 grams.

Table 4 - Determination of the moving mass used in calculations

Item	Weight (gram)
Linear slide rail, linear slide block, sliding bracket, accelerometer, and associated nuts and washers (measured)	249
Guide rod (measured)	18.84
Linear slide rail (calculated)	-145
Total	**122.84**

7.3.1 Pressure results

The data referenced below was collected when the pressure supplying the piston varied slightly from a low value of 49.9 psi to a high value of 54.3 psi. The graph of the pressure readings can be found

below in Figure 18, this data was consistent throughout the varied conditions. The experimental results closely match the theory, with pressure one being the unregulated airflow, pressure two the airflow after the regulator, pressure three the air flow out of the piston, and four the airflow entering the piston. Since it is difficult to observe, it should be noted that pressure two mimics pressure three until the switch, and afterwards mimics pressure four.

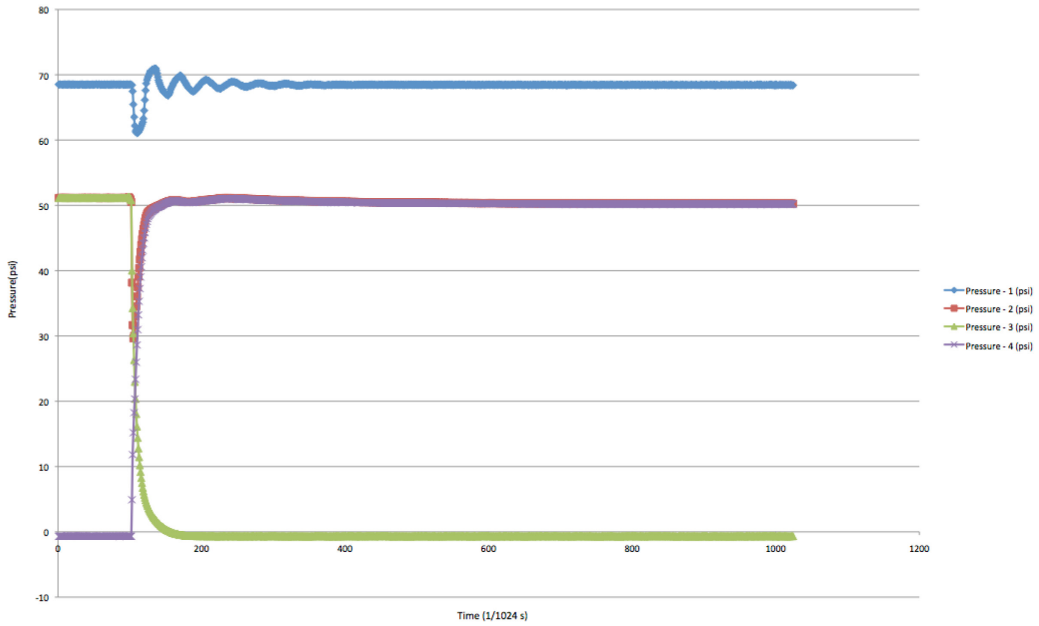

Figure 18 - Graph of pressure readings

The force exerted by the piston can be determined from the product of the pressure and the effective area of the piston. Since the effective area of the piston used is 0.12 in^2 for the outward stroke 0.10 in^2 for the inward stroke, and the pressures the trials were conducted at were recorded, the forces exerted are shown below in Table 5.

Table 5 - Forces calculated from piston pressure

Spring	Pressure(psi)	Outward Force (lbf)	Inward Force (lbf)
Red	52.3	6.2	5.2
Yellow	52.1	6.2	5.2
Green	54.3	6.5	5.4
Control	49.9	6.0	5.0
Short	24.1	2.9	2.4

7.3.2 Return stroke

The data below shows the force plots for the three standard springs during the return stroke. As shown below, the form of the force (and acceleration) is roughly the same, with just the magnitude changing. Figure 19 shows the force of the red spring, which has a maximum positive acceleration of 1.47g and a negative acceleration of 3.22g, which correlates to a force of 1.77N and 3.88N respectfully. Figure 20 shows the force of the yellow spring, which has a maximum positive acceleration of 1.70g and a negative acceleration of 2.95g, which correlates to a force of 2.05 N and 3.56N respectfully. Figure 21 shows the force of the green spring, which has a maximum positive acceleration of 1.56g and a negative acceleration of 1.58g, which correlates to a force of 1.88N and 1.90N respectfully.

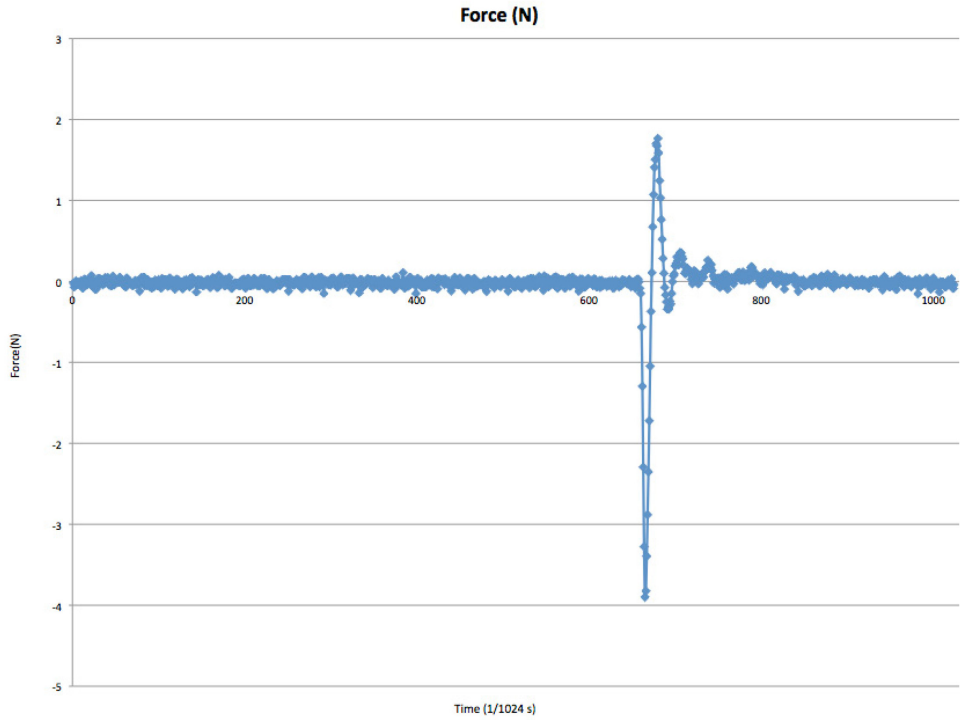

Figure 19 - Plot of force (N) versus time for the red spring in return stroke at 52.3 psi

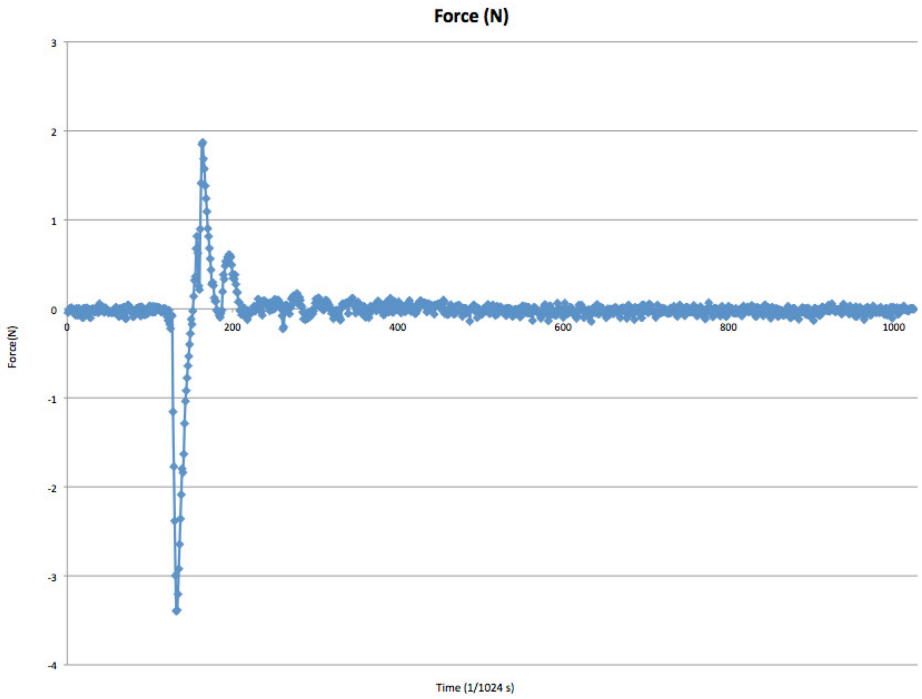

Figure 20 - Plot of force (N) versus time for the yellow spring in return stroke at 52.1 psi

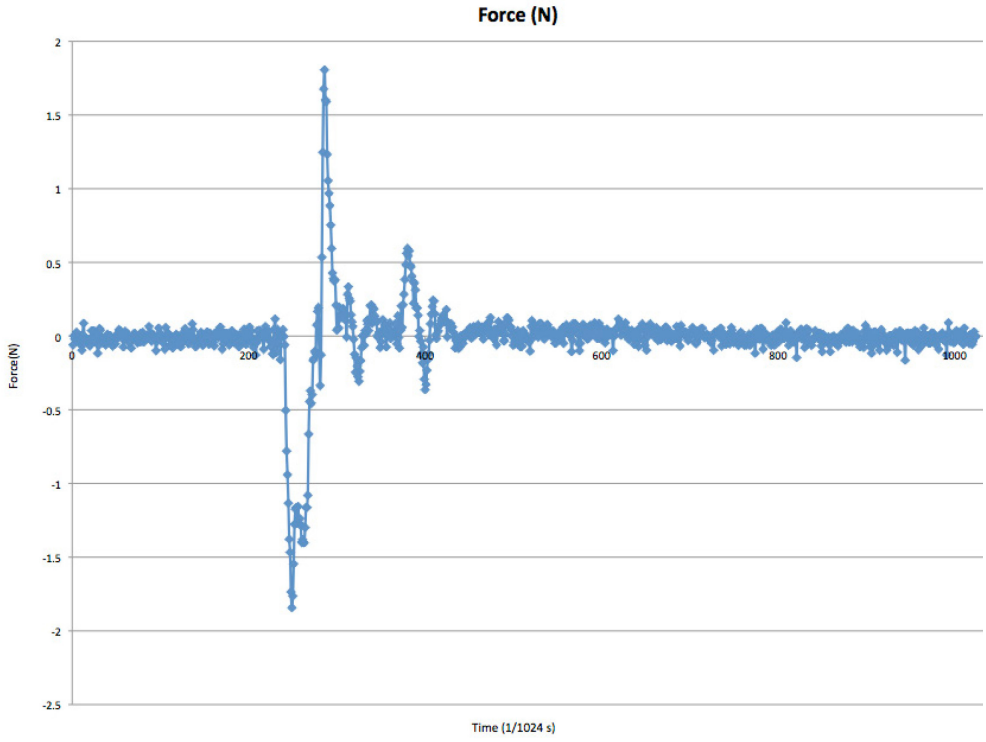

Figure 21 - Plot of force (N) versus time for the green spring in return stroke at 54.3 psi

7.3.3 Outward stroke

The data below shows the force plots for the three standard springs during the outward stroke. As with return stroke, the form of the force (and acceleration) is roughly the same, with just the magnitude changing. Figure 22 shows the force of the red spring, which has a maximum positive acceleration of 4.76g and a negative acceleration of 2.29g, which correlates to a force of 5.74N and 2.76N respectfully. Figure 23 shows the force of the yellow spring, which has a maximum positive acceleration of 5.84g and a negative acceleration of 3.26g, which correlates to a force of 7.04N and 3.93N respectfully. Figure 24 shows the force of the green spring, which has a maximum positive acceleration of 5.23g and a negative acceleration of 2.78g, which correlates to a force of 6.30N and 3.35N respectfully.

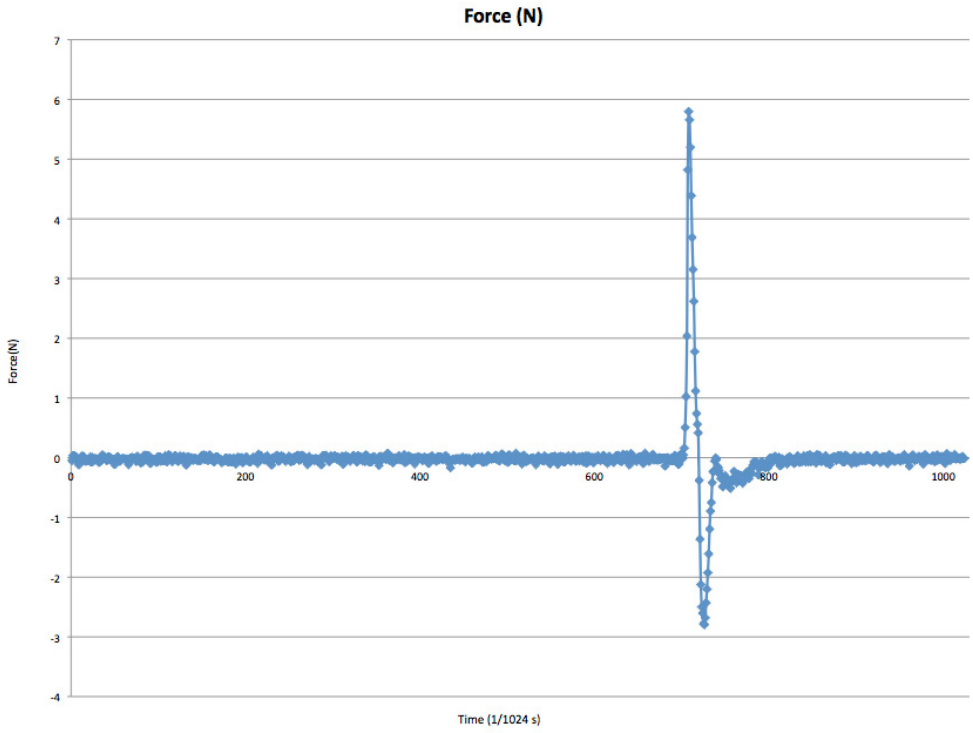

Figure 22 - Plot of force (N) versus time for the red spring in outward stroke at 52.3 psi

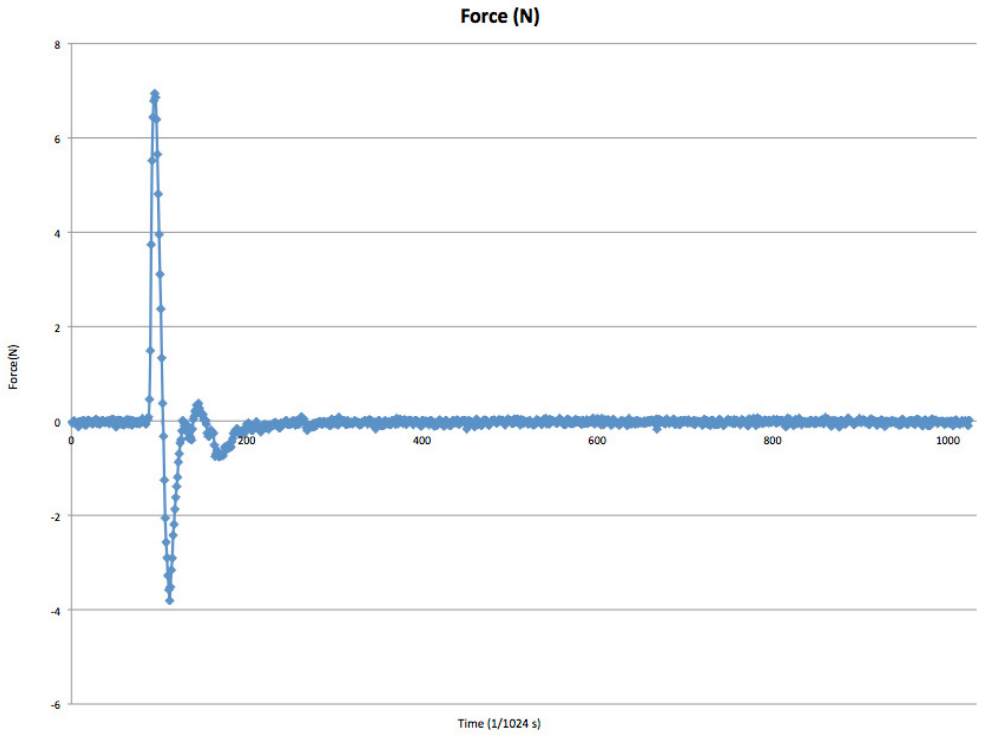

Figure 23 - Plot of force (N) versus time for the yellow spring in outward stroke at 52.1 psi

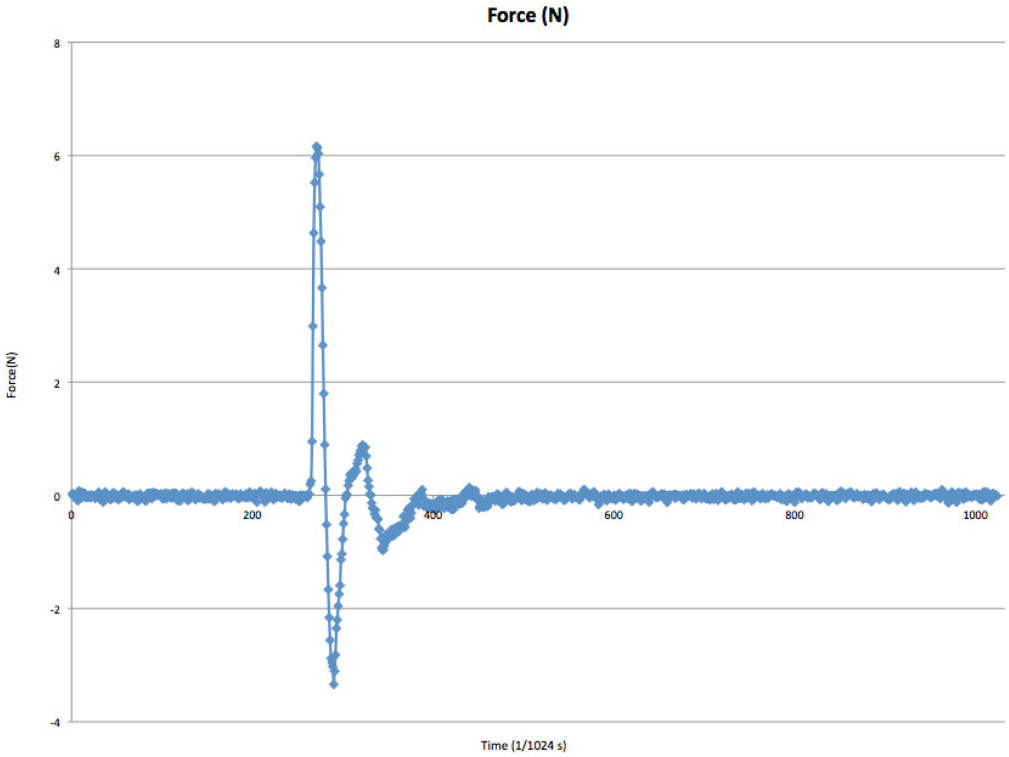

Figure 24 - Plot of force (N) versus time for the green spring in outward stroke at 54.3 psi

In order to consider the device without the effects of the spring, a run was conducted without a main spring, although the small piston spring remained. To allow for comparative results the test was conducted at the same pressure, which resulted in violent operation and likely caused higher than actual results to be recorded due to the impact. The return stroke, as shown in Figure 25, has a maximum positive acceleration of 0.46g and a negative acceleration of 0.68g, which correlates to a force of 0.55N and 0.83N respectfully. The outward stroke, as shown in Figure 26, has a maximum positive acceleration of 13.57g and a negative acceleration of 44.38g, which correlates to a force of 16.35N and 53.48N respectfully

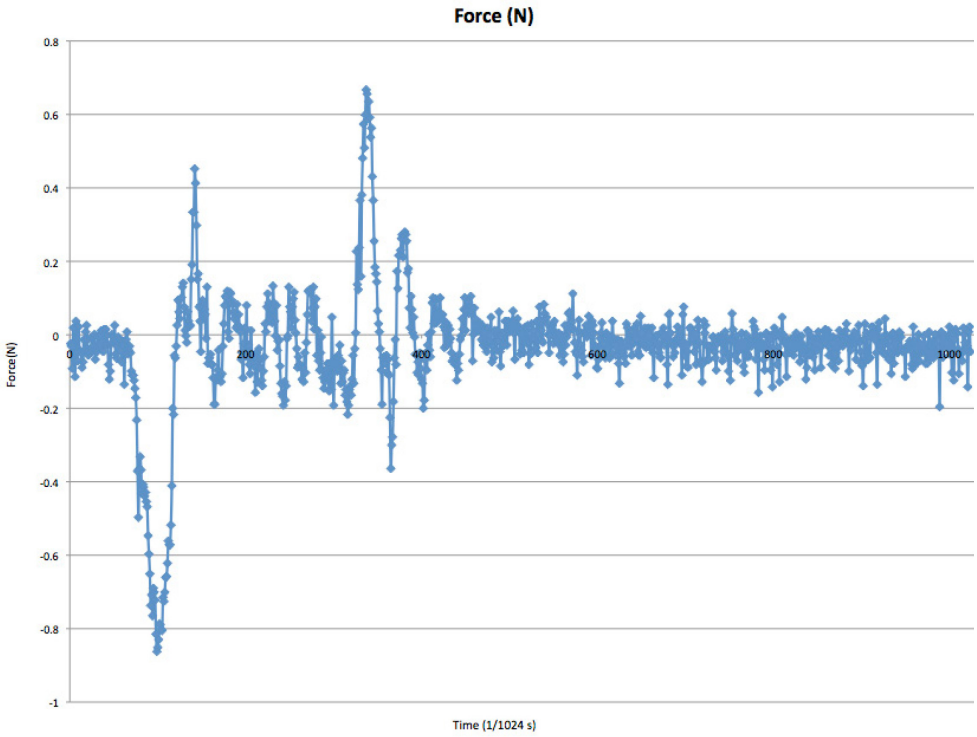

Figure 25 - Plot of force (N) versus time for the control test in return stroke at 50 psi

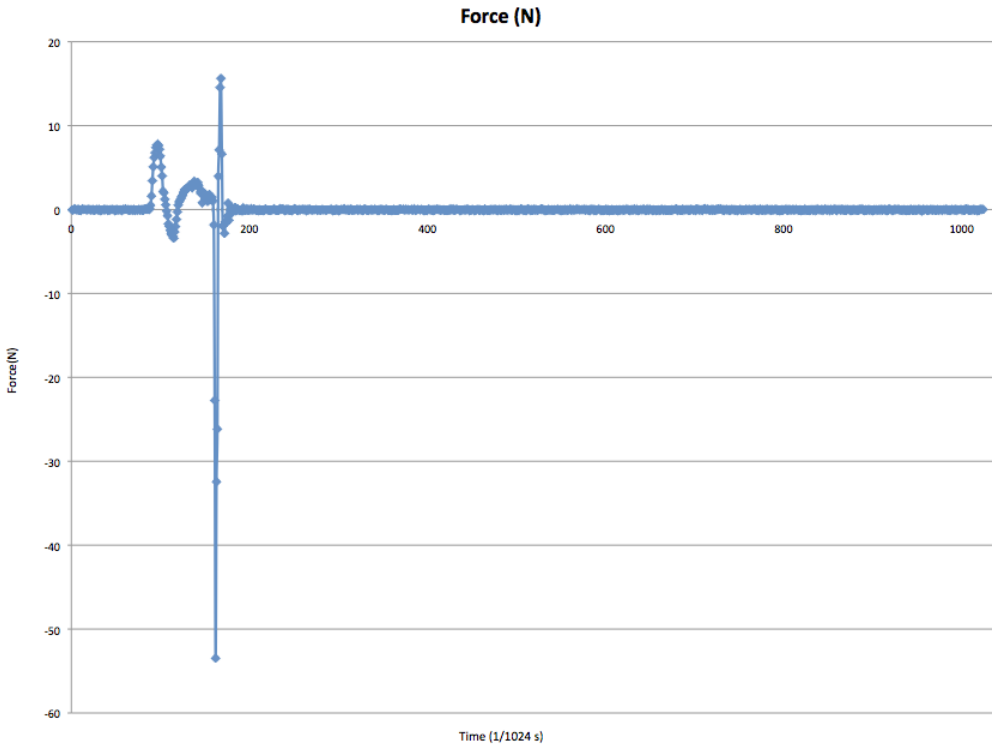

Figure 26 - Plot of force (N) versus time for the control test in outward stroke at 50 psi

The following table summarizes the results of experimental analysis of the final design. All values are of the resultant acceleration of the pneumatic spring-mass system in units of 'g' (1 g=9.81 m/s^2). It is important to note that the positive and negative values of acceleration are extremely high on the outward stroke for the control experiment (in the absence of springs). This is because one of the valves in the piston-cylinder was adjusted to compensate for a higher force required to compress a compression spring on the outward stroke, and is expected behavior of the system. The previously stated results are compiled below in Table 6 and Table 7, the control spring referenced denotes the results when the device was run with no main spring present.

Table 6 - Compilation of acceleration results in g's

Spring	Pressure (psi)	Outward Stroke		Return Stroke	
		Positive	Negative	Positive	Negative
Red	52.3	4.76	2.29	1.47	3.22
Yellow	52.1	5.84	3.26	1.70	2.95
Green	54.3	5.23	2.78	1.56	1.58
Control	49.9	13.57	44.38	0.46	0.68

Table 7 - Compilation of force results in Newtons

Spring	Pressure (psi)	Outward Stroke		Return Stroke	
		Positive	Negative	Positive	Negative
Red	52.3	5.74	2.76	1.77	3.88
Yellow	52.1	7.04	3.93	2.05	3.56
Green	54.3	6.30	3.35	1.88	1.90
Control	49.9	16.35	53.48	0.55	0.83

7.3.4 Short Spring

Also tested was the much shorter spring, which resulted in slightly different data. Due to the small size and relatively small resistance value, this spring had to be tested at a lower pressure due to the destructive force it caused when operated at 50 psi. Even when operated at 24.1 psi, the device saw some large acceleration data, as shown the return stroke data in Figure 27. The return stroke has a maximum positive acceleration of 1.03g and a negative acceleration of 2.33g, which correlates to a force of 1.24N and 2.81N respectfully, while the outward stroke has a maximum positive acceleration of 2.22g and a negative acceleration of 2.87g, which correlates to a force of 2.67N and 3.46N respectfully.

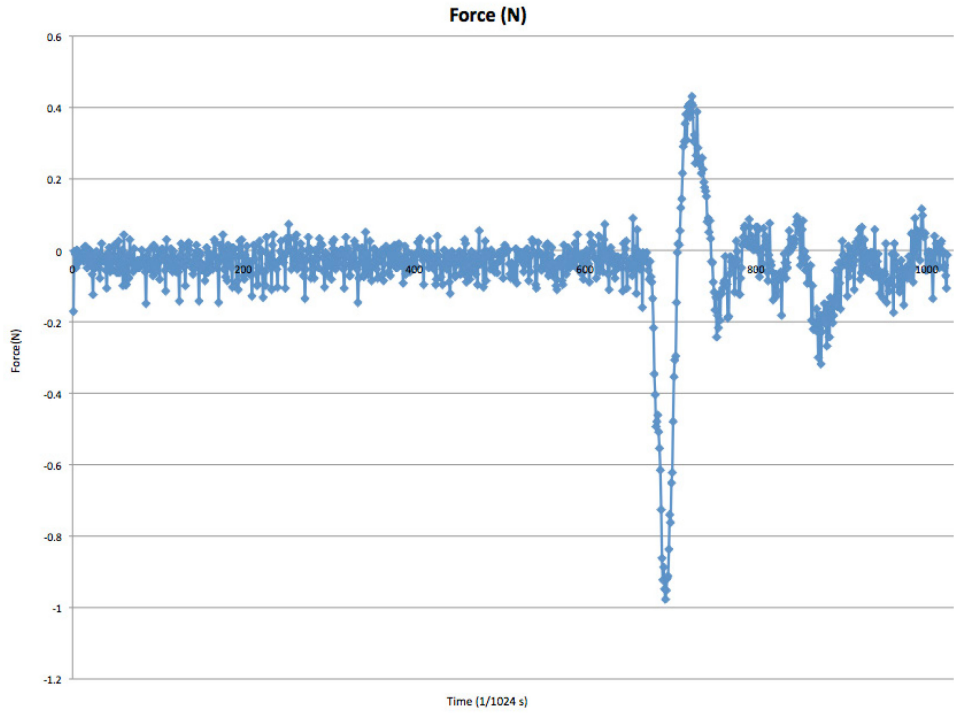

Figure 27 - Plot of Force (N) versus time for the short spring in return stroke at 24.1 psi

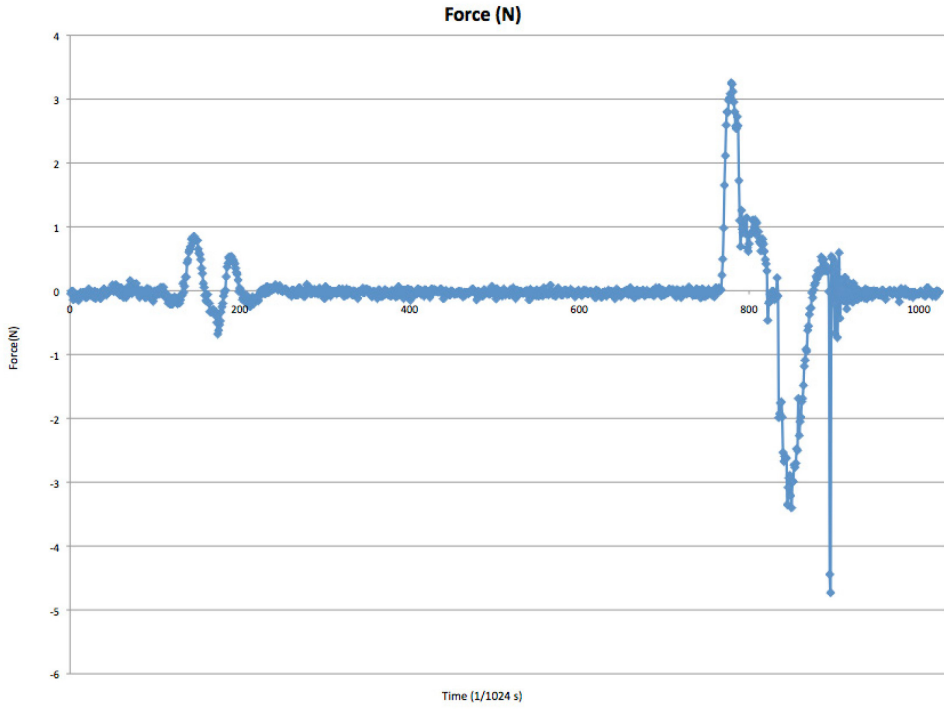

Figure 28 - Plot of Force (N) versus time for the short spring in outward stroke at 24.1 psi

7.4 Analysis

The mathematical model was created before construction of the device was finished. This model assumed a sinusoidal pressure versus time function, which is not created in our model with the solenoid. In addition, fluid dynamics within the pneumatic portion of the system was not considered. Also, assumptions were used to determine the dampening and resistance for the first system, while experimental data was used for the bond graph system. Besides using experimental data, the bond graph system also assumes, like the first model, that the piston is of infinite length, when it has a limit of motion.

The comparison is made between the final iteration of the mathematical model, and the final iteration of the bond graph model. Observations of the system for this comparison are those taken by human eye and instrumentation. The experimental data that the bond graph uses does not account for spring dampening (the spring was removed during testing), which will undoubtedly skew data, but the spring dampening was assumed small compared to the friction and piston dampening.

For the variation of pressure with respect to time, the bond graph method did not provide a function that was similar to the original function in magnitude or behavior. While both the original mathematical model and the bond graph function are both harmonic, the bond graph function also quickly approaches zero, while the first model pressure function never does. When compared to physical system behavior of the device, the bond graph function shows better relation to the behavior, as the motion of the system quickly ceases with a spring installed.

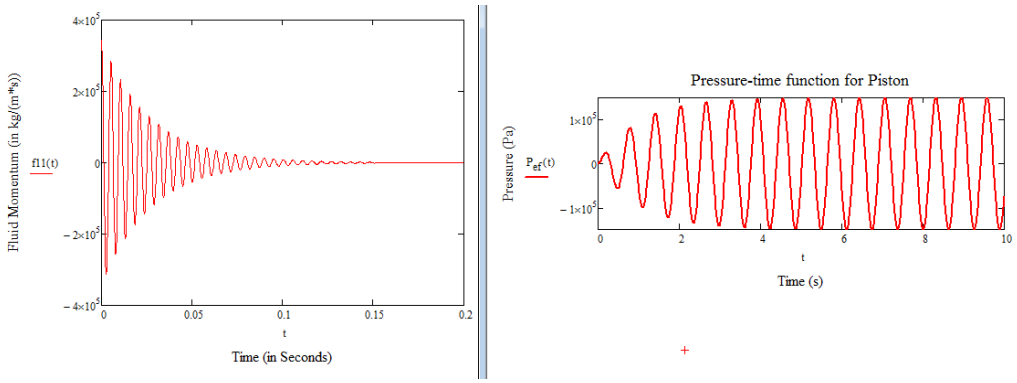

Figure 29- Pressure vs. Time functions

A property measured by the bond graph is noted here as fluid charge. This is the “charge” a fluid capacitance element for a bond graph holds. For the fluid charge data, measured in cubic meters there is no standard approach counterpart. The harmonic change is to be expected, and agrees with the

overall behavior of the standard mode. It is important to note that the magnitude of the charge is far too large for the pressures seen in the system itself. This assertion is made based on the ideal gas law which dictates that $P_1V_1=P_2V_2$, where P_1 is the atmospheric pressure, V_1 is the fluid charge recorded by the bond graph, P_2 is the system pressure, and V_2 is the volume of the pneumatic tubing (which comprises the capacitance of it). It is plausible that the behavior of this prediction is correct, but the magnitudes cannot be so.

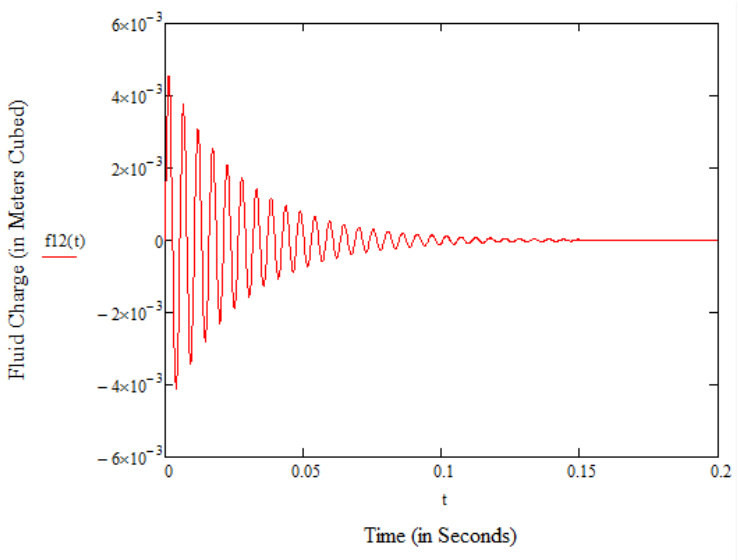

Figure 30- Calculated fluid charge versus time of pneumatic system capacitance (Element C5)

For the momentum data, the behavior of the curve seems to fit with the harmonic aspect of the first model, but the magnitude indicates extreme velocities and acceleration. This is not the case, but the harmonic behavior of the momentum function is a step in the correct direction for further analyzing the system, as is the progression to zero momentum. However, the negative momentum predictions are incorrect, as there is no indication in the experimental data or group observations that the piston changes direction.

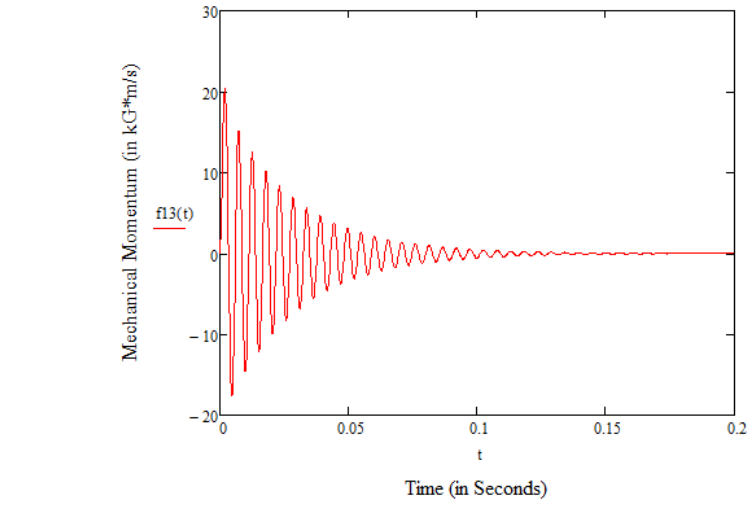

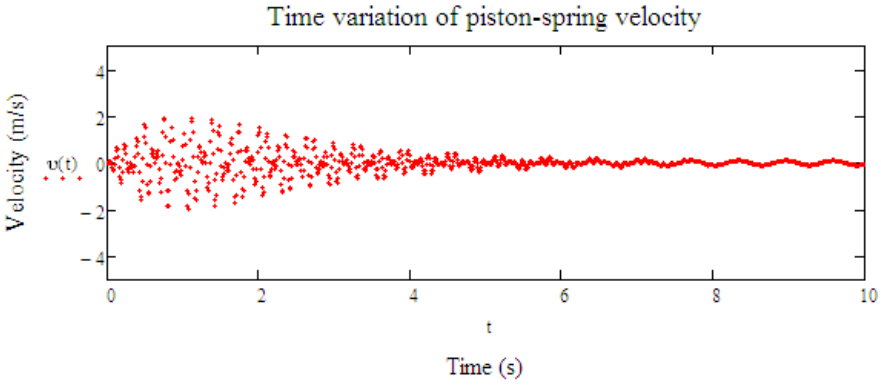

Figure 31- Bond Graph Momentum and Standard Approach Velocity

The last aspect predicted by the bond graph model is the charge, or mechanical displacement of the spring. This data approaches expected behavior of the physical system, but is still ten times larger than any displacement observed by the device, and this displacement goes to zero with time, rather than staying at a steady point. The presence of oscillations in the data agrees with the mathematical model, but the magnitudes of the functions disagree. Figure 32 is a comparison of the mechanical spring charge (displacement) and the standard approach displacement.

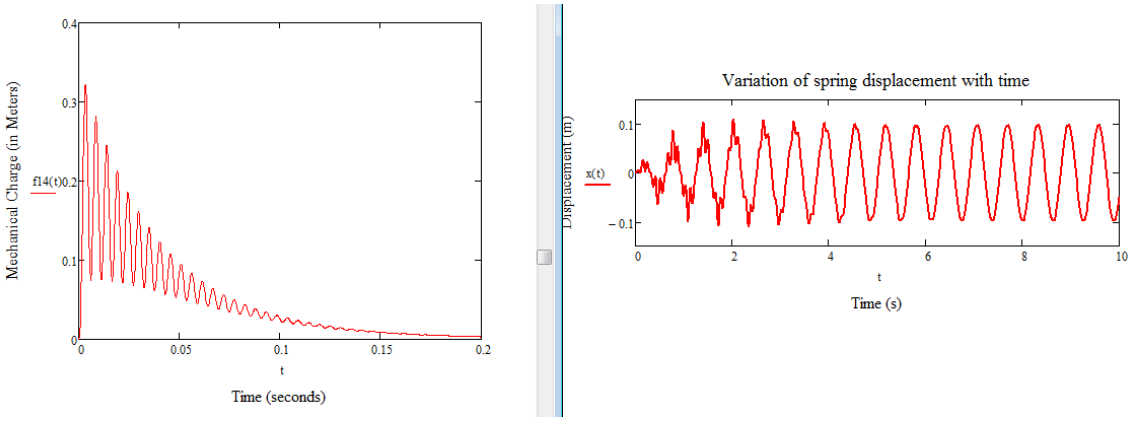

Figure 32- Bond Graph Mechanical Charge vs. Standard Approach Displacement

The data above for the bond graphs, while not agreeing with the original model except for the presence of harmonics, does show another sign of being correct. This sign is in the fact that all the bond graph readouts decay to nearly zero within the time span of the acceleration data taken from the machine during in operation. The data above for the bond graph equations are for the "out-stroke" of the piston, with the assumption that the pressure is maintained at a constant level.

Another indication that the bond graph, while not being a perfect predictor, could be applicable to the device, is the readings for the out stroke momentum, when differentiated, match the behavior of the acceleration data very well, when the peaks of the positive readings are compared to the accelerometer data. The momentum derivative graph from the bond graph approach is shown below. The magnitudes are incorrect, but the behavior and decay hold some similarity to the acceleration data.

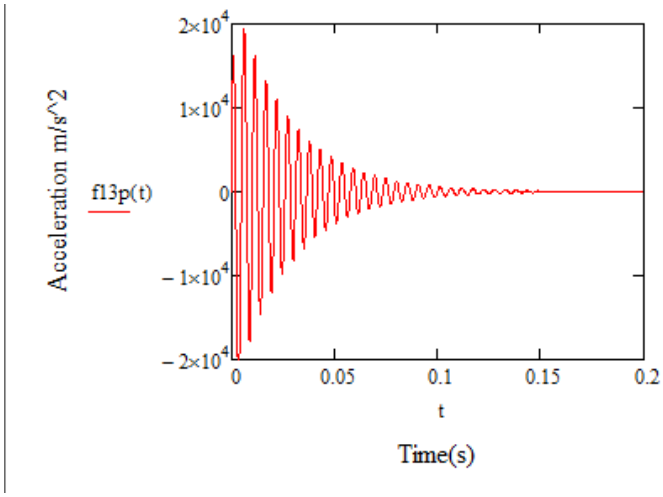

Figure 33- Derivative of Out Stroke Bond Graph Mechanical Momentum

While the mathematical models created to analyze the system do not fully correspond to standard predictions, or to measured system behaviors, they do serve their illustrative purpose. They demonstrate that even though a mathematical model may exist to predict the properties of a physical system, mathematical models are only as accurate as the assumptions made, and aspects analyzed in the system at hand.

The work in the previous section, concerning bond graph behavior, compared the behavior of the system when analyzed. The difference in the correlations, at least in terms of duration of time and some magnitude behaviors, are interesting. The sections prior, however, used the resistance calibration data, which did not include a main spring. The graphs below are acceleration functions taken from the system when a spring was in place. They have been trimmed, and are below for reference. In the previous Bond Graph Section, it was noted that there was a correlation between the springs' calculated acceleration results and those that were measured. While the correlation is in the behavior of the positive peaks of the sine wave, its presence indicates that the bond graph approach to analyzing this system may be worth continuing investigation. Below are figures from an out stroke and an in stroke, demonstrating that the partial correlation is present in the spring runs as well.

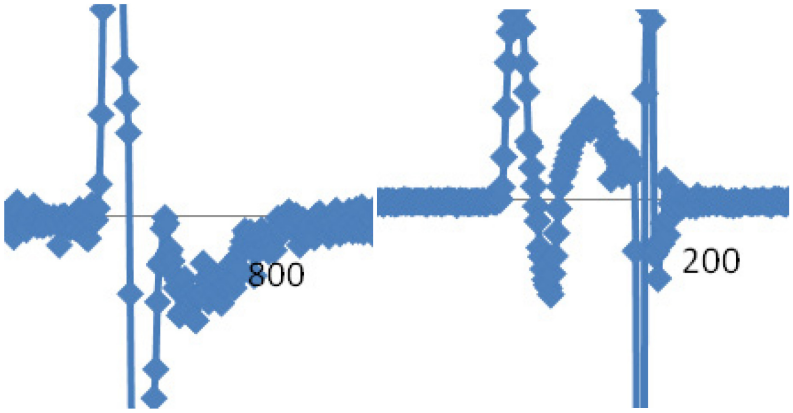

Figure 34- Acceleration Data (magnified) Out and Return Strokes Respectively

The data above demonstrates that, while the Bond Graph results do somewhat match the behavior of the device, the device does not experience such violent harmonics. There are two assumptions that immediately come to mind, which the bond graph relies on, that could be the source of this. The first is assuming that the air flowing through the system is in laminar flow. The velocities are too high for this. The second is that the correlation of the experimentally derived resistance to the acceleration data for the near springless run is correct. If this project is used for the basis of another project, it is recommended that the next team investigate formulas for turbulent resistance for a bond

graph element. Further investigation into the nature of the lumped mechanical resistance is also recommended.

8 Conclusions and Recommendations

Over the three terms that this MQP was designed, engineered, fabricated, and tested, our group gained valuable insight into the design process and advanced our knowledge in pneumatic systems and engineering in general. We feel that the constructed device can be used as a valuable teaching tool in Professor Cobb's Modeling and Analysis of Mechatronic Systems course, whose value could be greatly improved through subsequent project work.

8.1 Conclusions

The device constructed fulfils the goals and objectives that were established at the beginning of this project. The following section will detail our insight into the device and the need that it fulfills.

8.1.1 Differences between Three Models

The theoretical results are slightly different from experimental values obtained, as was expected at the outset of the design process. This is because there are several external conditions that influence the actual behavior of the system, such as friction inside the piston, the compressibility of air, the response time of the overall system, as well as the accuracy of the measurement devices. These factors contribute to a slight variation between theoretical and experimental values which cannot be avoided without making the theoretical computations extremely tedious and time consuming.

8.1.2 Use as an Educational Tool

This device will be a beneficial teaching aid to convey the differences and similarities between a bond graph model of a system and a system's actual behavior. Since it is exceedingly difficult if not impossible to account for all the variables that affect a system, an analytical solution must strike a balance between accounting for enough to provide an accurate and useful model, and simplifying the model enough to allow for easy computation.

As a teaching tool, this device will assist students in learning what assumptions to make and when they are valid. In addition, it will show that even if a system is perfectly modeled, you cannot expect its physical representation to perfectly match, as shown by the data collected from the device. Throughout this process, familiarity with electrical, mechanical, and pneumatic systems will be improved.

8.1.3 The Final Design

After multiple design iterations, we feel that the final design of the device represents a superior device that is capable of providing a pneumatic platform that applies force to a variety of springs. The design is also capable of measuring and recording accelerations and pressures to allow for the analysis of the forces applied and exerted in the system.

8.2 Recommendations

Based on our testing as well our experiences throughout the design phase of the project, multiple improvements and additions could have been made to improve the device, had additional time, resources, and or skill sets been available. The following describes improvements that a subsequent MQP group could make to improve the quality of the device is so desired.

8.2.1 Improvement of the Reliability and Accuracy of the Pressure Transducers

Through testing of the completed device, it was found that the 9V battery power supply delivers a decreasing amount of voltage to the sensors as the battery drains. This changing voltage results in a pressure reading that is artificially low. To rectify this situation, a DC power supply that operates off of a standard outlet should be specified and purchased, as well as circuitry that will provide a constant 5.25 volts at 40 milliamperes to the existing breadboard.

While a constant power supply will provide reliable pressure readings, more accurate pressure results would require additional work. The current method of pressure sensor calibration is to attach a pressure transducer from the device to a three gallon tank with a pressure gauge found in HL031. Several factors prevent this method from accurately calibrating the transducers. The primary factor is the precision of the gauge used to determine the pressure in the tank, since the calibration of the gauge itself is unknown. Additionally, the gauge only provides tick marks in increments of 1 psi, which when combined with the fluctuation of the tank and human error, results in a significant margin of error. Should pressure reading accurate to more than plus or minus a few pounds per square inch be desired, a calibrated pressure gauge of greater accuracy should be sought out or purchased.

8.2.2 Force Transducer

During the initial design phase multiple methods of force measurement were considered and researched, before the use of an accelerometer was finally decided upon. At the time the thought process was to use only one method of force measurement of the spring, although in retrospect employing an additional measurement instrument would improve the device by allowing for an

additional set of force data to be read. If desired a strain gauge could be added to the bushing bracket to measure the deflection caused by the force applied by the spring.

8.2.3 Improve Relationship between the Three Models

As discussed previously, there is significant deviation between the mathematical model, bond graph model, and experimental results. Even though these deviations were expected, and required for the purpose of this device, it would still be beneficial to identify the sources of the error and remove or reduce them.

The most obvious source of error would be due to the friction present throughout the device. Friction between the piston rod and piston cylinder, between the linear slide block and linear slide rail, and between the guide rod and bushing would result in a varying reduction of force throughout the system.

Some means to reduce the friction present include the purchase of a low friction piston that has not been abused by the robotics department, the replacement of the linear slide with one that has a lower friction coefficient or its possible removal from the system, and better alignment of all the components, so all the force is applied through one axis.

In addition to the mechanics of the system, the bond graph could also be improved to account for more factors of the system. The constructed bond graph includes numerous assumptions and simplifications that could be reconsidered to create a more accurate, albeit more complicated, model of the system.

Much like Professor Norton's "fourbar linkage demonstrator," this device could have a set of mechanical and bond graph improvements. These changes could be added sequentially to show how the experimental and theoretical models approach each other as sources of error are removed from the mechanical system, and ignored factors are taken into consideration in the bond graph.

8.2.4 Use as an Educational Product for Resale

Throughout the development of this device, the concept of selling the product as an educational tool was considered. The market for educational devices is both limited and generally expensive. The use of VEX components in the theoretical product varied from being based entirely VEX based to entirely custom parts.

Before this device could be considered for mass sale, various topics would have to be investigated. First and foremost, the market interest for such a device would have to be researched to determine the number of people who would be interested in such a device. Additionally, the pervasiveness of pneumatic VEX components, as well as computer hardware and software capable of sampling and storing the data generated from the sensors needs to be considered.

8.3 Concluding Remarks

In final conclusion, this MQP was an overall success, meeting the project's goals and objectives, and providing a launching point for the continuation of this project. Our hope is that future MQP groups improve the pneumatic test bed, following our recommendations and expanding it to fulfill the device's needs.

9 Bibliography

[1] WPI. (2006). *2006-2007 undergraduate catalog,* 2010, from http://www.wpi.edu/Images/CMS/Pubs-Catalogs-Ugrad/wpiugradcat0607.pdf

[2] Korane, K. J. (2007). *Motion control on a budget.* Retrieved Sep 17, 2009, from http://mechatronic-design.com/features/motion_control_budget/index1.html

[3] Michigan Occupational Safety and Health Administration. (2004). *Compressed air,* 2010, from http://www.michigan.gov/documents/CIS_WSH_talk13_73400_7.htm

[4] Society of Robots. *ACTUATORS - SOLENOIDS.*http://www.societyofrobots.com/actuators_solenoids.shtml

[5] Gonzalez, A. *Solenoid valve.* http://en.wikipedia.org/wiki/File:Solenoid_Valve.png

[6] Machine Design. (2002). *Pneumatic pressure regulators.*http://machinedesign.com/article/pneumatic-pressure-regulators-1115

[7] Omega. *Introduction to pressure transducers.*, 2010, from http://www.omega.com/prodinfo/pressuretransducers.html

[8] Omega. *Introduction to load cells.* http://www.omega.com/prodinfo/LoadCells.html

[9] Kistler. *The force transducer.*, 2010, from http://www.kistler.com/force-transducer_en

[10] Omega. *Introduction to accelerometers.*, 2010, from http://www.omega.com/prodinfo/accelerometers.html

[11] Lee Spring Company. *Overview: COMPRESSION SPRINGS,* 2010, from http://www.leespring.com/int_learn_compression.asp

[12] Young, H., & Freedman, R. (2004). *University Physics 11th Edition*

[13] Dixon Valves. (2002). *Pneumatic tubing fittings,* 2010, from http://www.dixonvalve.com/fgal/lit_pdf/2006/pneumatic_tubing_2006.pdf

[14] Norgren. (2008). *CLEAN COMPRESSED AIR - THE NORGREN GUIDE TO EFFECTIVE AIR PREPARATION.*, 2010, from http://www.omega.com/auto/pdf/CleanCmprsdAir.pdf

[15] Belizaire, J. (2009). *Inquiries about products, technologies and CAD data*

[16] THK. *Accessories for lubrication.* Retrieved February 28, 2010, from http://www.thk.com/documents/us_pdf/products/generalB/Lubrication/en_B_863options.pdf

[17] EBay. *THK MG70 GREASE GUN UNIT.* Retrieved February 28, 2010, from http://cgi.ebay.com/THK-MG70-GREASE-GUN-UNIT_W0QQitemZ290396898336QQihZ019QQcategoryZ26229QQcmdZViewItemQQ_trksidZp3286.m7QQ_trkparmsZalgo%3DLVI%26itu%3DUCI%26otn%3D2%26ps%3D63%26clkid%3D8180349970291446001#ht_1928wt_1133

[18] National Instruments. *NI USB DAQ hardware features.* Retrieved February/28, 2010, from http://sine.ni.com/np/app/culdesac/p/ap/daq/lang/en/pg/1/sn/n17:daq,n24:USB/docid/tut-8240

[19] Tongue, B. *Principles of vibration (second edition)* (pp. 173)

[20] Karnopp, D. C., Margolis, D. L., & Rosenberg, R. C. (2006). *System dynamics modeling and simulation of mechatronic systems* (Fourth Ed.). Hoboken New Jersey: John Wiley and Sons.

Appendices

Appendix A - Installation Manual

Appendix B - Operation Manual

Appendix C – Maintenance

Appendix D – Purchases

Appendix E – Engineering Drawings

Appendix F – Bond Graph MathCAD and MATLAB Calculations

Appendix G – Experimental Procedure for Bond Graph Mechanical Resistances

Appendix A. ***Installation Manual***

The following installation manual will show how to assemble the device from parts. Although not specified here, engineering drawings are available in Appendix E for custom parts, and part numbers for purchased parts are available in Appendix D.

Step 1

To begin assembly of the Pneumatic Test Bed device, locate the aluminum base with the printed side down. For reference purposes, locate the end with the set of mounting holes located on the edge, as noted in Figure 35.

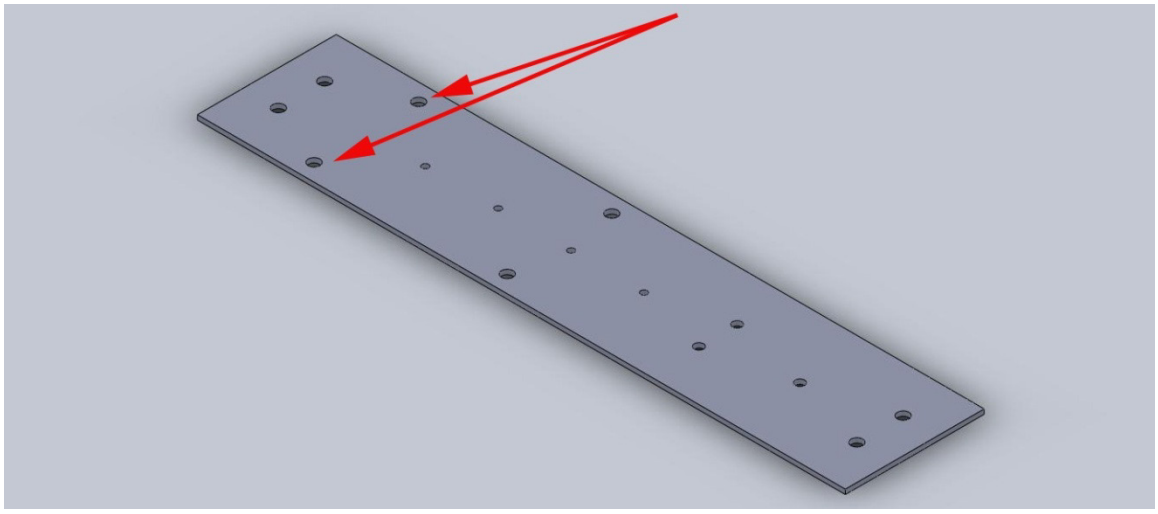

Figure 35 – Assembly Step 1

Step 2

Mount the piston riser to the aluminum base with two large bolts as shown in Figure 36. Note that the tapped hole is located between the bolts and the back of the device. Secure the bolts with a pair of washers and nuts, keeping it loose enough to align later.

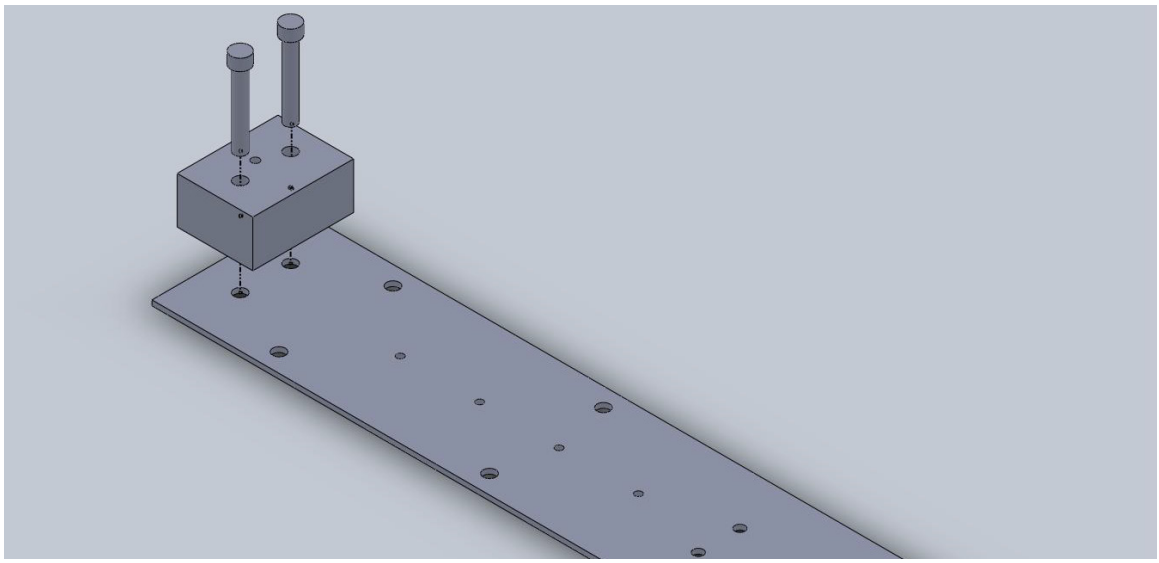

Figure 36 - Assembly Step 2

Step 3

Next, mount the linear slide assembly to the aluminum base as shown in Figure 37. Note that the linear slide assembly can be mounted in either direction. Secure each screw with a washer and nut, again loosely to allow for alignment.

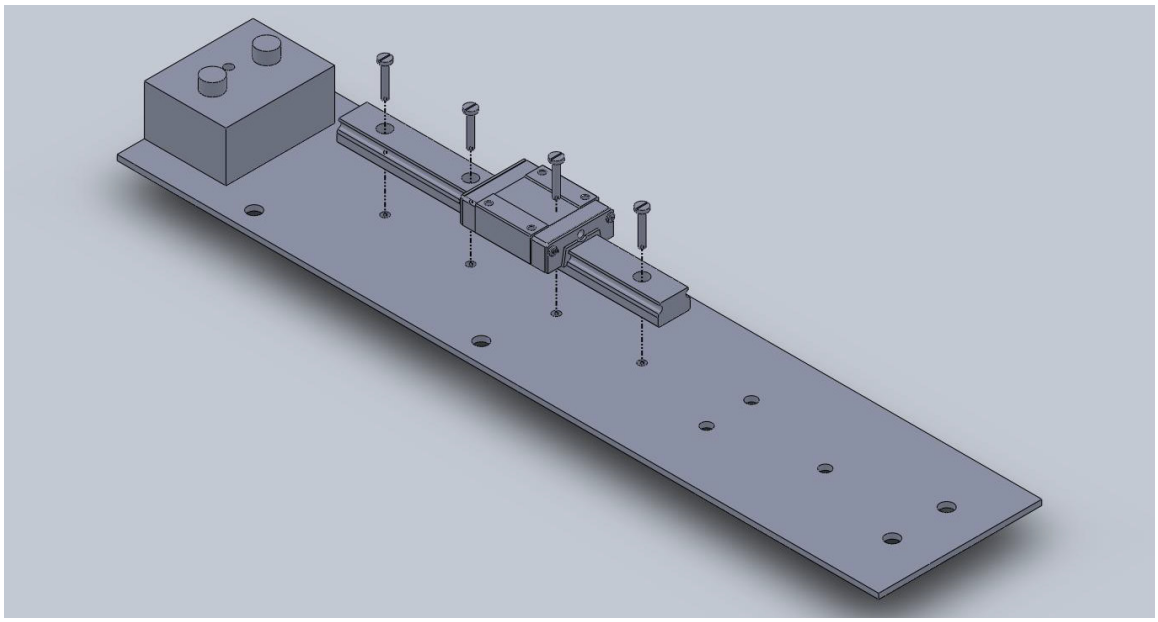

Figure 37 - Assembly Step 3

Step 4

Securely attach the sliding bracket to the linear slide block with the four Philips countersunk screws. Note the orientation of the large and small holes as shown in Figure 38.

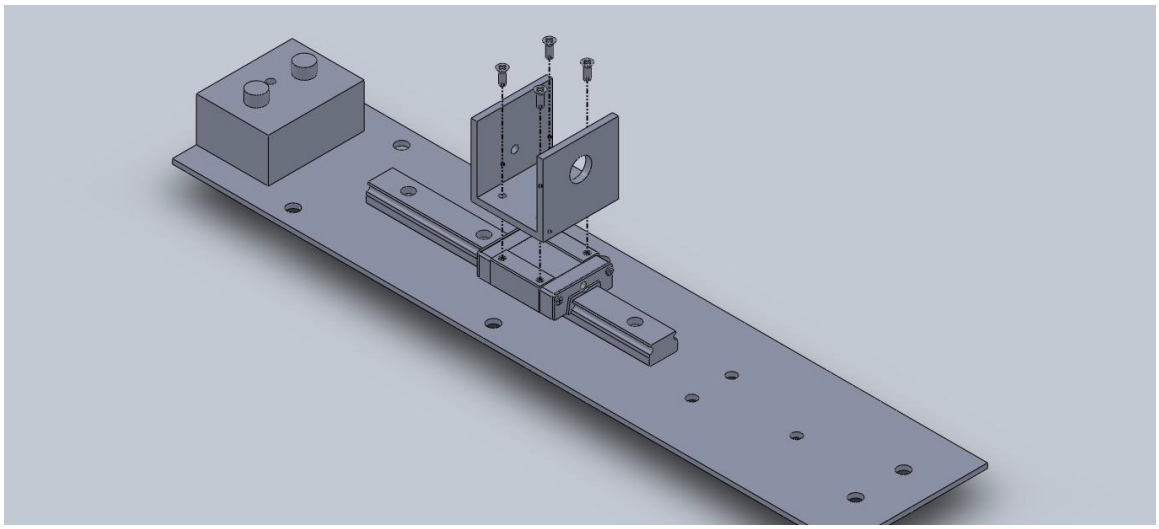

Figure 38 - Assembly Step 4

Step 5

Now mount the bushing bracket to the aluminum base. First place the plastic bushing in the bushing bracket as shown in Figure 39, and then loosely secure it to the aluminum base with the three round head hex screws, washers, and nuts.

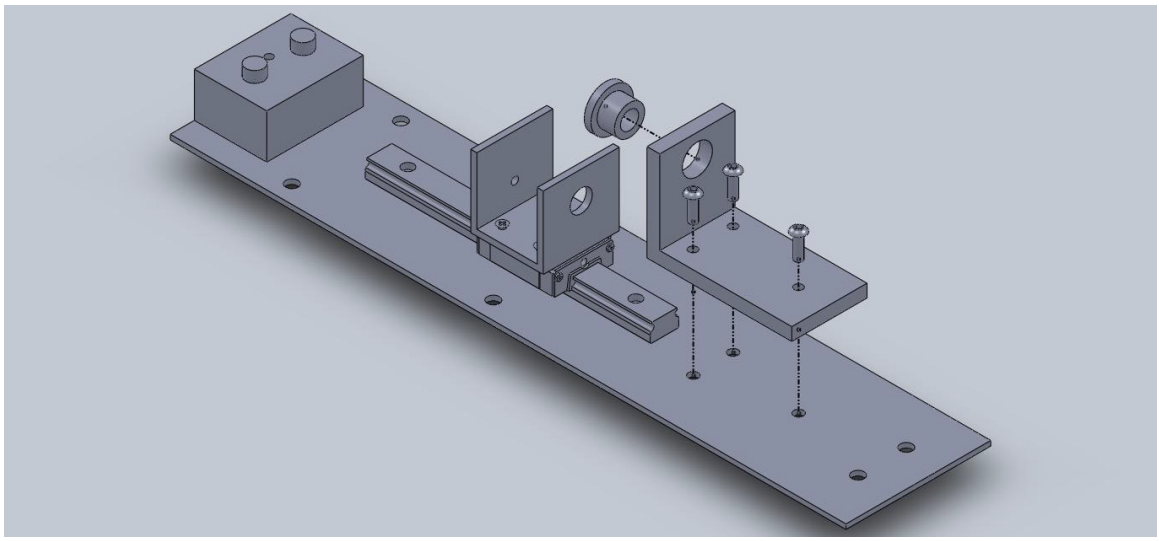

Figure 39 - Assembly Step 5

Step 6

Next attach the piston assembly to the piston riser, as shown in Figure 40, with a round head hex screw. Before inserting the piston rod into the sliding bracket, place the small spring, followed by a nut and washer on the threaded part of the piston as depicted. Note that the spring is not shown in the figure.

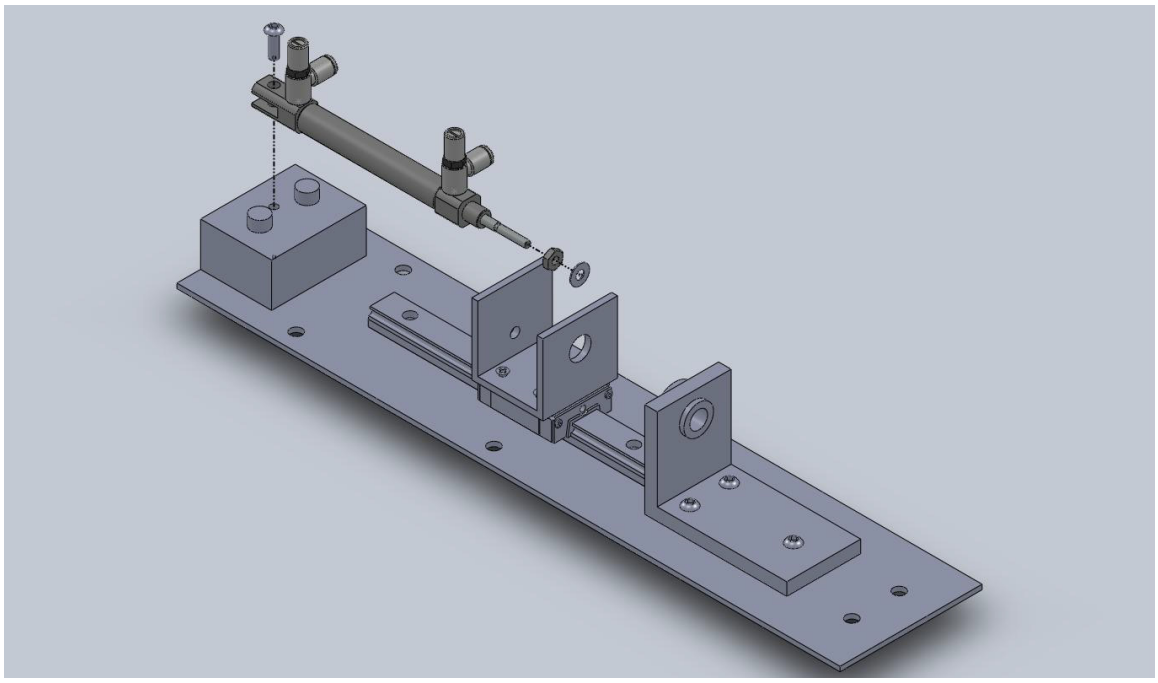

Figure 40 - Assembly Step 6

Step 7

As shown in Figure 41, it is now time to mount the guide rod, its retaining screw, and spring to the device. First place the short hex screw into the hole in the sliding bracket with a washer on either side. Second, place the spring between the washer and plastic bushing, and insert the guide rod into the back of the bushing and through the spring. Lastly, screw the guide rod into the screw tight enough to attach the two, but loose enough to allow for alignment.

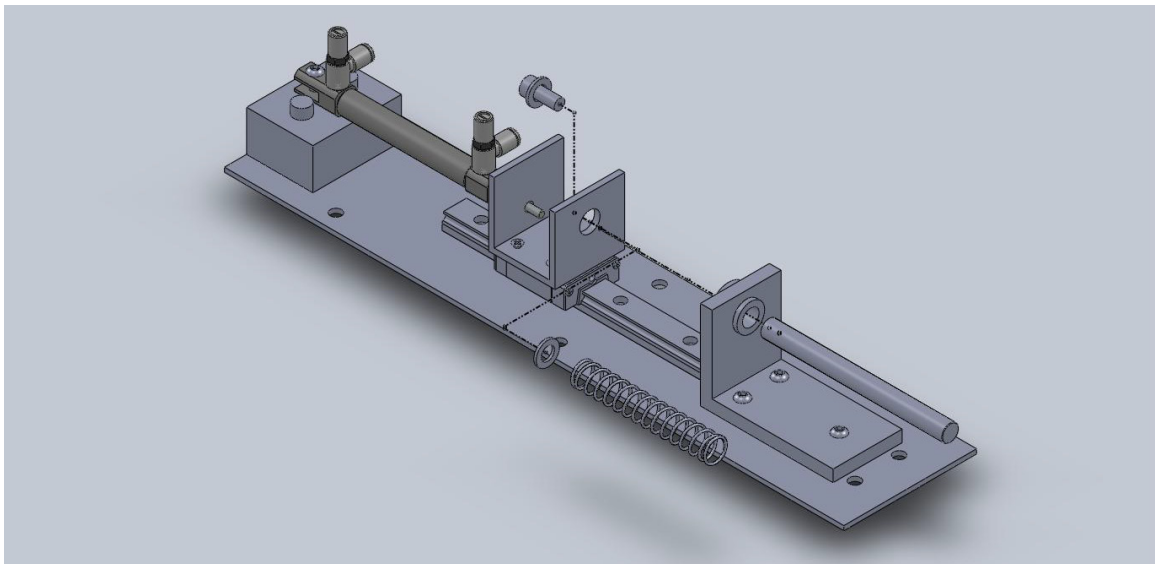

Figure 41 - Assembly Step 7

Step 8

Next, place a washer and nut onto the end of the piston rod as shown in Figure 42. This concludes the construction of the dynamic assembly portion of the device. The device should now be aligned to allow the piston assembly, linear slide assembly and guide rod to be parallel to each other. It is advised that the linear slide rail be first made parallel to the aluminum base, and then securely tightened (this may require the piston assembly and/or guide rod to be removed). Next, adjust the piston riser to make the piston assembly parallel to the linear slide assembly, and tighten that. The bushing bracket should be adjusted next to make the guide rod parallel to the linear slide assembly.

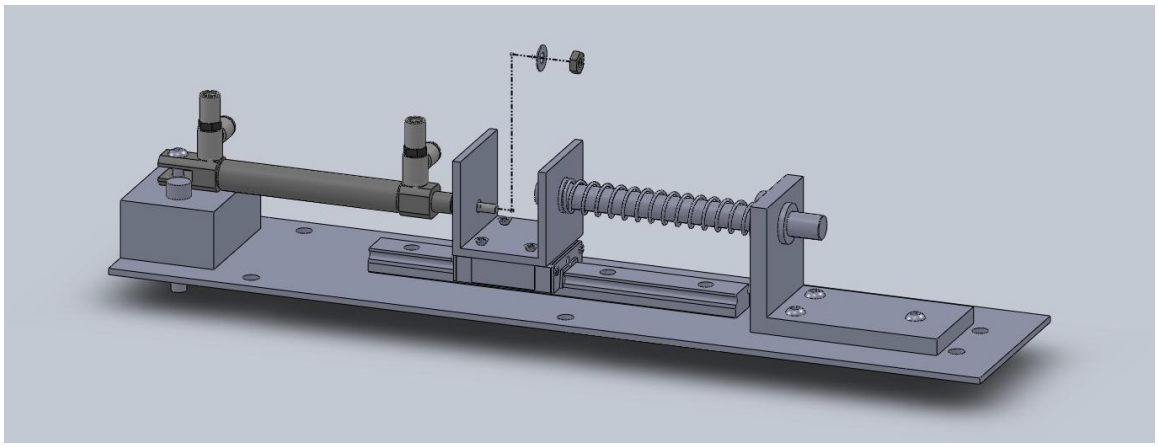

Figure 42 - Assembly Step 8

After all the components are securely attached to the aluminum base, the screw attaching the guide rod should be tightened once the guide rod is parallel to both the top and side of the aluminum base, and slides without resistance. Finally, adjust the nuts on the piston rod so that it is parallel with both the aluminum base and the linear slide assembly, and is at the correct distance so the spring is fixed in place.

Step 9

Now locate the wood base, and place it as shown with the majority of the countersunk holes facing up as shown in Figure 43.

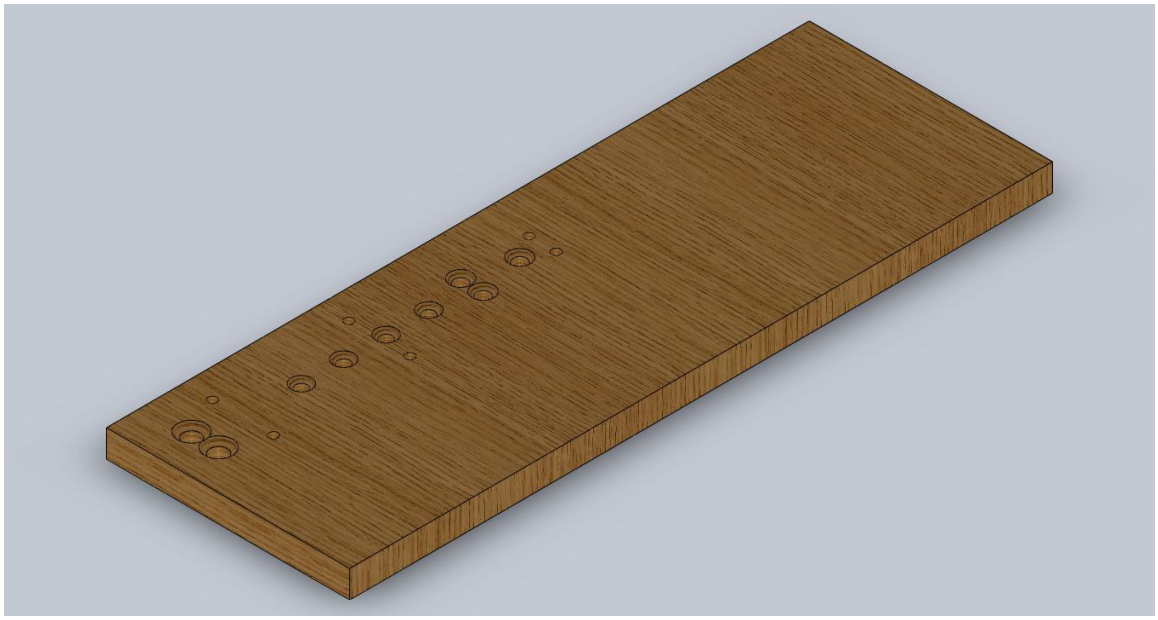

Figure 43 - Assembly Step 9

Step 10

Place the previously assembled dynamic assembly into the wood base as shown in Figure 44, and verify that the aluminum base is flush with the wood base, and that all of the bolts and washers clear their respectful countersunk areas. If clearance issues arise, adjusting the placement of the washers, or removing some wood material might be necessary. Next, insert the countersunk bolts from the bottom of the wood base, and tightly secure with the corresponding nuts.

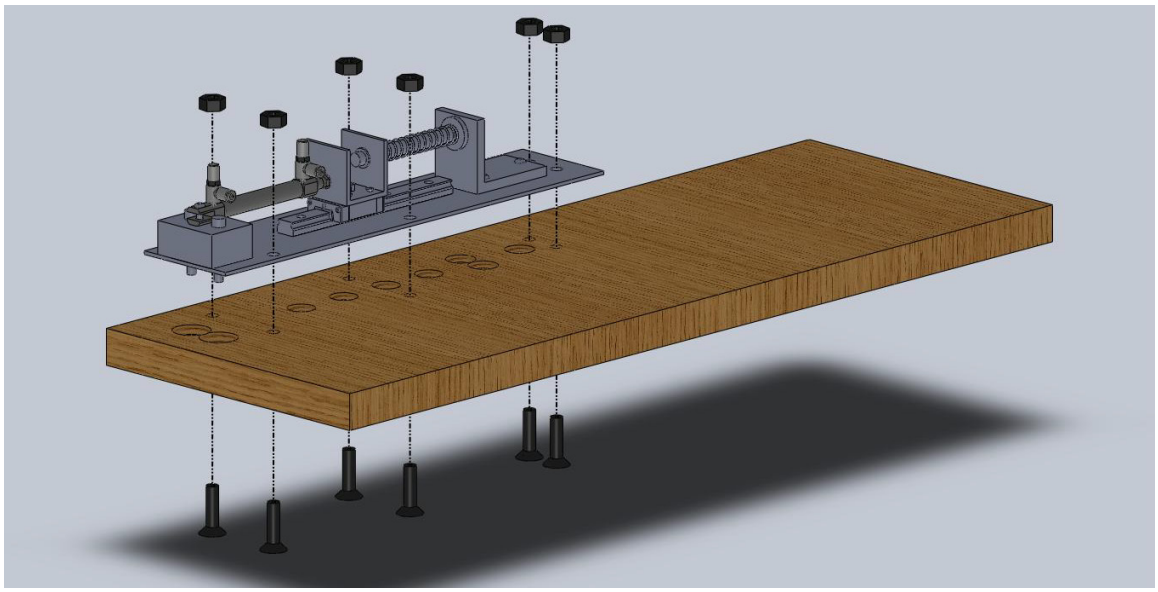

Figure 44 - Assembly Step 10

Step 11

Now attach all four pressure sensor and tee-fitting assemblies to the wood base with eight wood screws. Note that the air port on the side of the pressure sensor with the notch if for atmospheric pressure and should not be connected to the pressurized line. Screw in the sensors as shown in Figure 45, and as dimensionally documented in the engineering drawings.

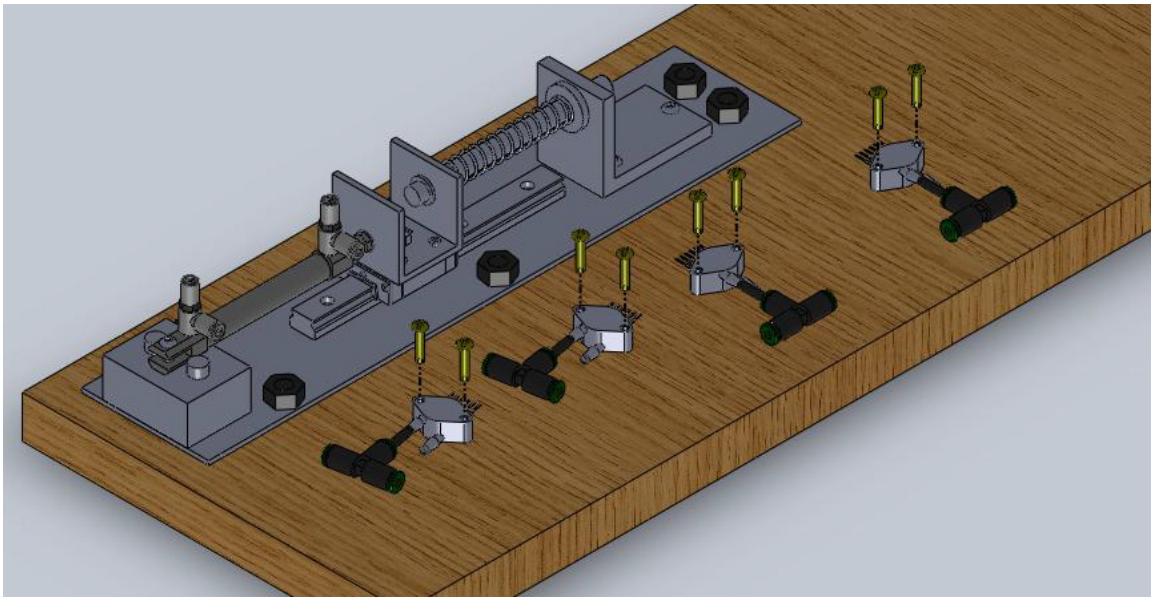

Figure 45 - Assembly Step 11

Step 12

Now place the solenoid, pressure regulator and on-off valve in place (attachment to the wood base not necessary) as shown in Figure 46. Note that the on-off valve is orientation specific and the arrows on the side denote the airflow.

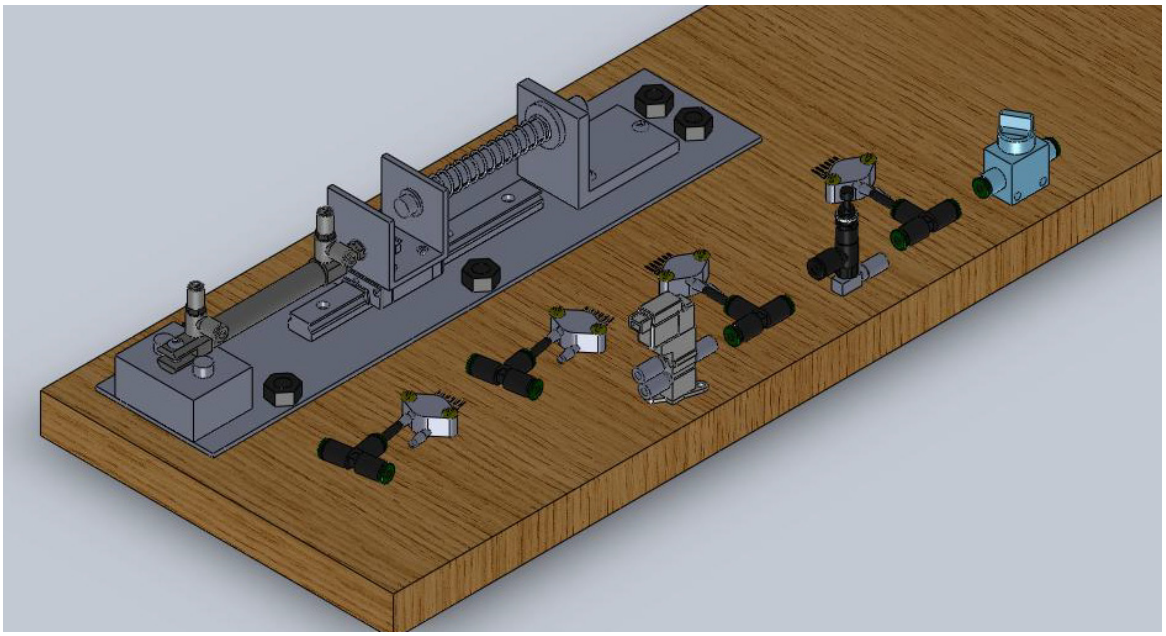

Figure 46 - Assembly Step 12

Step 13

Insert the tubing between the devices as shown in Figure 47, this should semi-secure the solenoid, pressure regulator, and on-off valve.

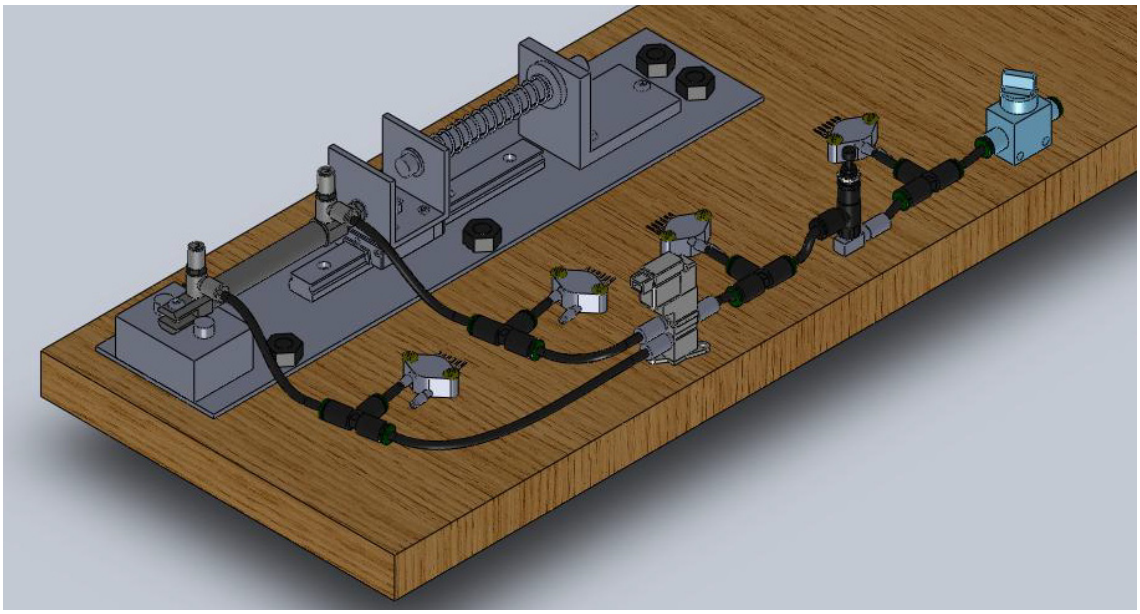

Figure 47 - Assembly Step 13

Step 14

Now attach the breadboard support to the wood base, as shown in Figure 48. First screw the breadboard risers into the breadboard support. In order to correctly align the breadboard risers, place the breadboard into the riser before tightening the screws. Second, use two wood screws to attach the breadboard support to the wood base.

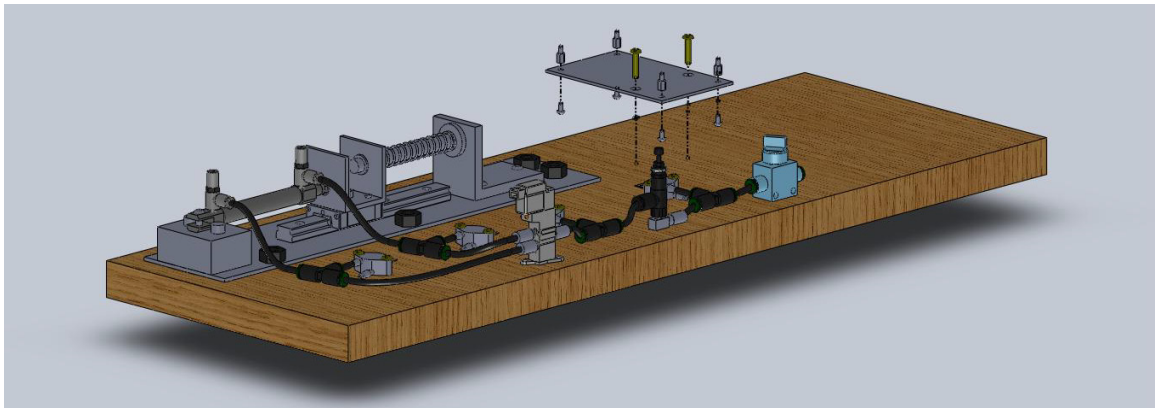

Figure 48 - Assembly Step 14

Step 15

No place the breadboard into the breadboard risers, and attach with the four corresponding nuts as shown in Figure 49.

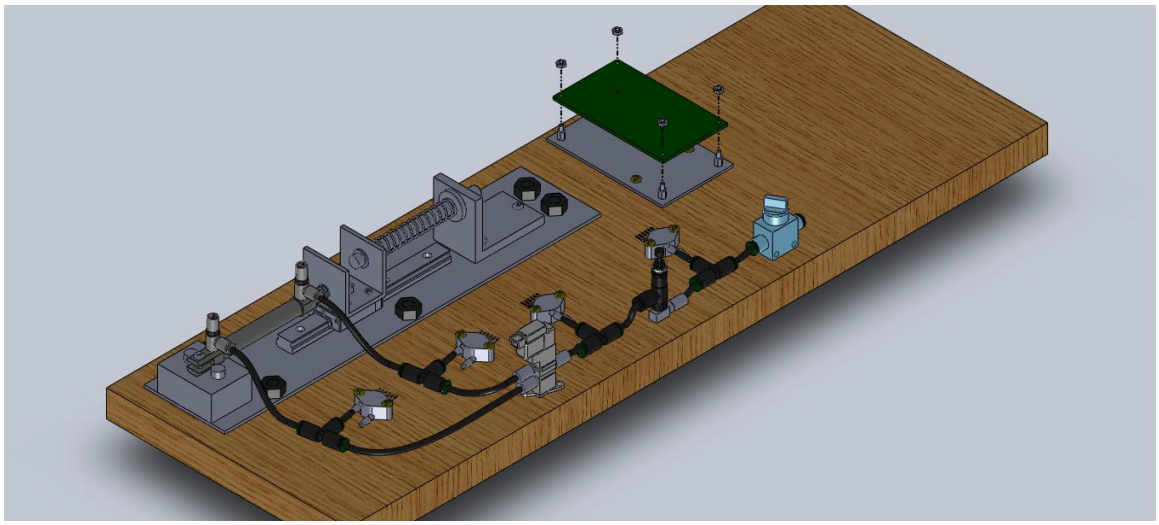

Figure 49 - Assembly Step 15

Step 16

Now attach the BNC bracket assembly to the wood base as shown in Figure 50. Screw the three wood screws through the BNC bracket into the wood base.

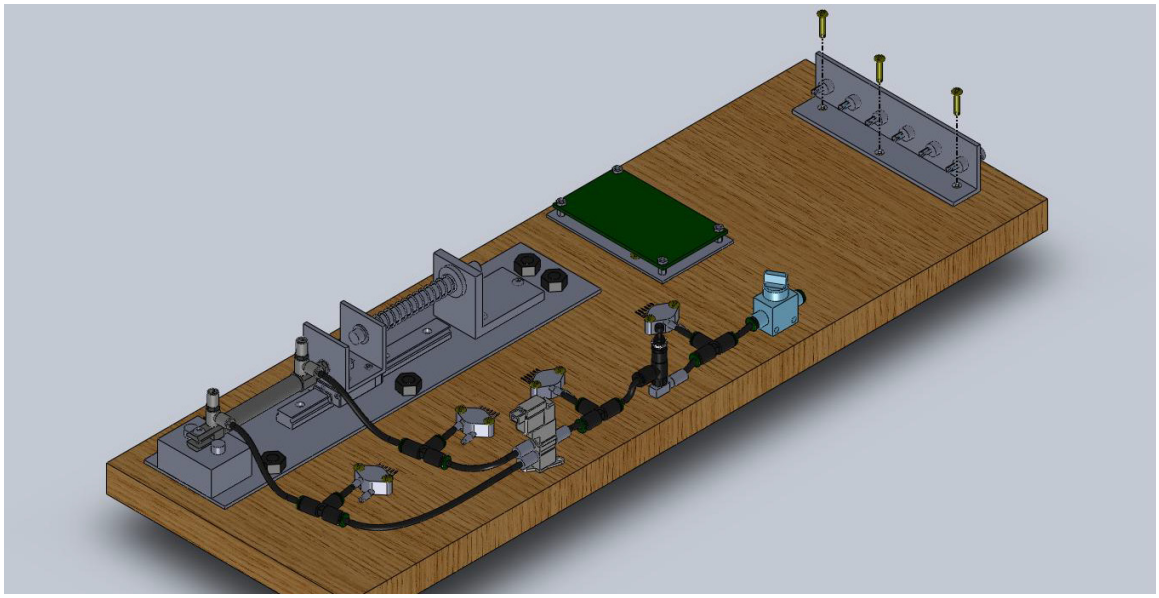

Figure 50 - Assembly Step 16

Step 17

Insert batteries and mount VEX controller to board as shown in Figure 51.

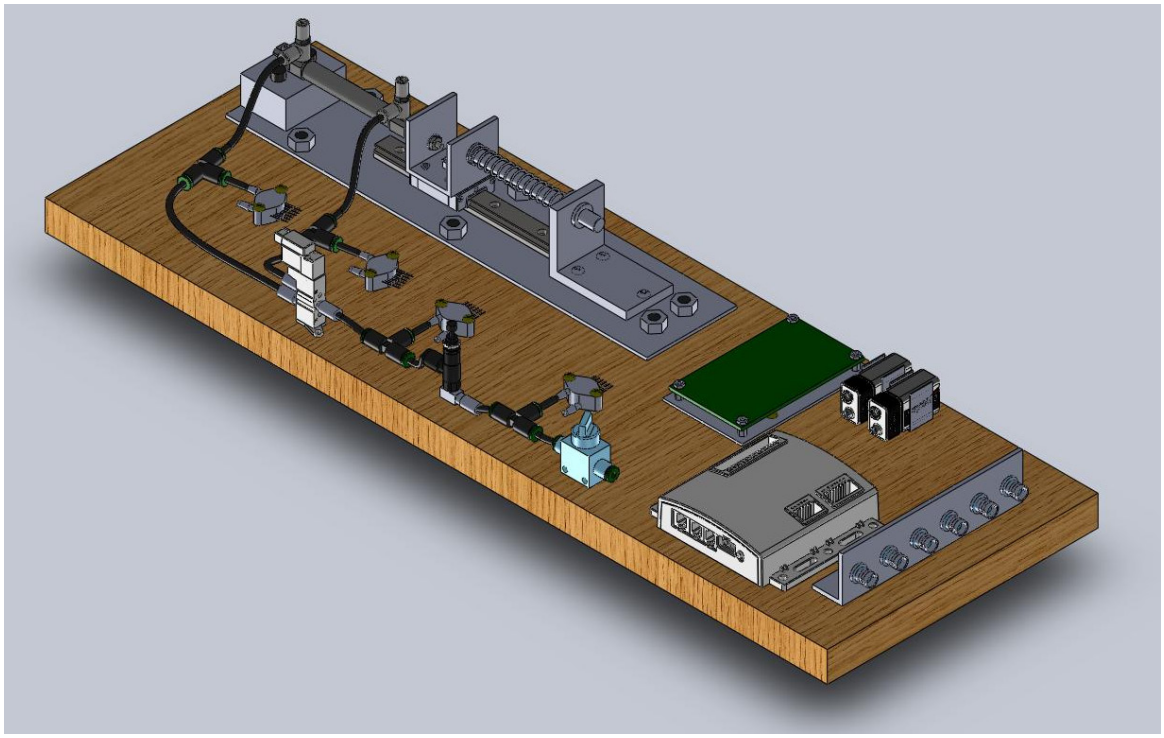

Figure 51 - Assembly Step 17

Step 18

Connect the wiring as shown in Figure 52 and Figure 53. First connect the pressure sensor leads from the breadboard to each pressure sensor. Note that each pressure sensor and lead are numbered and should be connected to the corresponding unit, and that the connector should be inserted so that the black wire connects to the pressure sensor pin with the notch, as illustrated in Figure 52. Finally, connect the wire from the solenoid to the VEX controller. Note that an extension for the default solenoid wire is provided, and that when connecting to the VEX controller, the pin connector should be inserted into port number 11 so that the white wire is facing the middle of the VEX controller and the black wire is facing the outside, as shown in Figure 53.

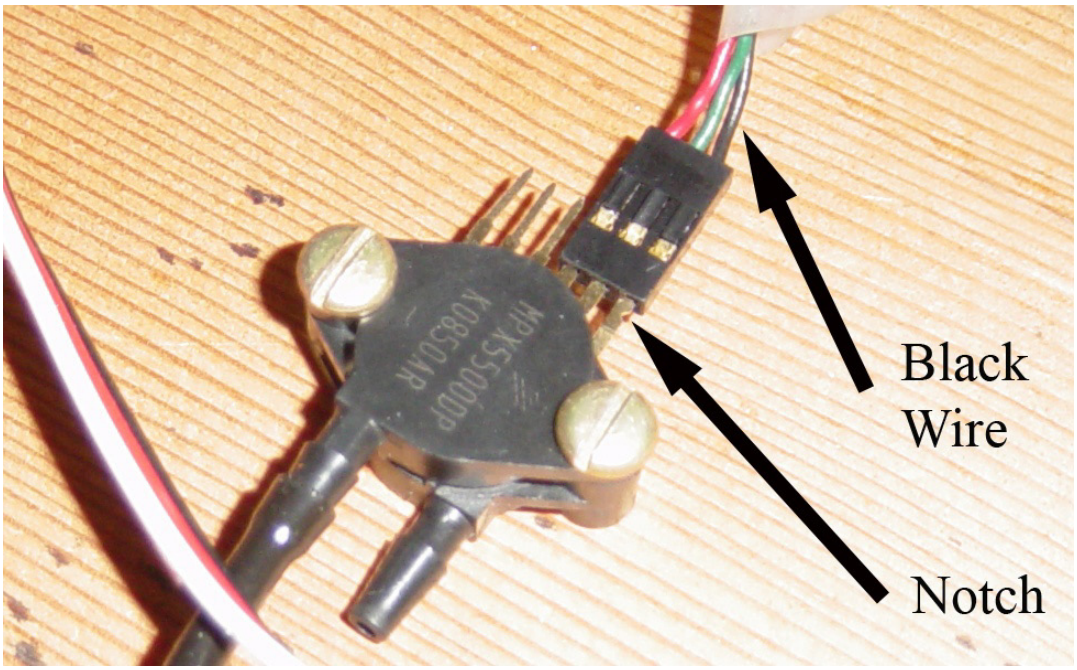

Figure 52 - Picture of the pressure sensor connector on the pressure sensor, depicting the orientation of the colored wires and the notch on the pressure sensor

Figure 53 - Image of the VEX controller and wire from the solenoid wire, noting order of the colored wires and port number of the connection

Appendix B. ***Operation Manual***

The following document provides instructions in the operation and maintenance of the Pneumatic Test Bed described in this document.

Step 1

The following instructions assume a fully assembled device as described in the installation manual, if the device is not fully assembled, please refer to Appendix A first.

Step 2

Operation of this device calls for the use of a VEX controller programmed to switch the flow of air within a solenoid every .8 seconds. In order to program the VEX controller, a simple while loop was created in Easy C, which is an integrated language that can be used in associated with the controller. The while loop switches the position of the solenoid valve from on (1) to off (0) every 800 milliseconds.

Step 3

Operation of the device requires a computer running LabVIEW and a DAQ. Connect the BNC ports on the device to the BNC ports on the DAQ using standard BNC cables. Due to the design of the VI, it is required that the accelerometer data connection be connected to “AI 0”, and that the pressure sensors be connected to “AI 1” through “AI 4”. The power to the accelerometer should be connected to “AO 0”.

Step 4

For best results it is recommended that the piston flow regulators be adjusted to the following recommended settings. The flow regulator that controls the outward stroke of the piston rod should be set to 1½ urns from the zero position (located where the screw is fully depressed), and the flow regulator that controls the return stroke of the piston rod be set to 4¾ turns from the zero position. Note that the numbers stated here are for the piston assembly that provided at the time of completion of this project, it was discovered that the internal resistance of the various identical piston assembles owned by WPI varies greatly due to improper operation and/or variances in manufacturing.

Step 5

The next step is to fill the air tank to power the pneumatics. Two tanks are available for use in HL031, a small three-gallon tank, and a larger twelve-gallon tank. The three-gallon tank will operate the device for about three to five minutes. In order to use the tanks in HL031, the threaded connection needs to be converted to 5/32-inch push to connect fitting, the conversion is shown in Figure 54, and can be found from parts in HL031. Since the pressure sensor has a maximum operating pressure of 72.5 psi, it is recommended that the tank be only filled to 70 psi. In order to get the best results the tank should be filled after going through a filter, which is available in the back of HL031 (Speed Aire Model 4ZL42), as shown in Figure 55. Once the tank is filled, connect the tank to the on-off valve on the device, while making sure that the on-off valve is closed.

Figure 54 - Fittings to convert threaded tank connection to 5/32 push-to-connect

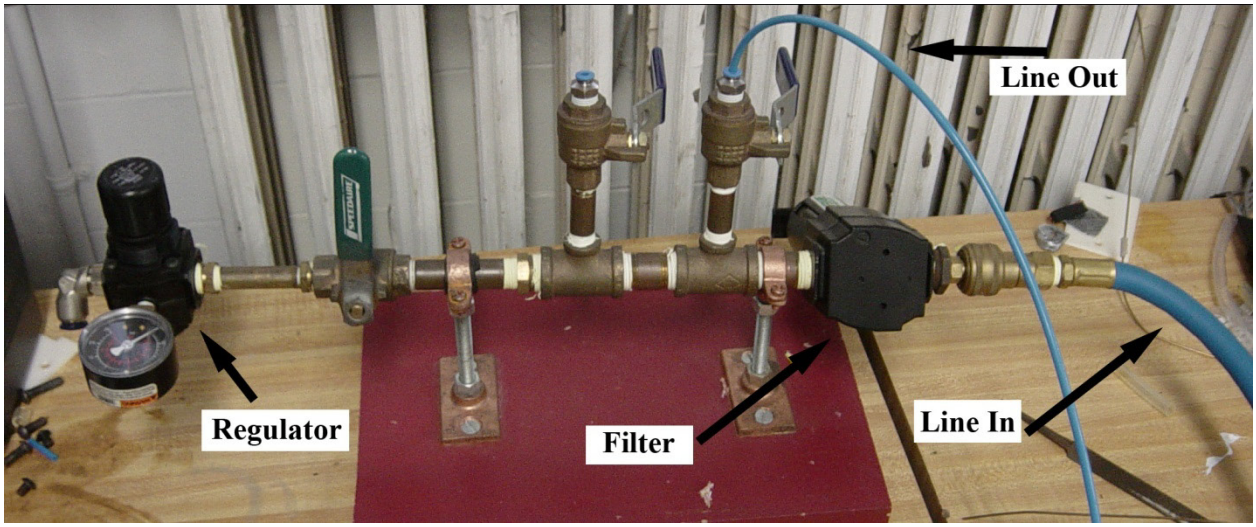

Figure 55 - Device with filter and dryer used to fill tank in HL031

Step 6

Connect the batteries for the device. First connect the two 9V batteries to the battery leads from the breadboard, and then the custom battery to the VEX controller.

Step 7

It is now time to set up the computer to display the desired data. Start by opening the file supplied with this report named PneumaticMQP_VI.vi in LabVIEW, the front panel should look like the screen shot seen below in Figure 56.

Step 8

The first step before running the VI is to set up the channels. As seen in the top left of Figure 56, the VI asks for the output voltage channel and the input channels. By clicking on the drop down box in output voltage, the user should select “ao0” of the device number that corresponds to the external DAQ. For the input channels, click on browse in the drop down menu and select “ai0” through “ai4” from the same device number.

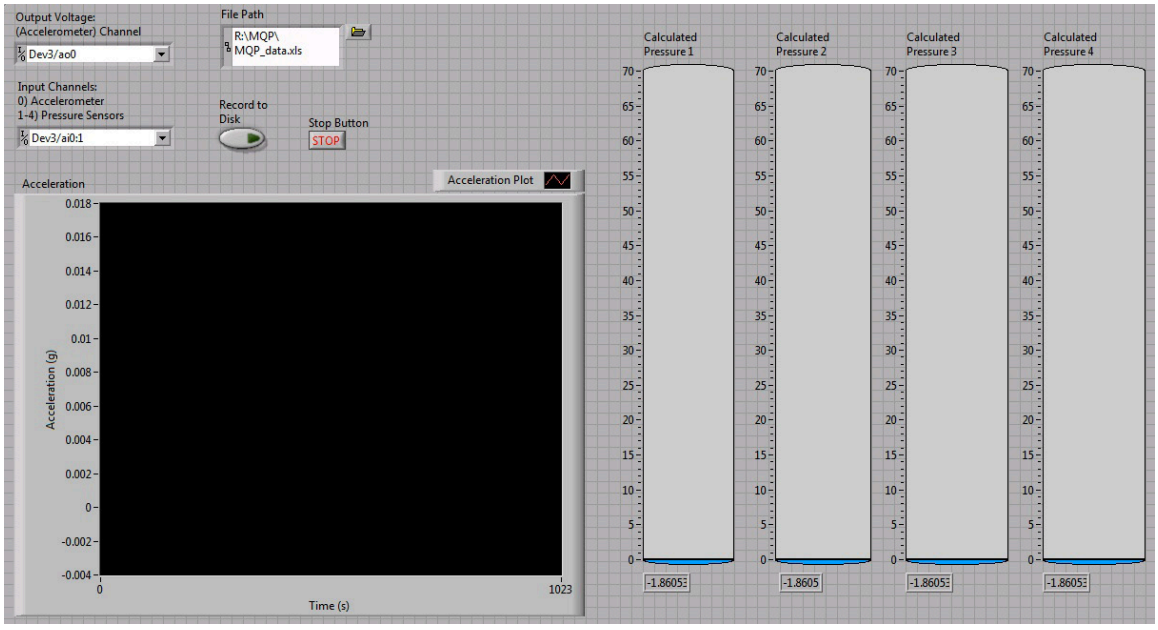

Figure 56 - LabVIEW VI initial screen

Step 9

In order to record the collected data to disk, a file path needs to be selected. By clicking on the folder icon next to the file path, browse to the location of an Excel .xls (not .xlsx) file the user created, where the data will be recorded to.

Step 10

It is now time to start the VI, press the start arrow, and the front panel should change and display constant noise in the accelerometer plot, and around zero psi in the pressure gages. At this point the on-off valve can be turned on (as well as the valve on the tank if closed), if the calculated pressure at point one is not consistent with the pressure of the tank, it may be necessary to recalibrate the sensors, as detailed in the maintenance section of this manual. The regulator can now be adjusted to bring the regulated pressure to a recommended 50 psi.

Step 11

The operation of the device can be initiated by switching on the VEX controller that operates the solenoid. Data can be recoded to the Excel file by pressing the green record to disk button, and stopped by pressing it again.

Step 12

To stop the device, turn the on-off valve to the off position, switch off the VEX controller, and stop the VI. Also disconnect the 9V batteries if device will be off for an extended period of time to conserve battery power.

Step 13

When the recoded data file is opened in Excel 2007, a few messages will be displayed due to the formatting of the data, the first should be answered “yes” and the next “finish.” The Excel spreadsheet shows each forward or backward motion of the device in sets of seven rows. The first set of rows show the content of each row in a set, specifically elapsed time, calculated pressure at each sensor,

acceleration, and force. Since the time value is only displayed in column one, and is zero for every other column in its row, the row of zeros can be used as an indicator of a different in or out stroke.

Step 14

In order to get different resistance values, the spring in the device has to be exchanged. To switch a spring the guide rod has to first be unscrewed, note that the spring should be under compression and will want to pop out. Then the spring in place has to be taken out and its replacement inserted in its place. Now the guide rod needs to be reinserted through the bushing, through the spring, and then screwed in. Before fully tightening the guide rod, make sure it is parallel to the linear slide in both the front and top plane.

There are three full sized springs, and one short spring available for use, the three full sized springs are color coded by resistance, where the red colored spring has a ‘k’ value of 15.59 b/in, while the yellow spring has a ‘k’ value of 5.27 lb/in, while the green spring has a ‘k’ value of 3.31 lb/in. The short spring is uncolored, and has a ‘k’ value of 3.14 lb/in, note that the short spring makes the device operate very violently, and should only be used at low pressures (start at around 5 psi).

Appendix C. Maintenance

Recalibrating the Pressure Sensors

Sometimes it is necessary to calibrate the pressure sensors, this may occur if the sensors read a number significantly different from 0 psi when no pressure is applied to the sensors, or the gage pressure of the tank differs from the calculated pressure in the sensor before the regulator. Due to the design limitations of the input voltage, as the capacity of the 9V batteries that power the sensors decreases, the voltage to each sensor also decreases, resulting in a varying voltage coming from each sensor. This means that the batteries in use should be kept fresh, and the sensors recalibrated frequently for best results. Possible solutions to this problem are discussed further in Section 8.2.1.

In order to calculate the slope and intercept, fill the tank to around 70 psi and hook it up to the device. Since only the sensor before the regulator is to be considered, the rest of the devise need not be operational. Next start the VI and switch the “calibrate pressure” switch to the on (bright green) position located in the maintenance section of the VI (below the main screen), as shown in Figure 57, and then enter the tank’s pressure into the box below the “gage pressure input” dial. Now record data in the VI for a few seconds, and then stop recording. Afterwards, drop the pressure in the tank by 10-15 psi, wait until the pressure has steadied out, record a few more seconds, and repeat until the tank is empty. Once all the readings have been taken, open the Excel file, which will show five columns with data, column one represents the voltage data for sensor one, column two, three and four sensor two, three and four respectfully, the last column contains the pressure values entered by the user. Next, plot the data with the voltage values from the first sensor on the X-Axis and the pressure values entered in the Y-Axis. Using a linear regression find the slope and intercept and input the numbers into the boxes shown in Figure 57. In order for the VI to reuse these values the next time the program is opened, select “Make Current Values Default” under the “Edit” menu. To make sure that the slope and intercept are accurate, empty the tank again while verifying that the calculated value is the same as the gage reading.

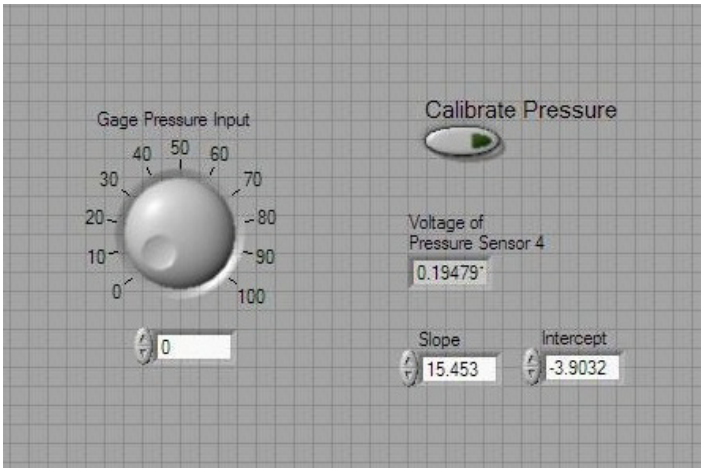

Figure 57 - Calibration front panel of the VI

For the simplicity of this VI, it has been assumed that the slope and intercept for each sensor is identical. Although this is not the case, the additional work required to calibrate the sensors was deemed too great for the minor accuracy increase that calibrating each sensor individually would cause. If the end user desired proper calibration of each sensor, the procedure above could be used on each sensor if the tank tube were connected to each sensor's tee-fitting. The VI would also have to be modified to apply a different slope and intercept value to each sensor.

Lubricating the Linear Slider

In order to keep the linear slider functioning properly it has to be lubricated on a regular basis. Lubricate the slider by applying some of the lithium grease as well as some WD-40 to the linear slide rail. Note, do not remove the linear slide block from the linear slide rail, as the remaining ball bearings will fall out of the assembly.

Tighten Bolts and Screws

Due to the repeated force that the device absorbs, the screws and bolts that hold the device together should be retightened occasionally to prevent one from loosening and failing.

Appendix D. Purchases

The following table contains all of the items that were purchased, acquired, or used in the construction of the final model. The costs shown reflect the price of the item at the time of purchase, and don't include tax or shipping. Manufacturer, supplier, model numbers, and other relevant information are included where available.

Part	Qty	Price (Unit)	Manufacturer	Supplier	Model
Pneumatic Components					
VEX Controler[1]	1	0.00	VEX	WPI	276-2170
Solenoid	1	0.00	VEX (Built by SMC)	WPI	SYJ3120-SMO-M3-F
Regulator[2]	1	0.00	VEX (Built by SMC)	WPI	ARJ1020F-M5-04
Piston Assembly[3]	1	0.00	VEX (Built by SMC)	WPI	NCJ2D10-200
On/Off Switch	1	0.00	VEX (Built by SMC)	WPI	VHK3-04F-04F
5/32" OD Tubing[4]	10	0.11	Coilhose Pneumatics	MSC Direct	NC2525-2500K
Tee-Fitting[5]	4	1.72	Parker	MSC Direct	364GC-5/32
Base Components					
Custom Aluminum Plate[6]	1	5.46	OnlineMetal	OnlineMetal	Custom
Custom Aluminum Block (Piston Riser)[7]	1	1.65	OnlineMetal	OnlineMetal	Custom
Aluminum Angle (Bushing Bracket)[8]	1	0.96	OnlineMetal	OnlineMetal	Custom
Aluminum Channel (Sliding Bracket)[9]	1	0.75	OnlineMetal	OnlineMetal	Custom
Aluminum Angle (BNC Bracket)[10]	1	1.50	OnlineMetal	OnlineMetal	Custom
Aluminum Rod[11]	1	0.00	UNKNOWN	WPI WB Scrap	N/A
Aluminum Plate (Breadboard Riser)	1	0.00	UNKNOWN	WPI WB Scrap	N/A
Plastic Bushing[12]	1	4.42	SmallParts	SmallParts	FBP-606104-02
Wood Base Plate	1	0.00	UNKNOWN	Self	N/A
Linear Slide[13]	1	95.11	THK	MSC Direct	RSR15ZMUU +150LM
Electronics					
Accelerometer[14]	1	0.00	Analog Devices	WPI	ADXL276 (AD22237)

Pressure Sensors	4	10.32	Freescale Semiconductor	Newark	MPX5500DP
Pressure Sensor Connector (plastic)	4	0.10	UNKNOWN	WPI ECE Shop	UNKNOWN
Pressure Sensor Connector (metal)	4	0.10	UNKNOWN	WPI ECE Shop	UNKNOWN
Solenoid Extension Wire	1	0.30	UNKNOWN	WPI ECE Shop	UNKNOWN
Wire	1	0.00	UNKNOWN	WPI	UNKNOWN
120 Ohm Resistor	1	0.10	UNKNOWN	WPI ECE Shop	UNKNOWN
75 Ohm Resistor	4	0.10	UNKNOWN	WPI ECE Shop	UNKNOWN
1 Micro Farad Capacitor	4	0.10	UNKNOWN	WPI ECE Shop	UNKNOWN
0.01 Micro Farad Capacitor	4	0.10	UNKNOWN	WPI ECE Shop	UNKNOWN
470 Pico Farad Capacitor	4	0.10	UNKNOWN	WPI ECE Shop	UNKNOWN
9V battery	2	1.00	UNKNOWN	WPI ECE Shop	UNKNOWN
BNC Connectors[15]	6	2.19	Amphenol	Newark	RF-31-10-RFX
Solderable Breadboard	1	1.00	UNKNOWN	WPI ECE Shop	UNKNOWN
Breadboard Riser and Hardware	4	0.10	UNKNOWN	WPI ECE Shop	UNKNOWN
Springs					
Short Spring (k=3.14) (set of 10)[16]	1	16.52	Gardner Spring, Inc	MSC Direct	2312031
Std. Spring (k=15.59) (set of 5)[16]	1	15.06	Gardner Spring, Inc	MSC Direct	2314441
Std. Spring (k=3.31) (set of 5)[16]	1	3.45	Lee Spring Company	MSC Direct	6811996
Std. Spring (k=5.27) (set of 5)[16]	1	3.45	Lee Spring Company	MSC Direct	6812077
Small Dia Spring (set of 12)[16]	1	7.91	Gardner Spring, Inc	MSC Direct	2311611
Other					
VEX Screws	4	0.00	VEX	WPI	UNKNOWN
Small Washer	7	0.00	UNKNOWN	WPI WB Shops	UNKNOWN
Medium Washer	3	0.00	UNKNOWN	WPI WB Shops	UNKNOWN
Large Washer	2	0.00	UNKNOWN	WPI WB Shops	UNKNOWN

Black Washer	2	0.00	UNKNOWN	WPI WB Shops	UNKNOWN
Long HEX Screws	2	0.00	UNKNOWN	WPI WB Shops	UNKNOWN
Short HEX Screws	1	0.00	UNKNOWN	WPI WB Shops	UNKNOWN
Countersunk Screws	4	0.00	UNKNOWN	WPI WB Shops	UNKNOWN
Flat Head Screws	4	0.00	UNKNOWN	WPI WB Shops	UNKNOWN
Small Nut	6	0.00	UNKNOWN	WPI WB Shops	UNKNOWN
Medium Nut	3	0.00	UNKNOWN	WPI WB Shops	UNKNOWN
Large Nut	2	0.00	UNKNOWN	WPI WB Shops	UNKNOWN
Wood Screw	13	1.00	UNKNOWN	WPI WB Shops	UNKNOWN
Countersunk Bolt	6	2.00	UNKNOWN	WPI WB Shops	UNKNOWN
Nut for Countersunk Bolt	6	3.00	UNKNOWN	WPI WB Shops	UNKNOWN
Multi-Purpose Lithium Grease (2-pack)[17]	1	4.74	LubriMatic	MSC Direct	11302
Unused					
Linear Slide[18]	1	3.31	Panasonic	DigiKey	PQ1060SA-ND
Std. Spring (k=8.67) (set of 5)[19]	1	3.57	Lee Spring Company	MSC Direct	6812150

Totals	
Total of Components	275.89
Budget	450.00
Funds Remaining	174.11

Note	**Comment**
1	Requires own battery, programming requires EasyC - see Professor Miller, Bradley A
2	Regulator also includes two bottom fittings

3	Piston includes two tamper proof speed controls, SMC model number AS1201F
4	MSC Direct Product Number:48635668 (quantity in feet, price/foot) Other colors available, sold in 10' increments
5	MSC Direct Product Number:84425412
6	14x3 inches, 0.1 Thick
7	1.5x2 inches, 0.8 Long
8	2"x3" Profile, 0.25'' Thick, 1.5" long
9	1.5"x1.5" Profile, 0.125'' Thick, 1.5" long
10	1"x1.5" Profile, 0.125'' Thick, 6" long
11	Approximate value: $0.50
12	3/8"ID x 5/8"OD x 1/2" Length White
13	Requires lubrication, cheaper to buy directly through THK, 150mm rail length – 32x43mm block, MSC Direct Product number:71462477
14	Provided by Professor Furlong, Model no longer made, similar model priced around $10 (per 1000 units)
15	Newark: 93F7577
16	Model number is MSC Direct Product Number
17	MSC Direct Product Number:00041335
18	Device broke, inconsistent data, replaced by accelerometer
19	Model number is MSC Direct Product Number, MSC Direct listed spring constant incorrectly, and diameter of spring too small for guide rod

Appendix E. Engineering Drawings

The following section provides engineering drawings for all of the custom made components, and reference drawings for some of the other components. Electronic versions of all the following drawings along with a solid model of the device can be found in the supplied files.

Partial solid models of the on-off valve, solenoid, regulator, and piston assembly were provided courtesy of SMC Corporation of America. The solid model of the linear slider assembly was provided courtesy of THK. The solid model of the VEX controller was provided courtesy of VEX Robotics. The 9V battery was provided courtesy of Randy Thompson through 3D Content Central. The solid model of the BNC connector was provided courtesy of Amphenol.

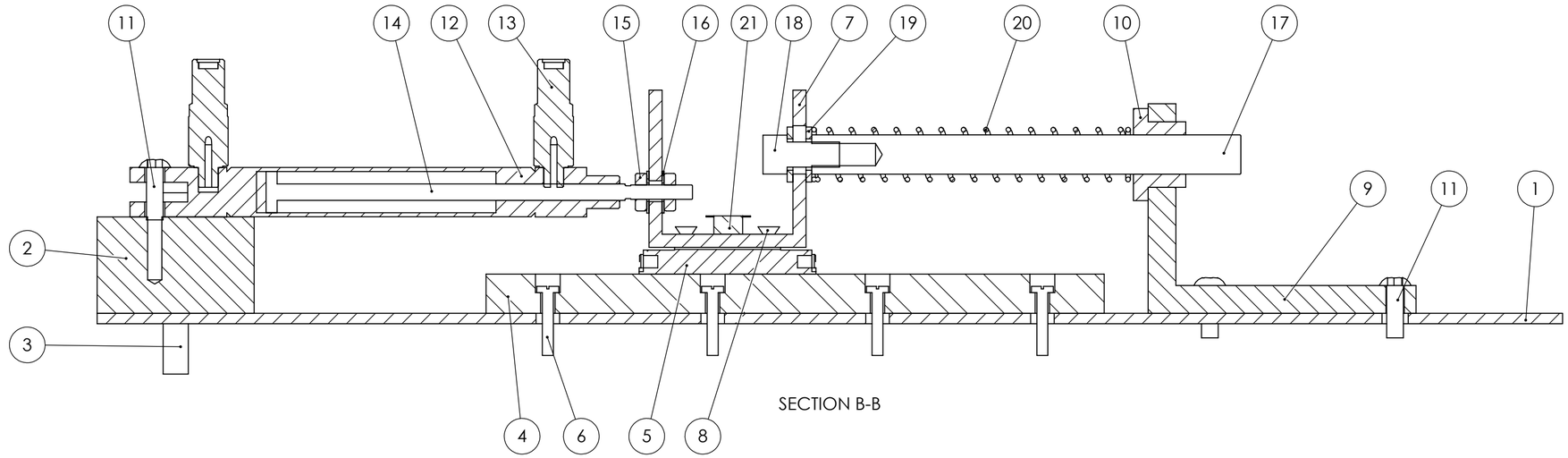

SECTION B-B

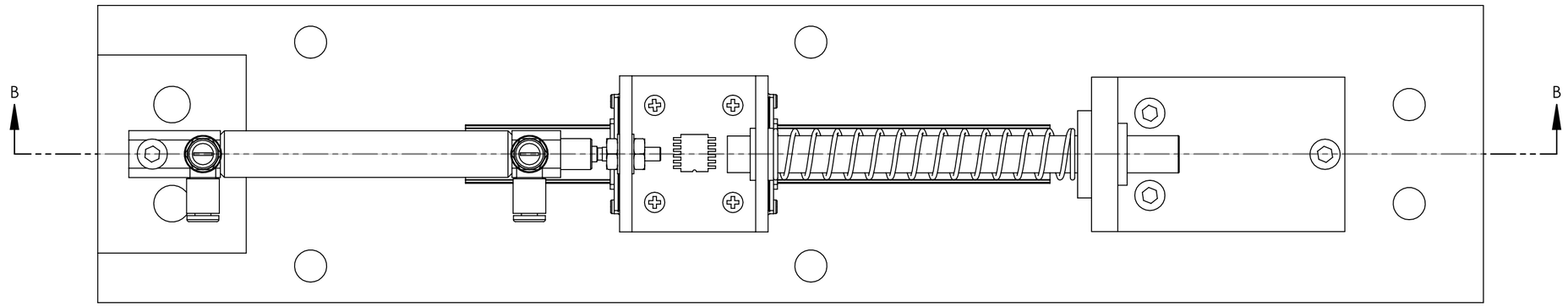

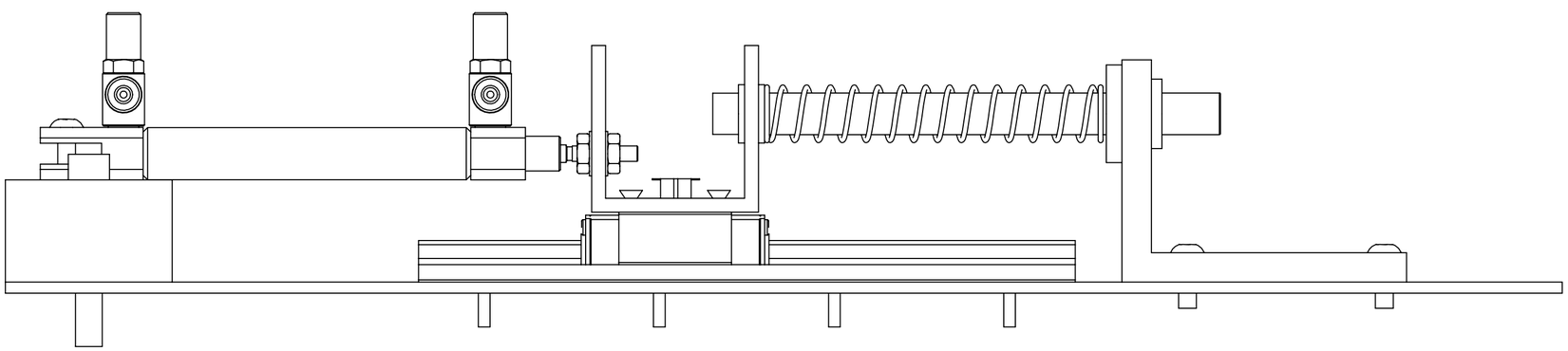

		UNLESS OTHERWISE SPECIFIED:		NAME	DATE
		DIMENSIONS ARE IN INCHES TOLERANCES: FRACTIONAL ±0.1 ANGULAR: MACH ±0.5 BEND ±0.5 ONE PLACE DECIMAL ± 0.1 TWO PLACE DECIMAL ± 0.05 THREE PLACE DECIMAL ± 0.005	DRAWN	BRW	2/25/10
			CHECKED		
			ENG APPR.		
			MFG APPR.		
			Q.A.		
		INTERPRET GEOMETRIC TOLERANCING PER:ASME Y14.5-2009	COMMENTS:		
		MATERIAL			
NEXT ASSY	USED ON	FINISH			
APPLICATION		DO NOT SCALE DRAWING			

TITLE:

Dynamic Assembly Cutaway View

SIZE	DWG. NO.	REV
C		A

SCALE: 1:1	WEIGHT:	SHEET 1 OF 2

ITEM NO.	DESCRIPTION	QTY.
1	Aluminum Base	1
2	Piston Riser	1
3	Piston Riser Bolt	2
4	Linear Slide Rail	1
5	Linear Slide Block	1
6	Linear Slide Bolt	4
7	Sliding Bracket	1
8	Sliding Bracket Screw	4
9	Bushing Bracket	1
10	Bushing	1
11	VEX Screw	4
12	Piston Cylinder	1
13	Piston Flow Valve	2
14	Piston Rod	1
15	Piston Rod Nut	2
16	Piston Rod Washer	2
17	Guide Rod	1
18	Guide Rod Screw	1
19	Guide Rod Washer	2
20	Spring	1
21	Accelerometer	1

NEXT ASSY | USED ON

APPLICATION

UNLESS OTHERWISE SPECIFIED:

DIMENSIONS ARE IN INCHES
TOLERANCES:
FRACTIONAL ±0.1
ANGULAR: MACH ±0.5 BEND ±0.5
ONE PLACE DECIMAL ± 0.1
TWO PLACE DECIMAL ± 0.05
THREE PLACE DECIMAL ± 0.005

INTERPRET GEOMETRIC TOLERANCING PER:ASME Y14.5-2009

MATERIAL

FINISH

DO NOT SCALE DRAWING

	NAME	DATE
DRAWN	BRW	3/10/10
CHECKED		
ENG APPR.		
MFG APPR.		
Q.A.		

COMMENTS:

TITLE:
Dynamic Assembly Cutaway View

SIZE **A** | DWG. NO. | REV **A**

SCALE: 1:1 | WEIGHT: | SHEET 2 OF 2

5 4 3 2 1

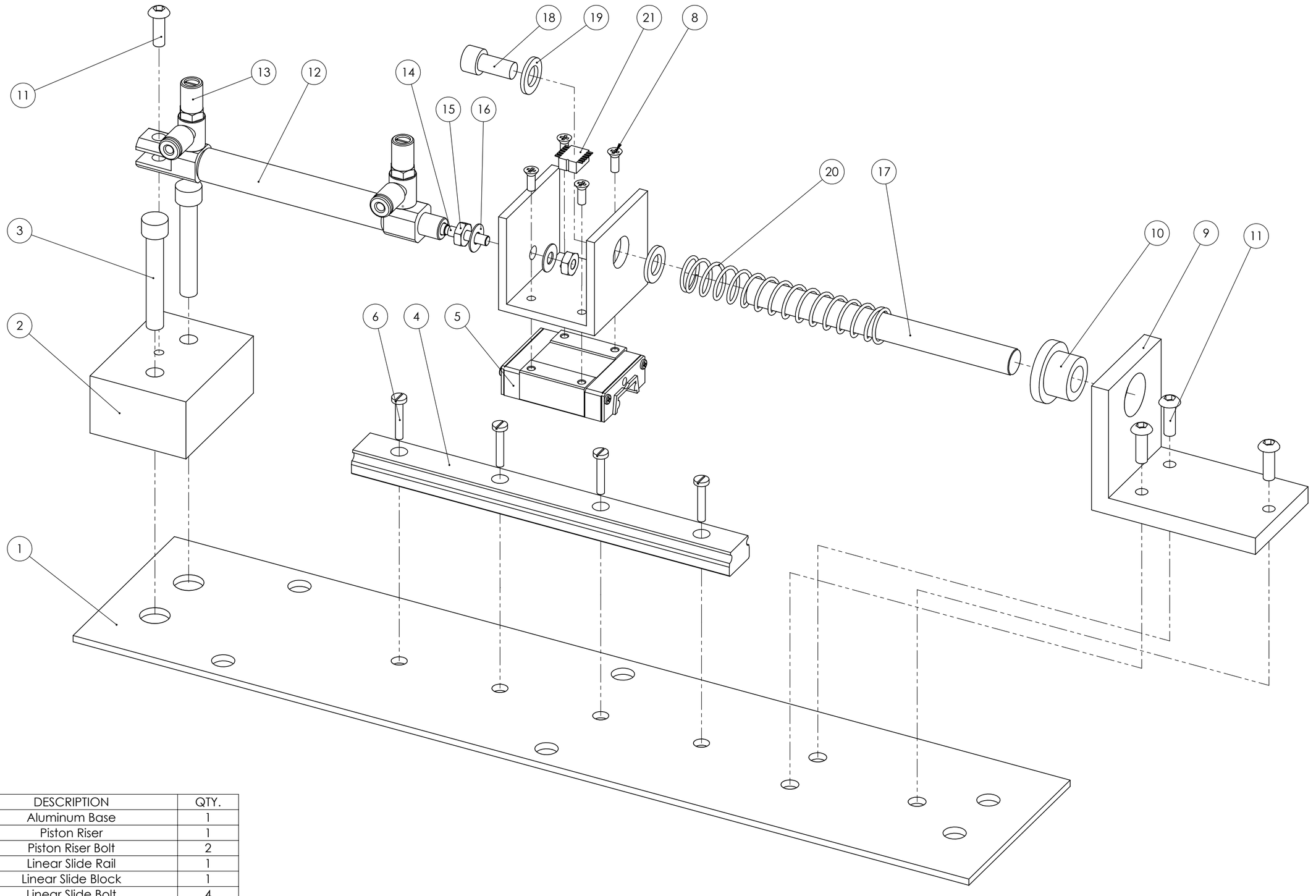

ITEM NO.	DESCRIPTION	QTY.
1	Aluminum Base	1
2	Piston Riser	1
3	Piston Riser Bolt	2
4	Linear Slide Rail	1
5	Linear Slide Block	1
6	Linear Slide Bolt	4
7	Sliding Bracket	1
8	Sliding Bracket Screw	4
9	Bushing Bracket	1
10	Bushing	1
11	VEX Screw	4
12	Piston Cylinder	1
13	Piston Flow Valve	2
14	Piston Rod	1
15	Piston Rod Nut	2
16	Piston Rod Washer	2
17	Guide Rod	1
18	Guide Rod Screw	1
19	Guide Rod Washer	2
20	Spring	1
21	Accelerometer	1

		UNLESS OTHERWISE SPECIFIED:		NAME	DATE
		DIMENSIONS ARE IN INCHES TOLERANCES: FRACTIONAL ±0.1 ANGULAR: MACH ±0.5 BEND ±0.5 ONE PLACE DECIMAL ± 0.1 TWO PLACE DECIMAL ± 0.05 THREE PLACE DECIMAL ± 0.005	DRAWN	BRW	2/23/10
			CHECKED		
			ENG APPR.		
			MFG APPR.		
		INTERPRET GEOMETRIC TOLERANCING PER:ASME Y14.5-2009	Q.A.		
		MATERIAL	COMMENTS:		
NEXT ASSY	USED ON	FINISH			
APPLICATION		DO NOT SCALE DRAWING			

TITLE:

Dynamic Assembly Exploded View

SIZE	DWG. NO.	REV
C		A

SCALE: 1:1	WEIGHT:	SHEET 1 OF 2

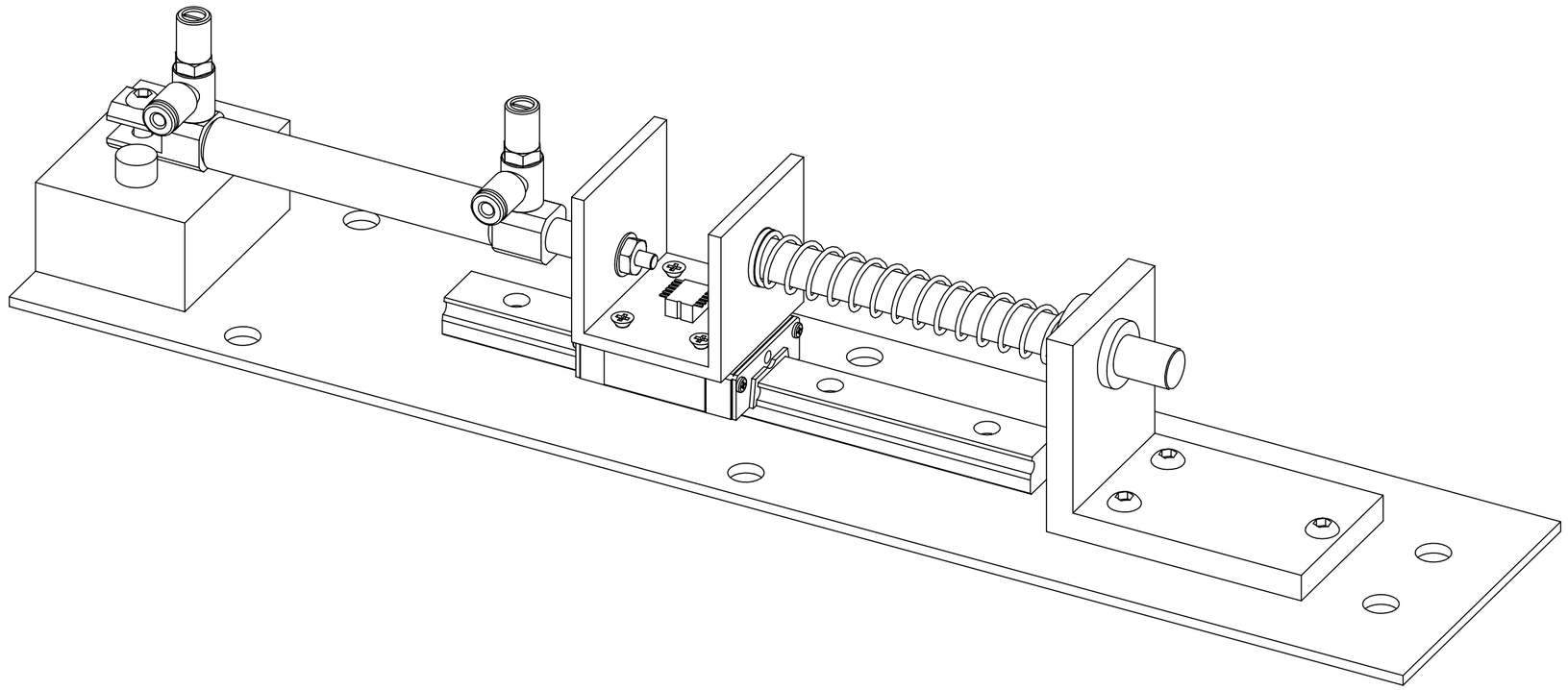

		UNLESS OTHERWISE SPECIFIED:		NAME	DATE
		DIMENSIONS ARE IN INCHES TOLERANCES: FRACTIONAL ±0.1 ANGULAR: MACH ±0.5 BEND ±0.5 ONE PLACE DECIMAL ± 0.1 TWO PLACE DECIMAL ± 0.05 THREE PLACE DECIMAL ± 0.005	DRAWN	BRW	3/10/10
			CHECKED		
			ENG APPR.		
			MFG APPR.		
		INTERPRET GEOMETRIC TOLERANCING PER:ASME Y14.5-2009	Q.A.		
		MATERIAL	COMMENTS:		
NEXT ASSY	USED ON	FINISH			
APPLICATION		DO NOT SCALE DRAWING			

TITLE:

Dynamic Assembly Exploded View

SIZE	DWG. NO.	REV
C		A

SCALE: 1:1	WEIGHT:	SHEET 2 OF 2

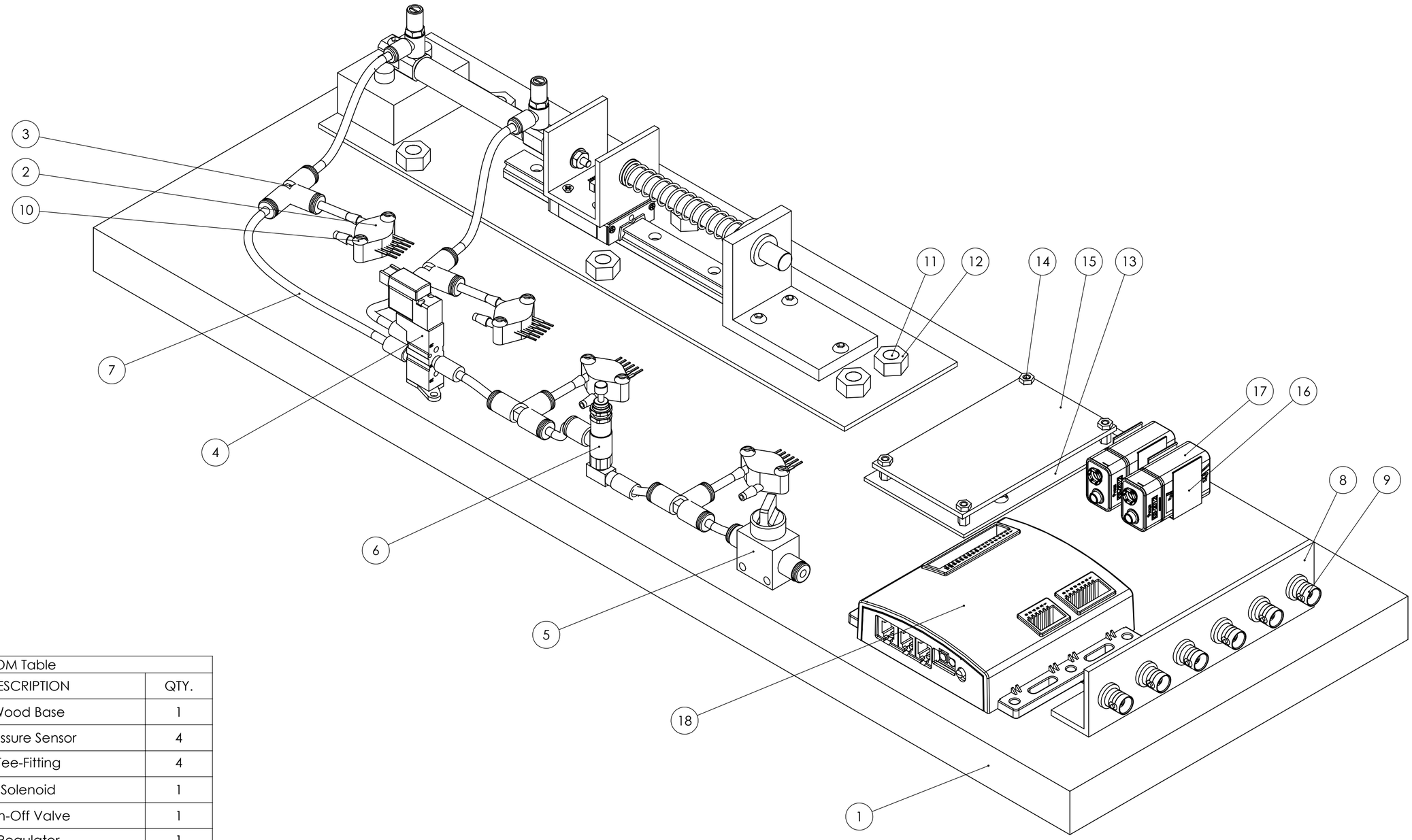

BOM Table		
ITEM NO.	DESCRIPTION	QTY.
1	Wood Base	1
2	Pressure Sensor	4
3	Tee-Fitting	4
4	Solenoid	1
5	On-Off Valve	1
6	Regulator	1
7	Pneumatic Tubing	1
8	BNC Bracket	1
9	BNC Connector	6
10	Wood Screw	13
11	Bolt	6
12	Nut	6
13	Breadboard Support	1
14	Breadboard Riser	4
15	Breadboard	1
16	Battery Holder	2
17	9V Battery	2
18	VEX Controler	1

		UNLESS OTHERWISE SPECIFIED:		NAME	DATE
		DIMENSIONS ARE IN INCHES TOLERANCES: FRACTIONAL ±0.1 ANGULAR: MACH ±0.5 BEND ±0.5 ONE PLACE DECIMAL ± 0.1 TWO PLACE DECIMAL ± 0.05 THREE PLACE DECIMAL ± 0.005	DRAWN	BRW	3/13/10
			CHECKED		
			ENG APPR.		
			MFG APPR.		
			Q.A.		
		INTERPRET GEOMETRIC TOLERANCING PER:ASME Y14.5-2009	COMMENTS:		
		MATERIAL			
NEXT ASSY	USED ON	FINISH			
APPLICATION		DO NOT SCALE DRAWING			

TITLE:
Full Assembly Isometric View

SIZE	DWG. NO.	REV
C		A
SCALE: 1:2	WEIGHT:	SHEET 1 OF 1

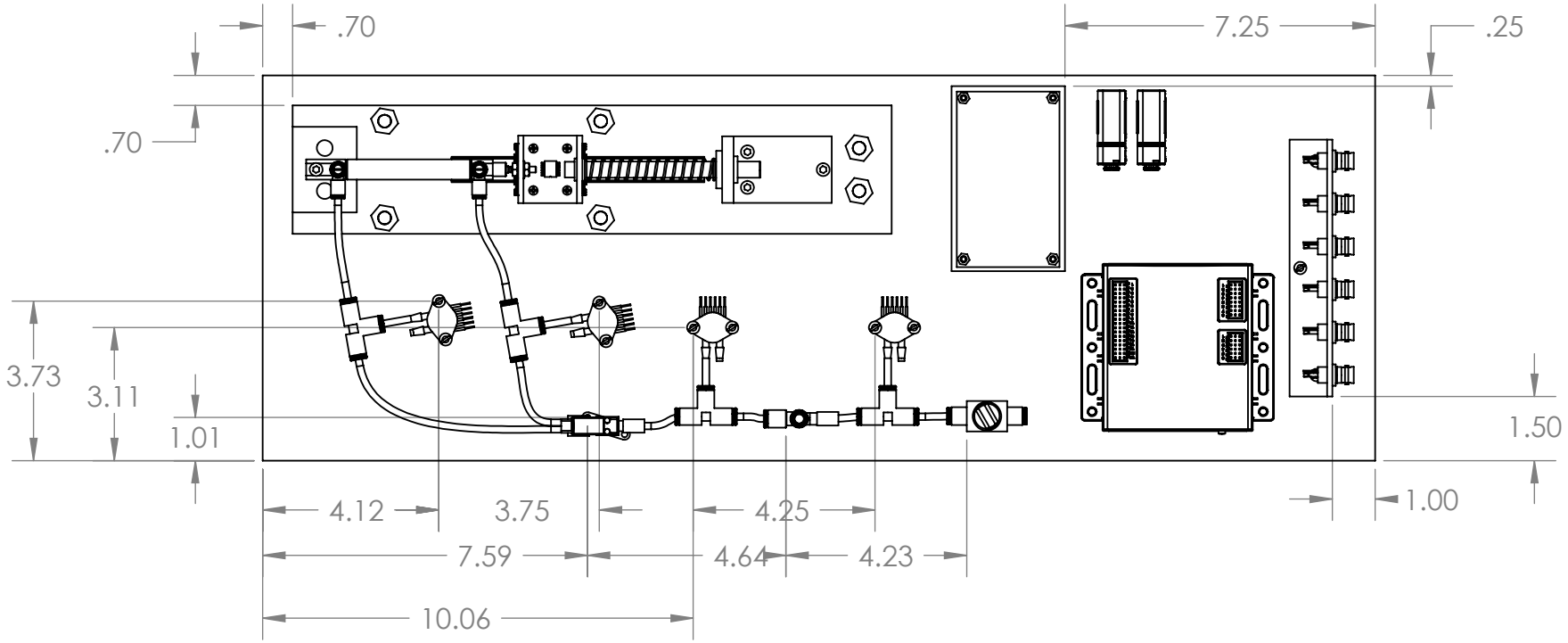

		UNLESS OTHERWISE SPECIFIED:		NAME	DATE
		DIMENSIONS ARE IN INCHES TOLERANCES: FRACTIONAL ±0.1 ANGULAR: MACH ±0.5 BEND ±0.5 ONE PLACE DECIMAL ± 0.1 TWO PLACE DECIMAL ± 0.05 THREE PLACE DECIMAL ± 0.005	DRAWN	BRW	2/20/10
			CHECKED		
			ENG APPR.		
			MFG APPR.		
		INTERPRET GEOMETRIC TOLERANCING PER:ASME Y14.5-2009	Q.A.		
		MATERIAL Aluminium	COMMENTS:		
NEXT ASSY	USED ON	FINISH			
APPLICATION		DO NOT SCALE DRAWING			

TITLE:
Assembly Overview

SIZE	DWG. NO.	REV
A		A

SCALE: 1:4 | WEIGHT: | SHEET 1 OF 1

5 4 3 2 1

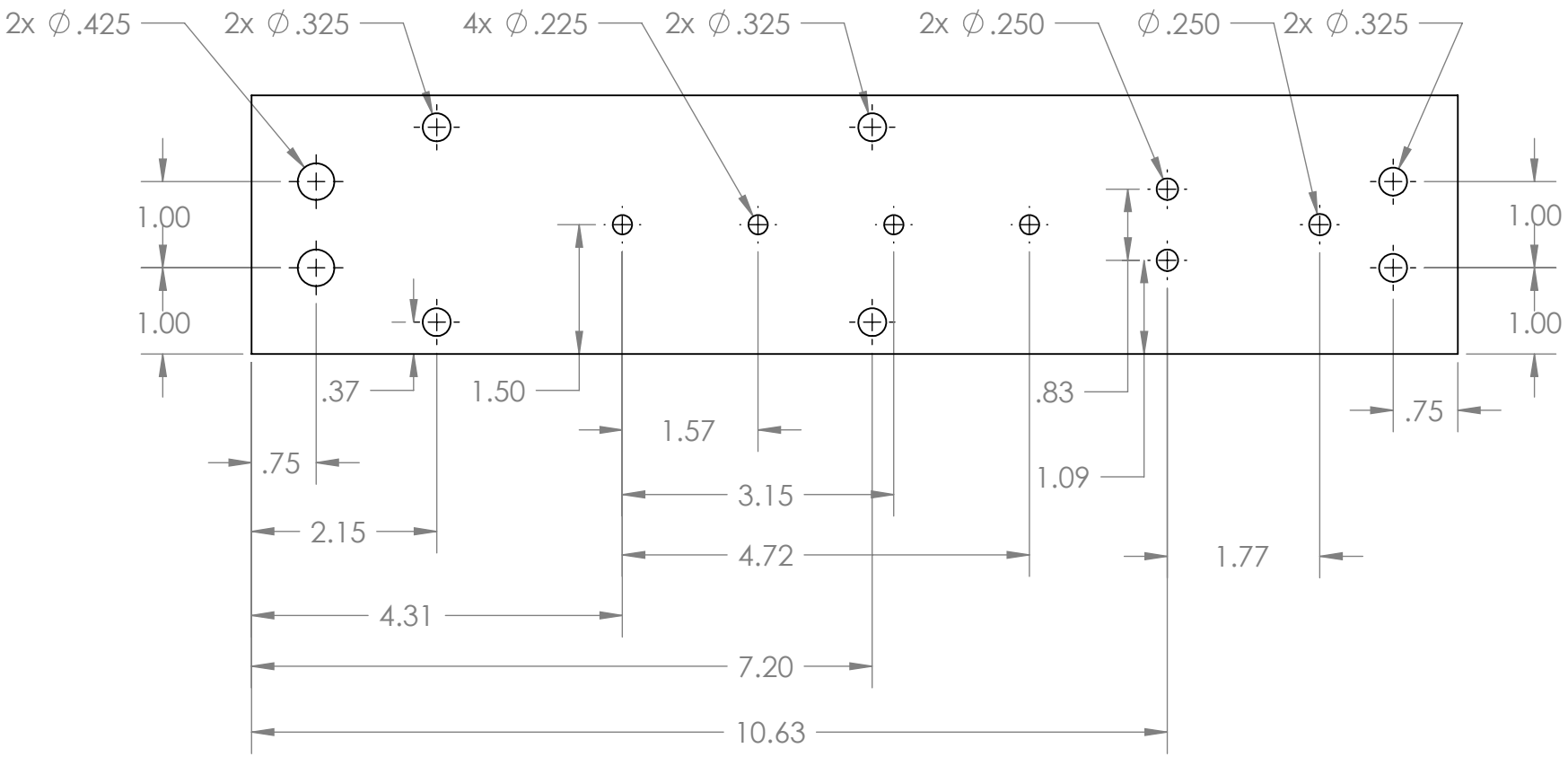

NOTE: Plate 0.1 Inches Thick

		UNLESS OTHERWISE SPECIFIED:		NAME	DATE
		DIMENSIONS ARE IN INCHES TOLERANCES: FRACTIONAL ±0.1 ANGULAR: MACH ±0.5 BEND ±0.5 ONE PLACE DECIMAL ± 0.1 TWO PLACE DECIMAL ± 0.05 THREE PLACE DECIMAL ± 0.005	DRAWN	BRW	2/14/10
			CHECKED		
			ENG APPR.		
			MFG APPR.		
		INTERPRET GEOMETRIC TOLERANCING PER:ASME Y14.5-2009	Q.A.		
		MATERIAL Aluminium	COMMENTS:		
NEXT ASSY	USED ON	FINISH			
APPLICATION		DO NOT SCALE DRAWING			

TITLE:

Aluminum Base

SIZE	DWG. NO.	REV
A		B

SCALE: 1:2	WEIGHT:	SHEET 1 OF 1

5 4 3 2 1

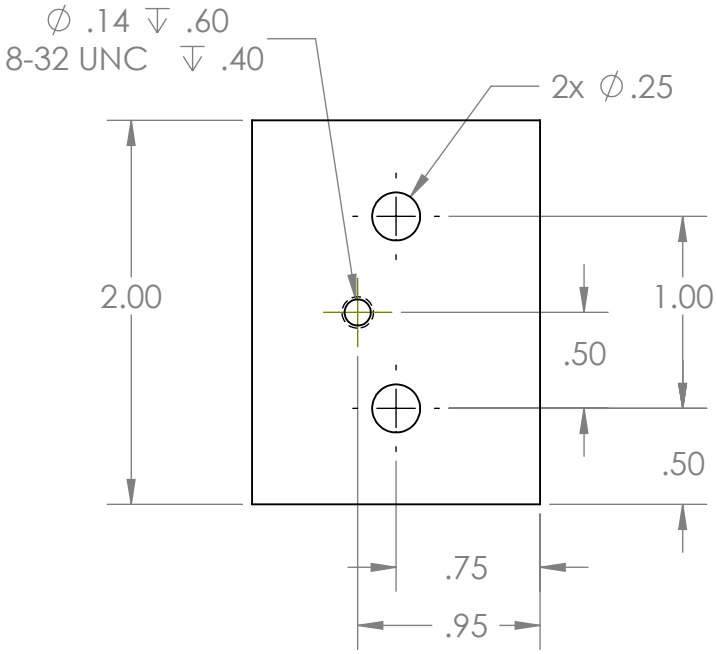

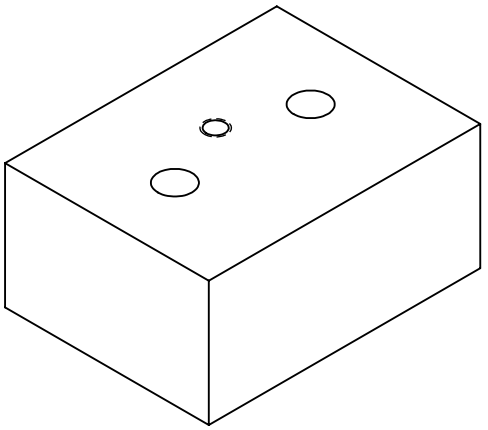

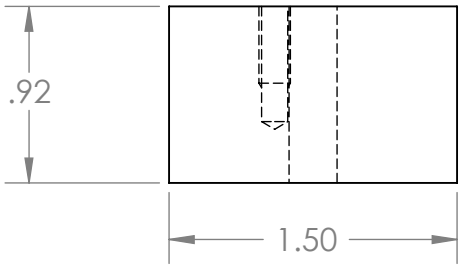

		UNLESS OTHERWISE SPECIFIED:		NAME	DATE
		DIMENSIONS ARE IN INCHES TOLERANCES: FRACTIONAL ±0.1 ANGULAR: MACH ±0.5 BEND ±0.5 ONE PLACE DECIMAL ± 0.1 TWO PLACE DECIMAL ± 0.05 THREE PLACE DECIMAL ± 0.005	DRAWN	BRW	2/14/10
			CHECKED		
			ENG APPR.		
			MFG APPR.		
			Q.A.		
		INTERPRET GEOMETRIC TOLERANCING PER:ASME Y14.5-2009	COMMENTS:		
		MATERIAL Aluminium			
NEXT ASSY	USED ON	FINISH			
APPLICATION		DO NOT SCALE DRAWING			

TITLE:

Piston Riser

SIZE	DWG. NO.	REV
A		A

SCALE: 1:1	WEIGHT:	SHEET 1 OF 1

5 4 3 2 1

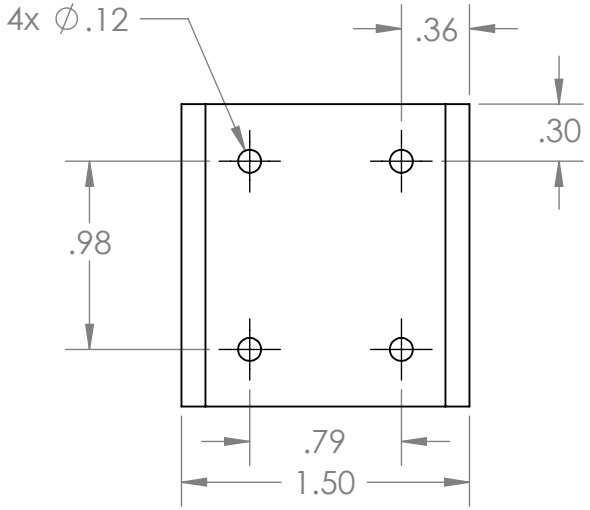

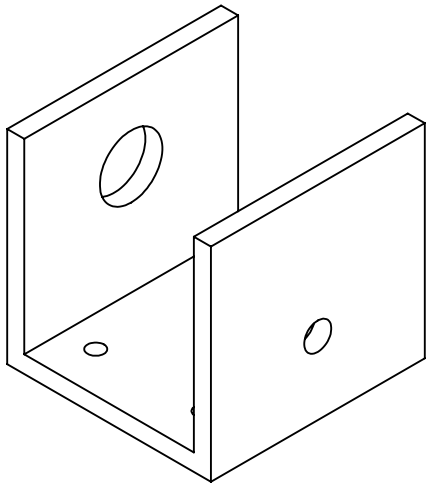

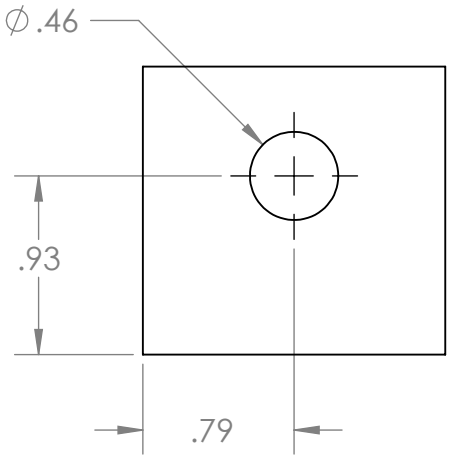

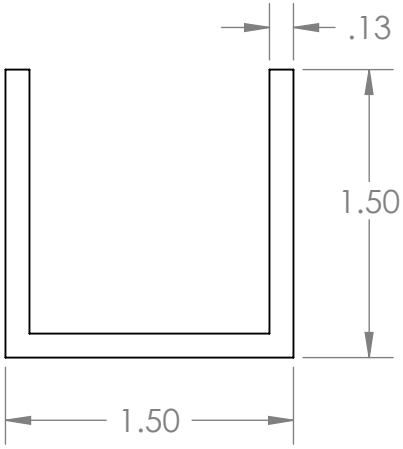

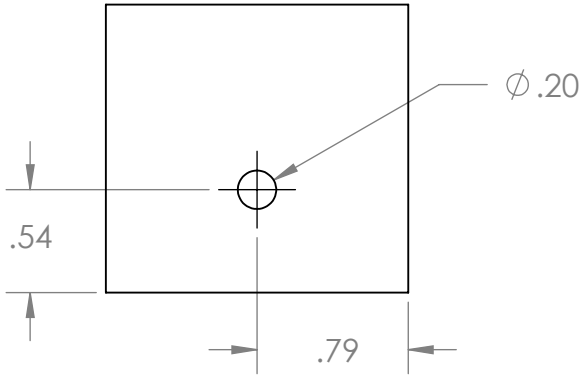

		UNLESS OTHERWISE SPECIFIED:		NAME	DATE
		DIMENSIONS ARE IN INCHES TOLERANCES: FRACTIONAL ±0.1 ANGULAR: MACH ±0.5 BEND ±0.5 ONE PLACE DECIMAL ± 0.1 TWO PLACE DECIMAL ± 0.05 THREE PLACE DECIMAL ± 0.005	DRAWN	BRW	2/16/10
			CHECKED		
			ENG APPR.		
			MFG APPR.		
		INTERPRET GEOMETRIC TOLERANCING PER:ASME Y14.5-2009	Q.A.		
		MATERIAL Aluminium	COMMENTS:		
NEXT ASSY	USED ON	FINISH			
APPLICATION		DO NOT SCALE DRAWING			

TITLE:

Sliding Bracket

SIZE	DWG. NO.	REV
A		B

SCALE: 1:1	WEIGHT:	SHEET 1 OF 1

5 4 3 2 1

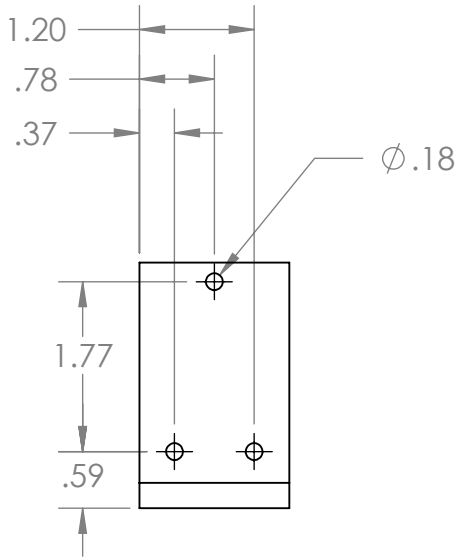

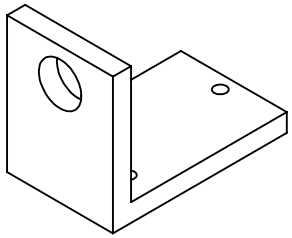

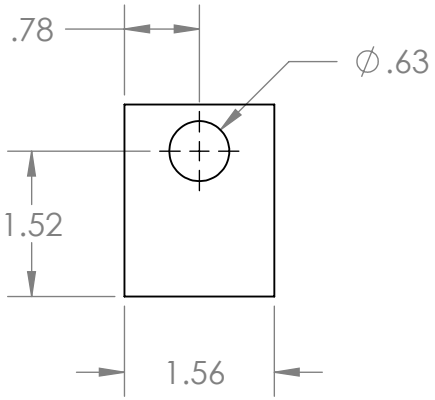

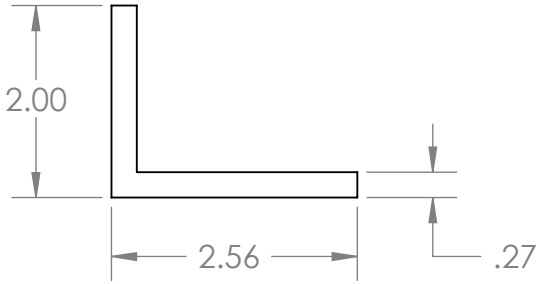

		UNLESS OTHERWISE SPECIFIED:		NAME	DATE
		DIMENSIONS ARE IN INCHES TOLERANCES: FRACTIONAL ±0.1 ANGULAR: MACH ±0.5 BEND ±0.5 ONE PLACE DECIMAL ± 0.1 TWO PLACE DECIMAL ± 0.05 THREE PLACE DECIMAL ± 0.005	DRAWN	BRW	3/1/10
			CHECKED		
			ENG APPR.		
			MFG APPR.		
		INTERPRET GEOMETRIC TOLERANCING PER:ASME Y14.5-2009	Q.A.		
		MATERIAL Aluminium	COMMENTS:		
NEXT ASSY	USED ON	FINISH			
APPLICATION		DO NOT SCALE DRAWING			

TITLE:

Bushing Bracket

SIZE	DWG. NO.	REV
A		B

SCALE: 1:2 | WEIGHT: | SHEET 1 OF 1

5 4 3 2 1

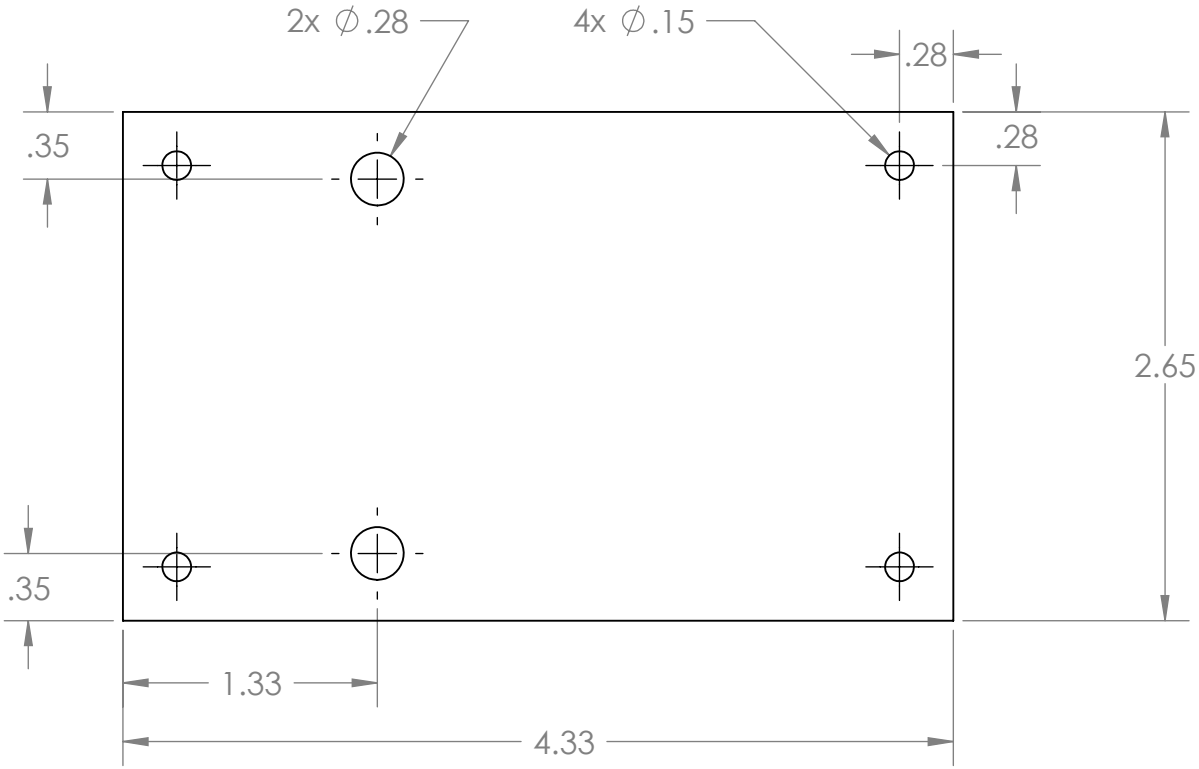

NOTE: Plate .075 Thick

		UNLESS OTHERWISE SPECIFIED:		NAME	DATE
		DIMENSIONS ARE IN INCHES TOLERANCES: FRACTIONAL ±0.1 ANGULAR: MACH ±0.5 BEND ±0.5 ONE PLACE DECIMAL ± 0.1 TWO PLACE DECIMAL ± 0.05 THREE PLACE DECIMAL ± 0.005	DRAWN	BRW	2/20/10
			CHECKED		
			ENG APPR.		
			MFG APPR.		
		INTERPRET GEOMETRIC TOLERANCING PER:ASME Y14.5-2009	Q.A.		
		MATERIAL Aluminium	COMMENTS:		
NEXT ASSY	USED ON	FINISH			
APPLICATION		DO NOT SCALE DRAWING			

TITLE:

Breadboard Support

SIZE	DWG. NO.	REV
A		A

SCALE: 1:1 | WEIGHT: | SHEET 1 OF 1

5 4 3 2 1

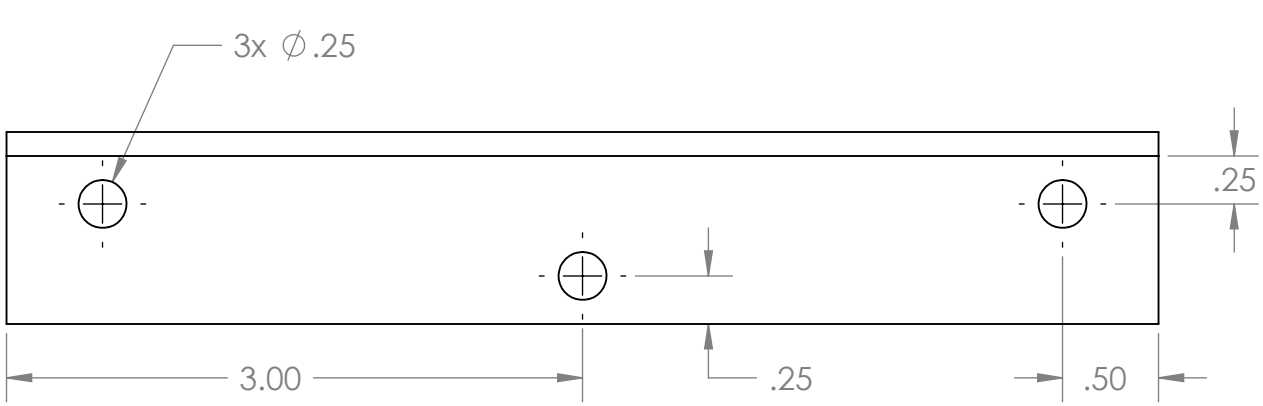

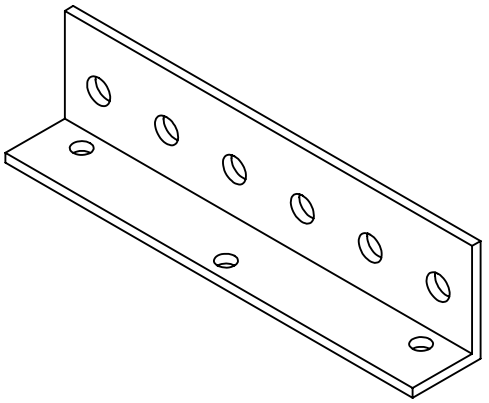

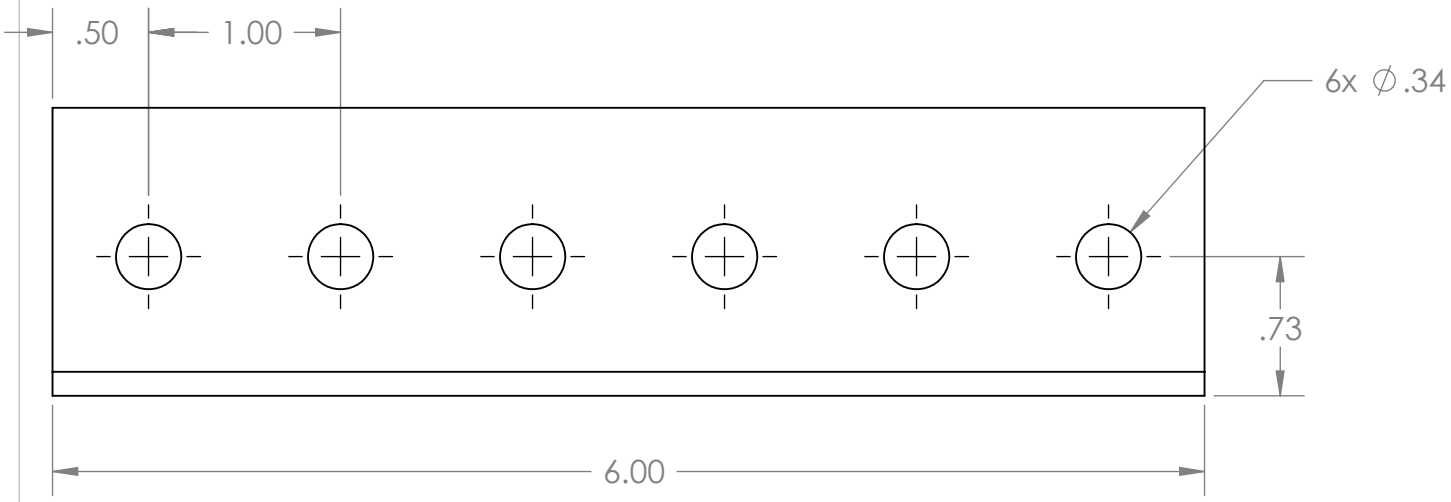

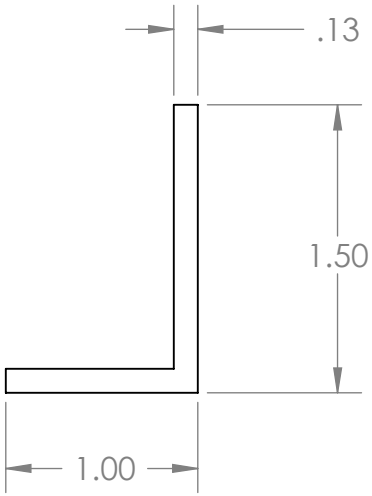

		UNLESS OTHERWISE SPECIFIED:		NAME	DATE
		DIMENSIONS ARE IN INCHES TOLERANCES: FRACTIONAL ±0.1 ANGULAR: MACH ±0.5 BEND ±0.5 ONE PLACE DECIMAL ± 0.1 TWO PLACE DECIMAL ± 0.05 THREE PLACE DECIMAL ± 0.005	DRAWN	BRW	2/2/10
			CHECKED		
			ENG APPR.		
			MFG APPR.		
		INTERPRET GEOMETRIC TOLERANCING PER:ASME Y14.5-2009	Q.A.		
		MATERIAL Aluminium	COMMENTS:		
NEXT ASSY	USED ON	FINISH			
APPLICATION		DO NOT SCALE DRAWING			

TITLE:

BNC Bracket

SIZE	DWG. NO.	REV
A		A

SCALE: 1:1	WEIGHT:	SHEET 1 OF 1

5 4 3 2 1

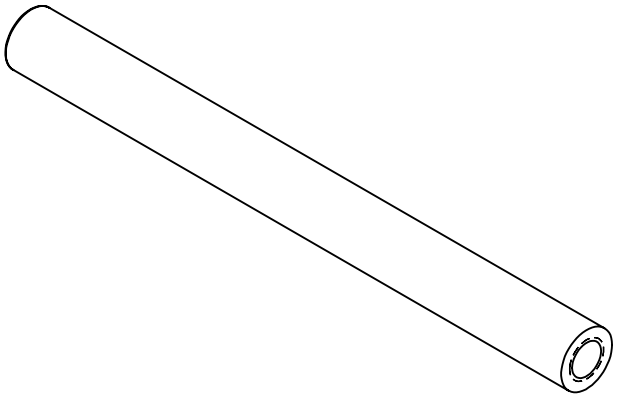

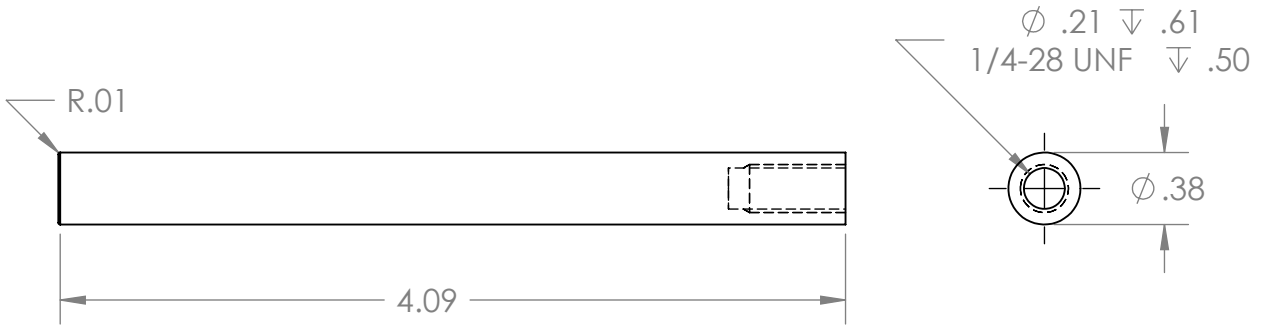

		UNLESS OTHERWISE SPECIFIED:		NAME	DATE
		DIMENSIONS ARE IN INCHES TOLERANCES: FRACTIONAL ±0.1 ANGULAR: MACH ±0.5 BEND ±0.5 ONE PLACE DECIMAL ± 0.1 TWO PLACE DECIMAL ± 0.05 THREE PLACE DECIMAL ± 0.005	DRAWN	BRW	2/23/10
			CHECKED		
			ENG APPR.		
			MFG APPR.		
			Q.A.		
		INTERPRET GEOMETRIC TOLERANCING PER:ASME Y14.5-2009	COMMENTS:		
		MATERIAL Aluminium			
NEXT ASSY	USED ON	FINISH			
APPLICATION		DO NOT SCALE DRAWING			

TITLE:

Guide Rod

SIZE	DWG. NO.	REV
A		B

SCALE: 1:1 | WEIGHT: | SHEET 1 OF 1

5 4 3 2 1

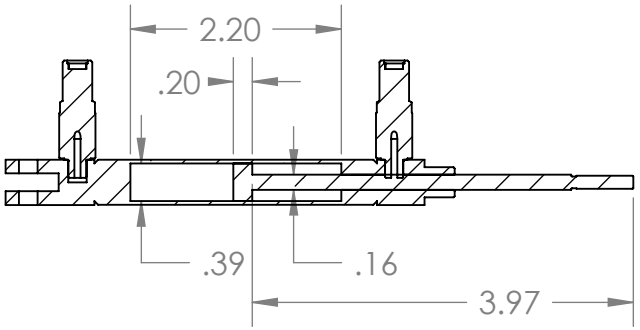

SECTION A-A

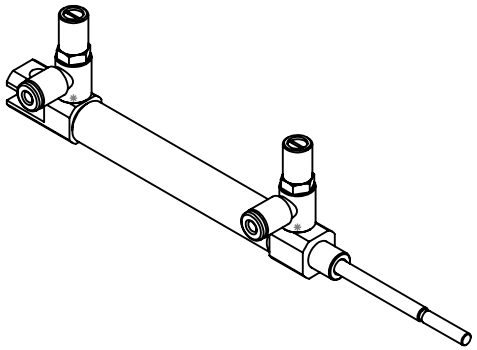

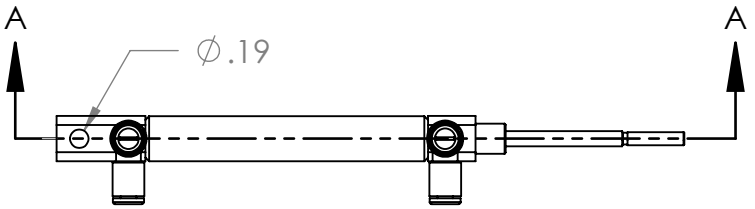

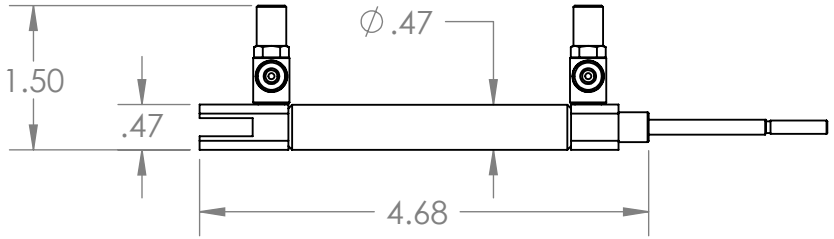

NEXT ASSY	USED ON
APPLICATION	

UNLESS OTHERWISE SPECIFIED:

DIMENSIONS ARE IN INCHES
TOLERANCES:
FRACTIONAL ±0.1
ANGULAR: MACH ±0.5 BEND ±0.5
ONE PLACE DECIMAL ± 0.1
TWO PLACE DECIMAL ± 0.05
THREE PLACE DECIMAL ± 0.005

INTERPRET GEOMETRIC TOLERANCING PER:ASME Y14.5-2009

MATERIAL

FINISH

DO NOT SCALE DRAWING

	NAME	DATE
DRAWN	BRW	2/16/10
CHECKED		
ENG APPR.		
MFG APPR.		
Q.A.		

COMMENTS:

TITLE:

Piston Assembly

SIZE	DWG. NO.	REV
A		A

SCALE: 1:2 | WEIGHT: | SHEET 1 OF 1

5 4 3 2 1

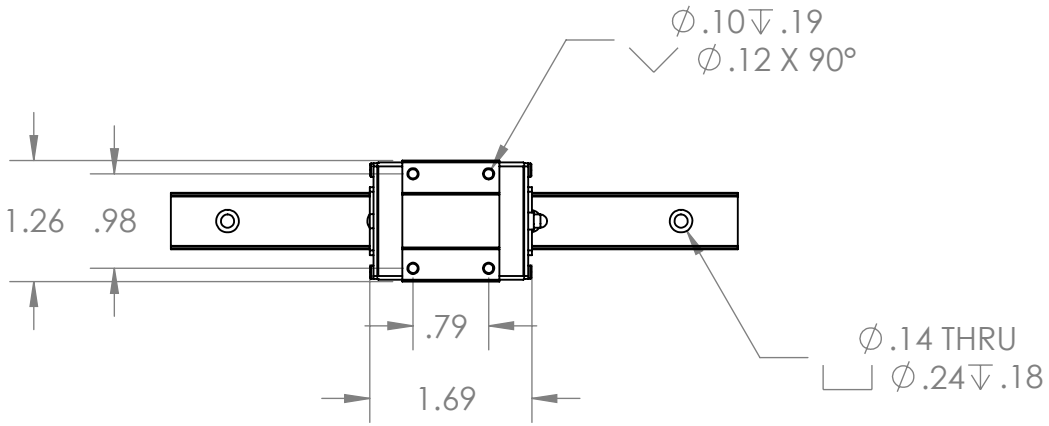

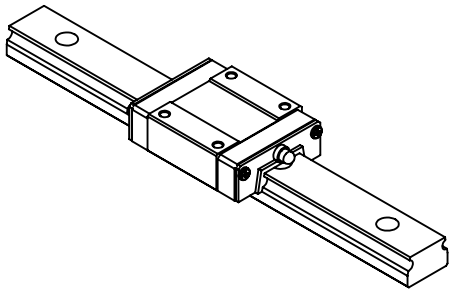

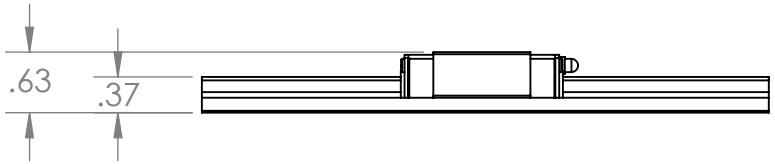

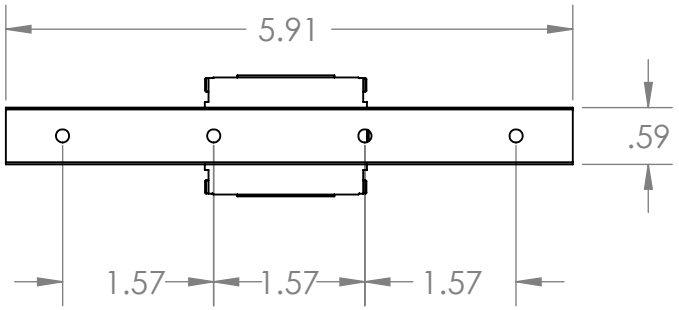

		UNLESS OTHERWISE SPECIFIED:		NAME	DATE
		DIMENSIONS ARE IN INCHES TOLERANCES: FRACTIONAL ±0.1 ANGULAR: MACH ±0.5 BEND ±0.5 ONE PLACE DECIMAL ± 0.1 TWO PLACE DECIMAL ± 0.05 THREE PLACE DECIMAL ± 0.005	DRAWN	BRW	2/16/10
			CHECKED		
			ENG APPR.		
			MFG APPR.		
		INTERPRET GEOMETRIC TOLERANCING PER:ASME Y14.5-2009	Q.A.		
		MATERIAL	COMMENTS:		
NEXT ASSY	USED ON	FINISH			
APPLICATION		DO NOT SCALE DRAWING			

TITLE:

Linear Slide Assembly

SIZE	DWG. NO.	REV
A		A

SCALE: 1:2 | WEIGHT: | SHEET 1 OF 1

5 4 3 2 1

Appendix F. Bond Graph MathCAD and MATLAB Calculations

This appendix contains all of the calculations used in the bond graph that were conducted in the programs MathCAD and MATLAB.

This is a MathCAD file, written by Richard MacKendrick, to evaluate Bond Graph Element Properties, and create the State Equations from a MATLAB print out. This Program, combined with the MATLAB script, gives the user the ability to rapidly change the system properties to observe their effects on system behavior. The values below are taken from a precursor program, also written in MathCAD.

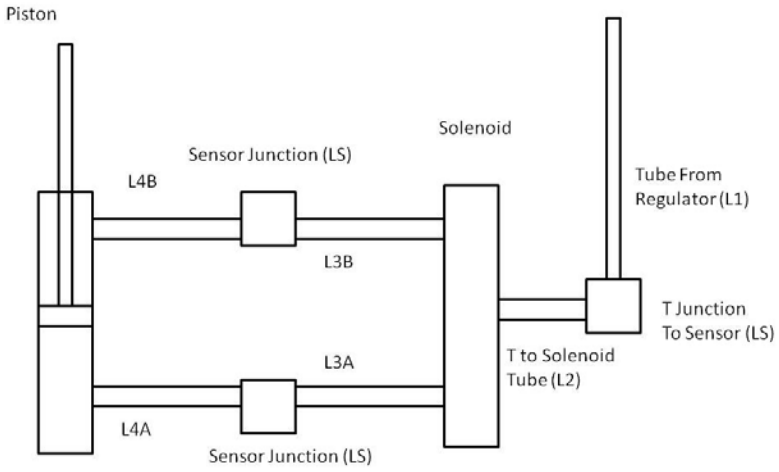

The Diagram above indicates which lengths belong to which pipes. Only a portion of the Pneumatic system is modeled here.

$L_1 := 0.325\text{in} = 8.255 \times 10^{-3}\,\text{m}$ $L_{3a} := 6.9\text{in} = 0.175\,\text{m}$ $L_{3b} := 2.62\text{in} = 0.067\,\text{m}$

$L_2 := 0.752\text{in} = 0.019\,\text{m}$ $L_{4a} := 2.68\text{in} = 0.068\,\text{m}$ $L_{4b} := 3.27\text{in} = 0.083\,\text{m}$

$L_s := 0.81\text{in} = 0.021\,\text{m}$

The properties below, also listed in the precursor program, are the inner and outer diameters of the Tubing, the elastic modulus of the material of the tubing (assumed to be Nylon 11, Youngs modulus taken from CES EduPack). The Bulk Modulus of Air for adiabatic conditions taken from www.wikipedia.org. Density of air taken from www.wolframalpha.com.

$Tu_{ID} := 0.1060\text{in} = 2.692 \times 10^{-3}\,\text{m}$ $Tu_{OD} := \frac{5}{32}\text{in} = 3.969 \times 10^{-3}\,\text{m}$

$E_{tu} := 0.19 \cdot 10^6 \cdot \text{psi} = 1.31 \times 10^9\,\frac{\text{kg}}{\text{m}\cdot\text{s}^2}$

$B_{air} := 1.52 \cdot 10^5\,\text{Pa} = 1.52 \times 10^5\,\frac{\text{kg}}{\text{m}\cdot\text{s}^2}$ $\rho_{air} := 0.001275 \cdot \frac{1}{\text{cm}^3}\left(10^{-3}\,\text{kg}\right)\cdot\left(\frac{100\,\text{cm}}{\text{m}}\right)^3 = 1.275\,\frac{\text{kg}}{\text{m}^3}$

The functions below are taken from the book *System Dynamics- Modeling and Simulation of Mechatronic Systems* by Dean C. Karnopp, Donald L. Margolis, and Ronald C Rosenberg, from pages 121 and 124 for the capacitance and inertance functions respectively.

$\text{TubeCap}\left(V_0, B, r_0, t_\omega, E\right) := \left[V_0 \cdot \left[\frac{1}{B} + \frac{\left(2 \cdot r_0\right)}{t_\omega \cdot E}\right]\right]^{-1}$ $\text{TubeInr}\left(\rho, L, r_0\right) := \frac{(\rho \cdot L)}{\pi \cdot r_0^{\,2}}$

V0 is volume, B is bulk modulus, r0 is the pipe inner radius, tω is the wall thickness, E is the Youngs modulus of the piping material, ρ is density, and L is the length of the pipe.

The Capacitance function is modified, as in the precursor program, to reflect the fact that the units work out to a relationship of effort*capacitance=charge, when the relationship should be effort=capacitance*charge.
As All pipes are of the same type, they are all assumed to have the same radius, which is half of the inner diameter. The thickness is half of the difference of the inner diameter from the outer diameter.

$$\tau := \frac{\left(Tu_{OD} - Tu_{ID}\right)}{2} = 6.382 \times 10^{-4}\,m \qquad r_p := \left(\frac{Tu_{ID}}{2}\right) = 1.346 \times 10^{-3}\,m$$

As the system properties for the liquid portion of the system depend on tube lengths, and as the liquid properties of the system are signal controlled depending on the path the solenoid allows fluid to travel, different lengths for each state and each Bond Graph Element are calculated Below. The Resistance function given for tubing below assumes incompressible laminar flow. While this may not necessarily be true, these assumptions will be made for mathematical simplicity. The formula is taken from page 116 of Karnopp et al. The viscosity of air is taken from page 556 in the appendix of Karnopp et al. The viscosity given is for air at STP, which is not the case in the system. This property is taken anyway for sake of simplicity, and due to the relatively small diference in pressure from 0 to 50 psi Gauge, which is the systems typical operating pressure.

$$\text{restube}(\mu, l, d) := \frac{(128 \cdot \mu \cdot l)}{\pi \cdot d^4} \qquad \mu_{air} := 1.8 \cdot 10^{-5}\,\frac{N \cdot s}{m^2}$$

$$L_{c5a} := L_1 + L_2 + 2 \cdot L_s + L_{3a} + L_{4a} \qquad L_{c5b} := L_1 + L_2 + 2 \cdot L_s + L_{3b} + L_{4b}$$

$$L_{r4a} := L_1 + L_2 + 2 \cdot L_s + L_{3a} + L_{4a} \qquad L_{r4b} := L_1 + L_2 + 2 \cdot L_s + L_{3b} + L_{4b}$$

$$L_{i2a} := L_1 + L_2 + L_{3a} + L_{4a} \qquad L_{i2b} := L_1 + L_2 + L_{3b} + L_{4b}$$

$$v_{c5a} := r_p^{\,2} \cdot \pi \cdot L_{c5a} = 1.775 \times 10^{-6}\,m^3$$

$$v_{c5b} := r_p^{\,2} \cdot \pi \cdot L_{c5b} = 1.242 \times 10^{-6}\,m^3$$

$$m_{2a} := \text{TubeInr}\left(\rho_{air}, L_{i2a}, r_p\right) = 6.062 \times 10^{4}\,\frac{kg}{m^4}$$

$$m_{2b} := \text{TubeInr}\left(\rho_{air}, L_{i2b}, r_p\right) = 3.963 \times 10^{4}\,\frac{kg}{m^4}$$

$$k_{5a} := \text{TubeCap}\left(v_{c5a}, B_{air}, r_p, \tau, E_{tu}\right) = 8.557 \times 10^{10}\,\frac{kg}{m^4 \cdot s^2}$$

$$k_{5b} := \text{TubeCap}\left(v_{c5b}, B_{air}, r_p, \tau, E_{tu}\right) = 1.223 \times 10^{11}\,\frac{kg}{m^4 \cdot s^2}$$

$$r_{4a} := \text{restube}\left(\mu_{air}, L_{r4a}, Tu_{ID}\right) = 4.352 \times 10^{6}\,\frac{kg}{m^4 \cdot s}$$

$$r_{4b} := \text{restube}\left(\mu_{air}, L_{r4b}, Tu_{ID}\right) = 3.044 \times 10^{6}\,\frac{kg}{m^4 \cdot s}$$

The Transformer modulus in this system, like the previous fluid properties, varies with time. A function for this is taken from the precursor program. The negative value indicates a reversal of motion direction and force application.

$$G_{67}(t) := \begin{cases} \text{return } 1.273 \times 10^{4} \dfrac{1}{m^2} & \text{if } \sin(2\cdot\pi\cdot t) \geq 0 \\ \text{return } \left[\dfrac{-1}{\left(7.855 \times 10^{-5} - 1.257 \times 10^{-5}\right)} \dfrac{1}{m^2} \right] \end{cases}$$

The outward stroke, which the "a" subscripted values above represent the fluid properties for, occurs first in the sequence of system actions. The reliance on t for time reflects this. Below are functions for the m2, r4 and k5 values.

$$k_{5f}(t) := \begin{cases} \text{return } k_{5a} & \text{if } \sin(2\cdot\pi\cdot t) \geq 0 \\ \text{return } k_{5b} \end{cases} \qquad m_{2f}(t) := \begin{cases} \text{return } m_{2a} & \text{if } \sin(2\cdot\pi\cdot t) \geq 0 \\ \text{return } m_{2b} \end{cases}$$

$$r_{4f}(t) := \begin{cases} \text{return } r_{4a} & \text{if } \sin(2\cdot\pi\cdot t) \geq 0 \\ \text{return } r_{4b} \end{cases}$$

The remaining system properties, the resistance, inertance, and capacitance of the mechanical system, are taken directly from the precursor program. These values have been found to be correct, and as such will be used for this program.

$$m_8 := 0.121\text{kg} = 0.121\ \text{kg}$$

$$k_9 := 15.59 \cdot \frac{\text{lb}}{\text{in}} \frac{1\text{in}}{2.54\text{cm}} \frac{100\text{cm}}{\text{m}} \frac{4.448\text{N}}{\text{lb}} = 2.73 \times 10^{3} \frac{\text{kg}}{s^2}$$

Possible Spring Constants are 15.59, 5.21 or 3.31 lbf/in. Other springs can be purchased, and their k values can be entered for k9 alternatively. Below is the adapted R4(t) function, taken from the precursor program. The values for resistance also vary with time due to signal control. The resistance values were taken experimentally, using a bond graph to find useable equations from which to base the resistance calculations.

$$r_{10}(t) := \begin{cases} \text{return } 131.550645 \dfrac{\text{kg}}{\text{s}} & \text{if } \sin(2\pi t) \geq 0 \\ \text{return } 51.00786845 \dfrac{\text{kg}}{\text{s}} \end{cases}$$

In order to transfer output into MATLAB for rapid evaluation, a vector is created with system properties as a function of time. To ensure that MathCAD will compute the vector, however, unitless render functions were taken from the original program. They are shown below.

$$ucf := \frac{m^4 \cdot s^2}{kg} \quad ucm := \frac{s^2}{kg} \quad urg := m^2$$

$$urf := \frac{m^4 \cdot s}{kg} \quad uim := \frac{1}{kg}$$

$$uif := \frac{m^4}{kg} \quad urm := \frac{s}{kg}$$

$$\text{MATLABVECT}(t) := \begin{pmatrix} ucf \cdot k_{5f}(t) \\ uif \cdot m_{2f}(t) \\ urf\ r_{4f}(t) \\ urg \cdot G_{67}(t) \\ uim \cdot m_{8} \\ ucm \cdot k_{9} \\ urm\ r_{10}(t) \end{pmatrix}$$

$$\text{MATLABVECT}(0.01) = \begin{pmatrix} 8.557 \times 10^{10} \\ 6.062 \times 10^{4} \\ 4.352 \times 10^{6} \\ 1.273 \times 10^{4} \\ 0.121 \\ 2.73 \times 10^{3} \\ 131.551 \end{pmatrix}$$

$$\text{MATLABVECT}(0.6) = \begin{pmatrix} 1.223 \times 10^{11} \\ 3.963 \times 10^{4} \\ 3.044 \times 10^{6} \\ -1.516 \times 10^{4} \\ 0.121 \\ 2.73 \times 10^{3} \\ 51.008 \end{pmatrix}$$

Below are initial conditions, and the applied pressure, to the system for the Out stroke.

$p_{20} := 0$

$q_{50} := 0$

$p_{80} := 0$

$q_{90} := 0.00\text{m}$

$\text{Papplied} := 50\text{psi} = 3.447 \times 10^{5}\ \frac{\text{kg}}{\text{m} \cdot \text{s}^{2}}$

Below are the roots for the characteristic equations for each possible set of bond graph element values. V1 is for the out stroke conditions, and V2 is for the in stroke conditions. Polyroots was used to get the roots.

$$v1 := \begin{pmatrix} \frac{1668615000000000}{52393} \\ \frac{39273696191163076054900944260272602808348343464145085697 1}{25558814382207201774316769413162685095874448588 8} \\ \frac{55083291758514002893242317079556973039 25}{36321259787836200095962296666209792} \\ \frac{81556659208216591}{70368744177664} \\ 1 \end{pmatrix}$$

$$\text{polyroots}(v1) = \begin{pmatrix} -1.064 \times 10^{3} \\ -36.793 + 1.189i \times 10^{3} \\ -36.793 - 1.189i \times 10^{3} \\ -21.161 \end{pmatrix}$$

$$v2 := \begin{pmatrix} \frac{91171225600000011375}{1417633792} \\ \frac{29821063931499301990792598135958262403247}{24777814544324913207899292958720} \\ \frac{11324815903126522249713331179}{360564656793211371520} \\ \frac{4297431529894477323}{9218305487273984} \\ 1 \end{pmatrix}$$

$$\text{polyroots}(v2) = \begin{pmatrix} -324.917 \\ -64.056 \\ -38.606 - 1.757i \times 10^{3} \\ -38.606 + 1.757i \times 10^{3} \end{pmatrix}$$

The results for the MATLAB laplace vectors have been used to create the state equations below. An important aspect of the equations below is that they are copied from MATLAB, but have their results rounded to four significant figures. This is different than what the MATLAB output will be, but is neccessary for MathCAD to produce results, as the numbers directly output by MATLAB have too high a number of significant digits for MathCAD to use in its invlaplace symbolic function.

f11(t) :=

The equations to the right have been fully executed in the MathCAD files accompanying this MQP. The evaluations performed to acquire these functions have been removed from the PDF due to file sizing and continuity reasons.

f12(t) :=

f13(t) :=

f14(t) :=

Using the functions generated above, the following plots appear below. The time interval selected is from 0 to 0.2 seconds, as the experimental data indicates that this is approximately equal the time required for the entire out stroke cycle from start to stall.

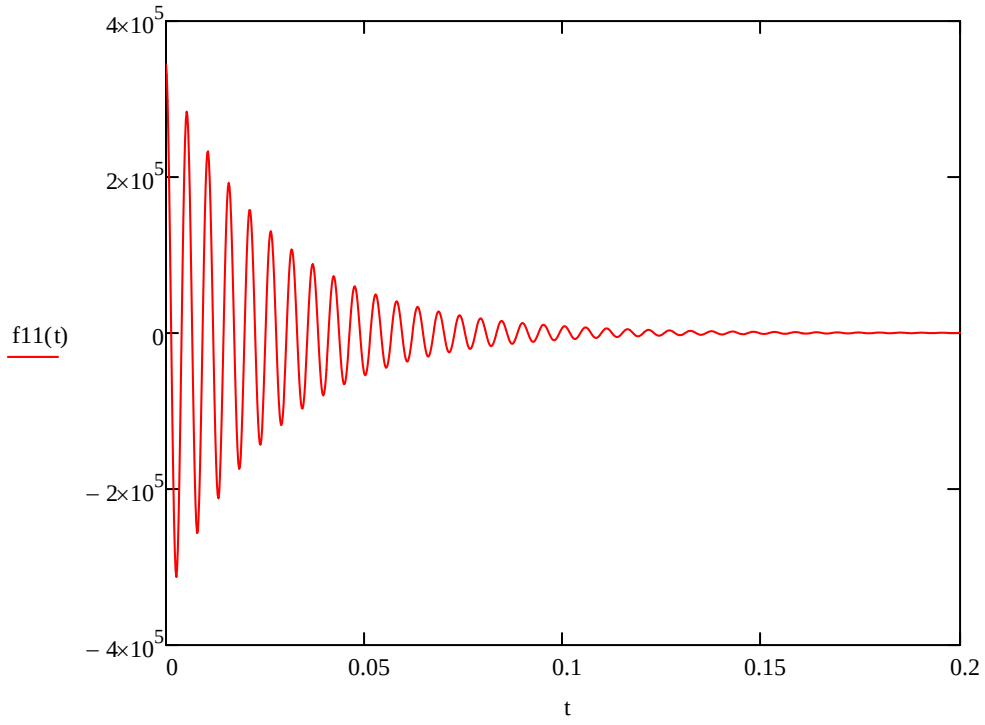

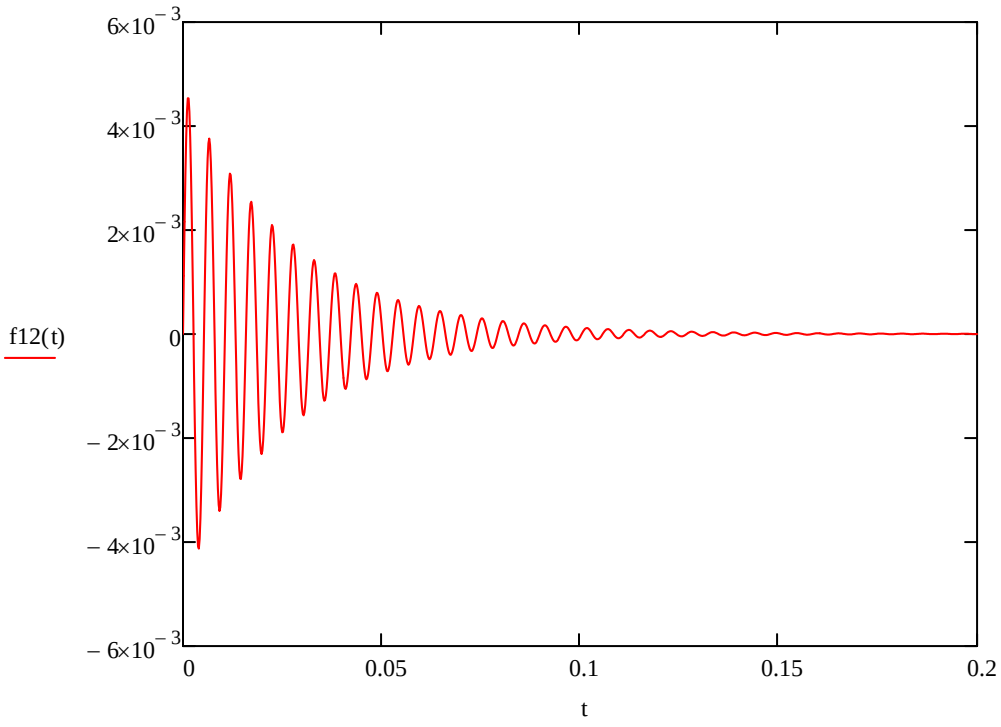
f12(t)
6×10⁻³
4×10⁻³
2×10⁻³
0
– 2×10⁻³
– 4×10⁻³
– 6×10⁻³
0
0.05
0.1
0.15
0.2
t

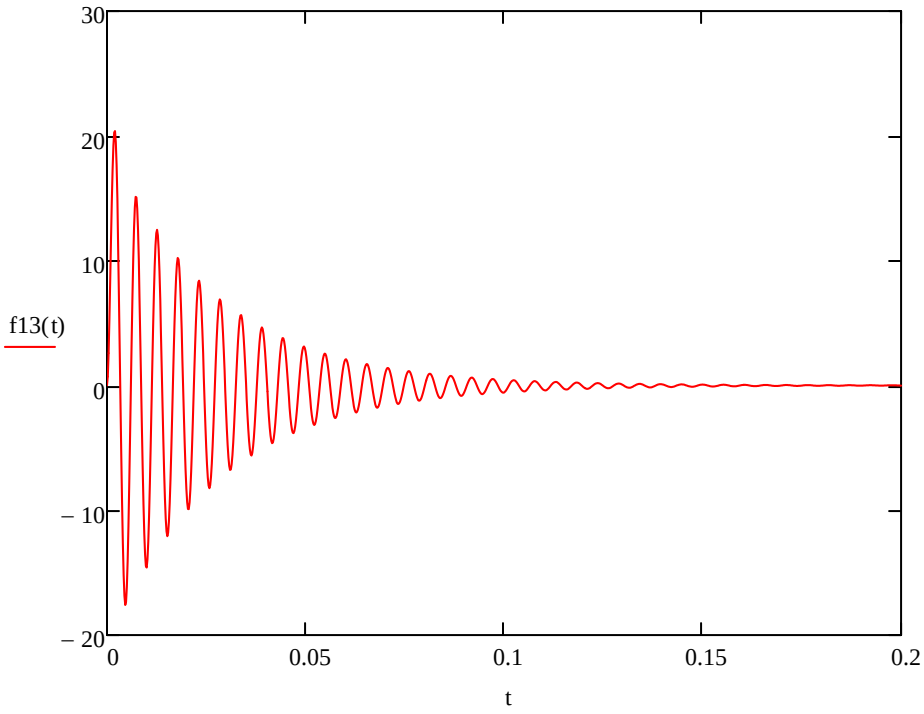
f13(t)
30
20
10
0
– 10
– 20
0
0.05
0.1
0.15
0.2
t

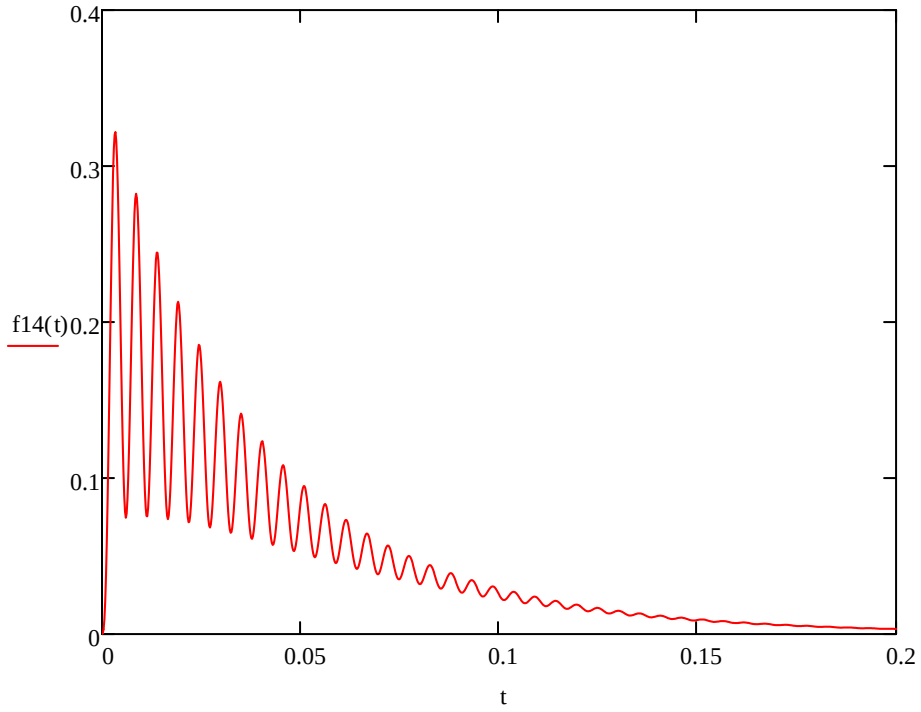

The symbollic evaluation to the right has been removed from the PDF for Continuity and File Size reasons. To view, access accompanying MathCAD File $f11p(t) := \frac{d}{dt} f11(t) \rightarrow$

Below is a plot of the derivative of the out stroke fluid momentum function.

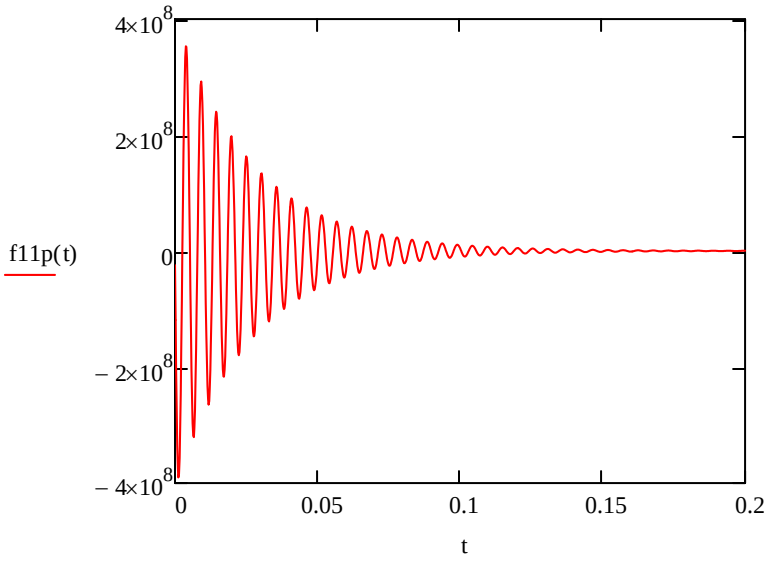

The symbollic evaluation to the right has been removed from the PDF for Continuity and File Size reasons. To view, access accompanying MathCAD File $f13p(t) := \frac{d}{dt} f13(t) \rightarrow$

Below is a plot of the derivative of the out stroke mechanical momentum function.

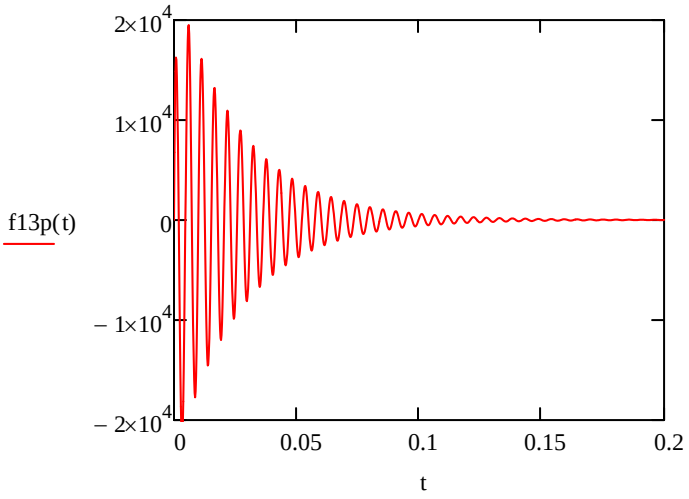

Below are initial conditions, and the applied pressure, to the system for the in stroke. It is assumed that the displacement of the spring is initially 0.0254 for the in stroke. These conditions were entered into MATLAB, and the resulting laplace domain equations had their numbers rounded to four significant figures. The results are below.

$p_{20} := 0$

$q_{50} := 0$

$p_{80} := 0$

$q_{90} := 0.0254m$

$P_{applied} := 50psi = 3.447 \times 10^5 \frac{kg}{m \cdot s^2}$

f21(t) :=

f22(t) :=

The equations to the right have been fully executed in the MathCAD files accompanying this MQP. The evaluations performed to acquire these functions have been removed from the PDF due to file sizing and continuity reasons.

f23(t) :=

f24(t) :=

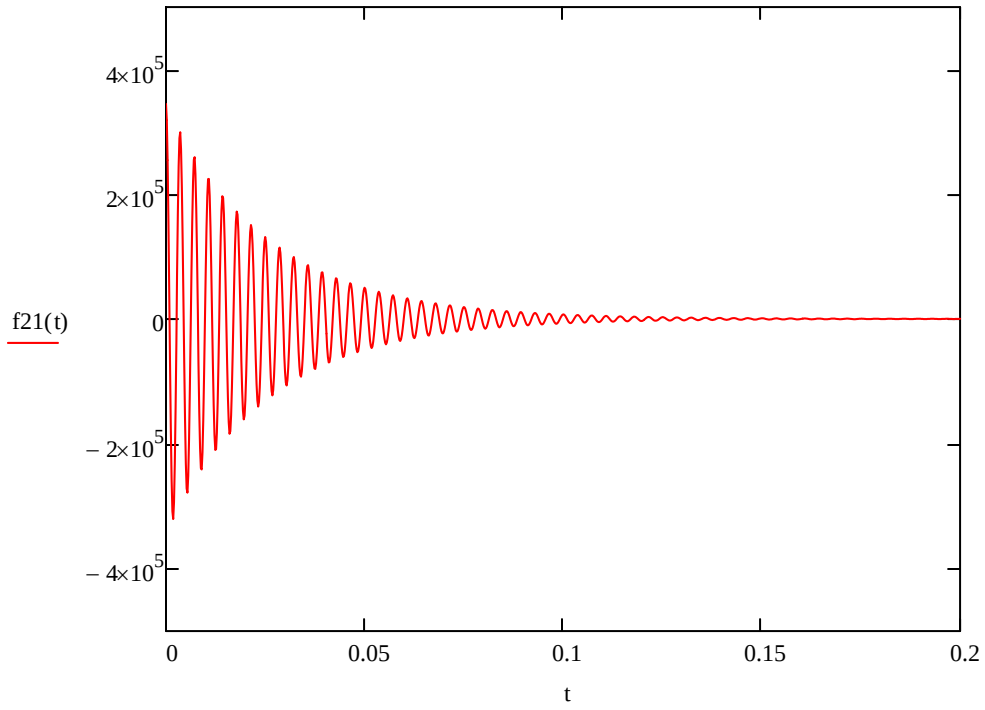

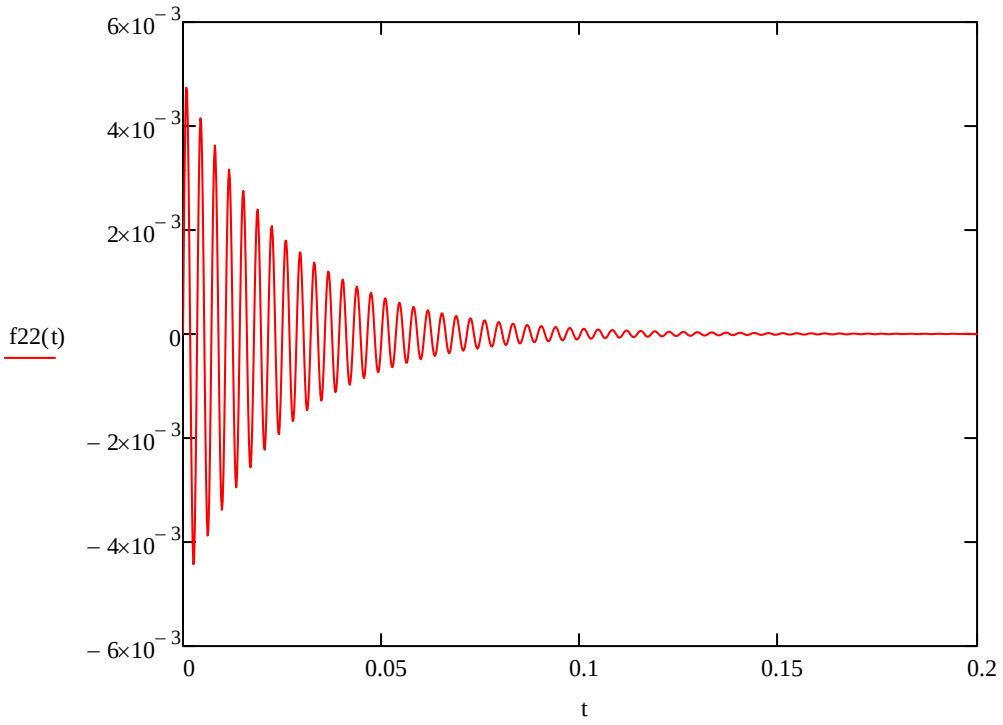
f22(t)
6×10⁻³
4×10⁻³
2×10⁻³
0
– 2×10⁻³
– 4×10⁻³
– 6×10⁻³
0
0.05
0.1
0.15
0.2
t

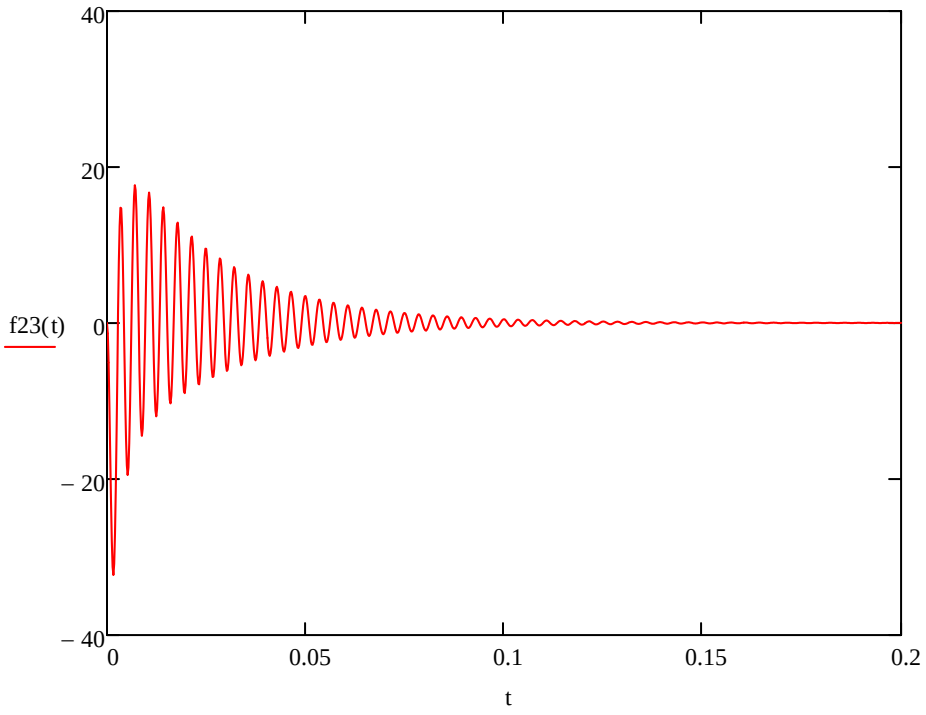
f23(t)
40
20
0
– 20
– 40
0
0.05
0.1
0.15
0.2
t

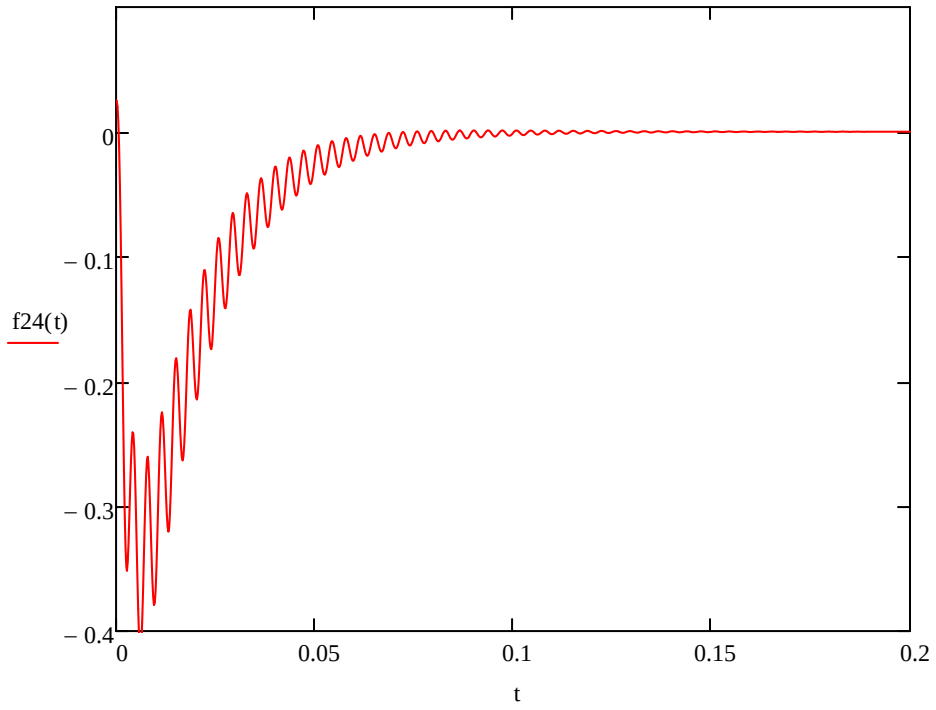

The graphs above show that, while the bond graph methods do not necessarily return the correct magnitudes of value, they do return useful behavior data concerning the system. Also, a useful note, is that the system, while not correlating with the physical system completely, does correlate quite well to itself, the in stroke behaviors being opposite in magnitude of their out stroke counterparts.

```
%This is a MATLAB script written by Richard MacKendrick for the
%Pneumatic Test Bench MQP. This script was written to evaluate
%A Bond Graph based approach that used a 4 state variable
%Bond Graph to predict Test Bench behaviors.

k5=8.557*10^10;%MathCAD Generated value for Fluid Capacitance
m2=6.062*10^4; %MathCAD Generated value for Fluid Inertance
r4=4.352*10^6; %MathCAD Generated value for Fluid Resistance
G67=1.273*10^4;%MathCAD Generated value for Transformer Modulus
m8=0.121;      %MathCAD Generated value for Mechanical Inertance
k9=2.73*10^3;  %MathCAD Generated value for Mechanical Capacitance
r10=131.551;   %MathCAD Generated value for Mechanical Resistance

amat=[-r4/m2,-k5  ,0           ,0;...  %This Matrix was generated using
      1/m2,   0   ,-1/(G67*m8) ,0;...  %the Bond Graph approach.The Bond
      0   ,k5/G67 ,-r10/m8     ,-k9;...%Graph on which this analysis is
      0   ,0      ,1/m8        ,0];    %based is in a separate file

  syms s;   % This symbolic variable is necessary for the output of
            % A polynomial which can be copied into MathCAD for more
            % Precise results than the MATLAB printout. The Matlab
            % Printout is provided to tell the user whether or not the
            % manual entry of the polynomial roots is worth their time
  roots(poly(amat))     %Gives indication on system stability/behavior
  det(s*eye(4)-amat)    %Gives roots of polynomial for MathCAD entry

  pause;
  clc;

  p20=0;               %User Selected Value for initial fluid momentum
  q50=0;               %User Selected Value for initial fluid charge
  p80=0;               %User Selected Value for initial mech. momentum
  q90=0;               %User Selected Value for initial mech. charge
  Papplied=3.447*10^5; %User Selected value for Applied Pressure
  invect=[(p20+Papplied);q50;p80;q90];
  %Below is the function that MATLAB uses to generate a vector of
  %Laplace Domain Equations for the Bond Graph State Equations.
  %These are entered into MathCAD for inversion, due to readability
  %Issues with MATLAB printouts.

  lapvect=inv(s*eye(4)-amat)*invect

  %Below, the script above is repeated to give results for the in stroke
  %behavior of the Pneumatic Test Bed.

  pause;
  clc;

  k5=1.223*10^11;   %MathCAD Generated value for Fluid Capacitance
  m2=3.963*10^4;    %MathCAD Generated value for Fluid Inertance
  r4=3.044*10^6;    %MathCAD Generated value for Fluid Resistance
  G67=-1.516*10^4;  %MathCAD Generated value for Transformer Modulus
```

```
  m8=0.131;          %MathCAD Generated value for Mechanical Inertance
  k9=2.73*10^3;      %MathCAD Generated value for Mechanical Capacitance
  r10=51.008;       %MathCAD Generated value for Mechanical Resistance

amat=[-r4/m2,-k5  ,0           ,0;...  %This Matrix was generated using
      1/m2,   0   ,-1/(G67*m8) ,0;...  %the Bond Graph approach.The Bond
      0   ,k5/G67 ,-r10/m8     ,-k9;...%Graph on which this analysis is
      0   ,0      ,1/m8        ,0];     %based is in a separate file

  roots(poly(amat))       %Gives indication on system stability/behavior
  det(s*eye(4)-amat)      %Gives roots of polynomial for MathCAD entry

  pause;
  clc;

  p20=0;                   %User Selected Value for initial fluid momentum
  q50=0;                   %User Selected Value for initial fluid charge
  p80=0;                   %User Selected Value for initial mech. momentum
  q90=0.0254;              %User Selected Value for initial mech. charge
  Papplied=3.447*10^5;     %User Selected value for Applied Pressure
  invect=[(p20+Papplied);q50;p80;q90]
  lapvect=inv(s*eye(4)-amat)*invect
```

Appendix G. Experimental Procedure for Bond Graph Mechanical Resistances

The procedure used to evaluate the mechanical resistance used in the bond graph is as follows.

Step 1- Remove the main spring from the device. Leave the return spring in place (its effects have been deemed negligible due to the fact that it does not act through the whole action of the device.)

Step 2- Run the device, collecting data for both piston out stroke and piston in stroke. Put the data into a spreadsheet file

Step 3- Using the spreadsheet file, turn the accelerometer readings into acceleration data.

Step 4- Trim out the acceleration readings associated with the impact, and with times in which the piston is not in motion. When the pipe is in motion, the direction of the motion is assumed positive in the direction that the piston is trying to move (IE- on the outstroke, the outward direction from the piston is positive. On the in stroke, the opposite is true).

Step 5- Apply a trend line to the acceleration data. The recommended trend-line is a sixth degree polynomial (if different software than Excel is used, a higher order polynomial is acceptable)

Step 6- Manually integrate the trend line equation given by Excel (or other software)

Step 7- Plot the integrated trend line equation as velocity, using starting at t=0, advancing by increments equal to the time between accelerometer readings, and collect velocity data for an equal amount of time as the trimmed acceleration data collects.

Step 8- Using the equation below, create a readout of resistance values. Take the natural logarithm of the ABSOLUTE value of the results of the equation within the natural logarithm to ensure numerical results. Alternately, results that do not evaluate can be thrown out for the creation of the average, but the approach above is far more convenient and has limited impact on accuracy for suitable intervals of time. The equation is $R = -\frac{m}{t}\ln\left(\frac{m}{Fa} * \int A(t)dt\right)$

Step 9- Average the resistance readings. Use this resistance for the bond graph based model. Take resistances for both out stroke and in stroke, as these numbers will be different.

The graph in Figure 58(below) is from the excel file used to obtain resistance values. This graph is the trimmed plot of the return stroke of the piston, from the time that the acceleration starts to just

before impact with the piston limit. Important to note is the sudden dip in acceleration towards the end. This is due to the return cushion spring gaining contact with the piston.

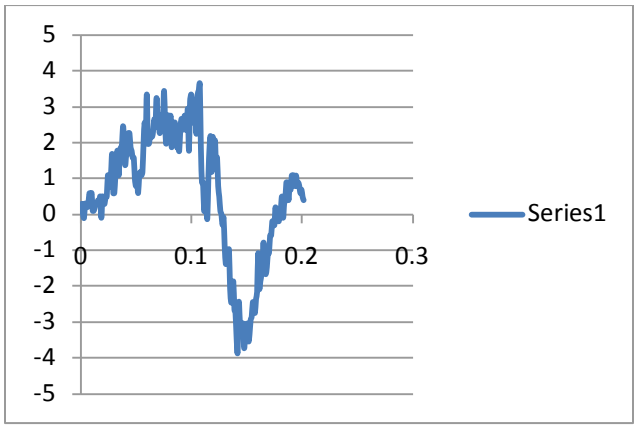

Figure 58 - Trimmed In Stroke Data

The graph in Figure 59 (below) is of the out stroke of the piston. The sharp initial increase in acceleration is due to the assistance of the return spring to the piston. The graph below, like that above, is trimmed to only encompass the times when the piston is in motion, but not impacting an end limit.

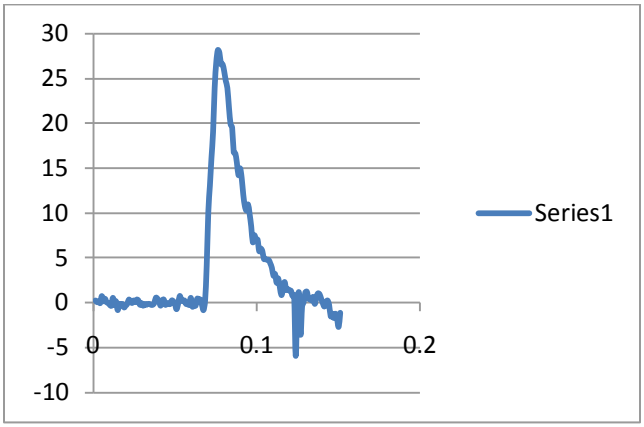

Figure 59 - Trimmed Out Stroke Data